Quantum Stretching: a quasi-copy technique of arbitrary qubits for quantum internet

Mario Mastriani

Quantum Stretching: a quasi-copy technique of arbitrary qubits for the quantum internet

Mario Mastriani

ORCID Id: 0000-0002-5627-3935

Abstract - Quantum stretching is a technique to make quasi-copies of an arbitrary qubit without violating the No-Cloning Theorem. These quasi-copies of the original qubit contain all the information of the original but at the cost of duplication in its size each time the technique is applied. Basically, a stretched bit or subit is obtained applying a single, unitary and reversible gate, i.e., we can recover the original qubit from its subit. Quantum stretching will allow us simultaneous teleportation to multiple destinations of the same subit, with the consequent potential that this has for the quantum internet in configurations from *1* to *N*, however, always taking into account the duplication of qubit size to be quasi-copied every time the technique is applied. Finally, quantum stretching is particularly useful to make satellite bifurcations in the quantum internet context.

Keywords: No-Cloning Theorem; Quantum Entanglement; Quantum Internet; Quantum Mechanics; Quantum Repeaters; Quantum Teleportation; Special Relativity.

1. Introduction

From the pioneering paper by Bennett *et al* [1], which establishes the theoretical beginning of quantum teleportation, until its first physical implementations by Bouwmeester *et al* [2, 3], Boschi *et al* [4], and Kurucz *et al* [5], the scientific community has been explicitly assuming the impossibility of instant quantum communication based on entanglement [6-11]. Actually, all this began with the so-called EPR paradox [12] due to Einstein, Podolsky, and Rosen, which was subjected to experimental scrutiny by the works of John Bell [13], and Clauser, Horne, Shimony, and Holt (CHSH) [14], and the physical implementation of their theorems in the works of Aspect [15] with loopholes, and Hensen *et al* [16], apparently, without loopholes. From these last works, a question arises about the problem of locality and causality raised in the EPR paradox [12], given that the experimental results seem to confer a non-local nature to the entanglement. This automatically results in a direct confrontation between two of the main pillars of the last century Physics: Special Relativity [17] and Quantum Mechanics [18]. It is in this context in which literature admits the instantaneity of entanglement but not for the transmission of useful information thanks to it [1, 19]. Since quantum teleportation is essentially based on entanglement, its original design incorporated this limitation known as non-signaling [6-11, 20, 21]. Besides, given that there is no quantum internet [22-28] without quantum teleportation [1-5], at least for now, quantum internet dragged several controversies around quantum teleportation and quantum entanglement in relation to the tempestuous relationship between Quantum Mechanics [18] and Special Relativity [17]. In other words, we begin to glimpse the conflict inference map: *quantum entanglement* → *quantum teleportation* → *quantum internet*. Therefore, the problems that Quantum Internet has faced since its inception in the physical layer have been:

1. the traditional quantum teleportation [1-5] uses a classical channel for disambiguation. The disambiguation bits travel along said channel at the speed of light and subject to the bandwidth of the said channel. Therefore, and given that the chain is broken by its weakest link, this classic channel leads to problems of latency or delays, limited bandwidth and exposure to hackers in the context of Quantum Key Distribution (QKD) [29], since, for the mere existence of the classic channel the hackers cannot make themselves of the main information but they can alter the integrity of such information the receiver will get when this one must reconstruct the teleported

state. Obviously, all these problems are aggravated as the distance between the transmitter and the receiver increases at both ends of the quantum teleportation process. Fortunately, this problem was solved by means of a modern technique [30] which will be mentioned in part in Section 3.3 and that allows us to dispense with the aforementioned classic channel, with all the advantages that this entails thinking in quantum internet [22-28] terms and without the slightest physical restriction or contradiction between Special Relativity [17] and Quantum Mechanics [18].

2. the traditional quantum teleportation [1-5] does not allow transmitting the same message (qubit to be teleported) to more than one destination at the same time, i.e., it does not allow us to make broadcasting. This restriction is due to the No-Cloning theorem, which states that an arbitrary qubit cannot be exactly copied. The solution to this problem is the leitmotiv of this work. Here, we present a technique known as quantum stretching which will allow us to make innumerable copies of the most relevant of a qubit in terms of information in the context of a quantum internet.

3. the traditional quantum teleportation [1-5] does not allow transmitting an object (lattice, matrix, or structure; with multiple qubits inside) using only one EPR pair. The practicality of this is obvious. Let us suppose that we want to transmit a picture of 1920 columns by 1080 rows by 3 colors by 8 bits per color channel (i.e., red-green-blue). The volume of information to be transmitted would be approximately 50 Million bits to be converted to their quantum counterpart. If we had to distribute an EPR pair for each qubit to be transmitted, then we would be talking about 50 Million EPR pairs to generate and distribute between both ends of the link, i.e., complete nonsense. Although the mere idea about the existence of this possibility seems mathematically absurd, we must bear in mind the results obtained in previous work [30], in which the exceptional attributes of entanglement to interact with large volumes of information were demonstrated theoretically and experimentally. Therefore, to continue exploring the scope of these attributes is not absurd at all. On the other hand, a reasonable scheme could be based on a numerical proportion of the type N qubits to be transmitted thanks to the distribution of M EPR pairs, for $M << N$, in some context of quantum compression (in principle lossless, but lossy). The solution of this complex problem, if it exists, would allow a more practical transfer of vectors, matrices, streamings, pictures, multi and hyperspectral satellite imagery, multi and hyper-slicing medical imagery, video, and TV on the quantum internet. Obviously, this problem is still open.

4. the short coherence time of the EPR pair conspires negatively, pro tem, with the main task that someday, not very far, we take the quantum internet from Earth to Mars. If we think in a delivery or a take-out of the entangled particle based on a spaceship or on a relay system as quantum repeaters, the distance to travel is so extravagant (in the best-case scenario, via any kind of optical link, the time of the trip is approximately 5000 times greater than the coherence time) that it makes the link completely unrealizable, given that: a) sending the element of the EPR pair by optical means would cause the collapse of the coherence before the arrival of said element, and b) for a system of satellite posts would require so many quantum repeaters that it would also be impractical,

5. all forms of quantum teleportation, i.e., the traditional [1-5], and even the most modern [30], destroy entanglement as an essential part of the teleportation process. This entails the need to create and distribute a new EPR pair at the end of each teleportation in order to enable the next transfer. If we think about the possibility that someday we can connect the Earth with Mars through the quantum internet, the problem of the redistribution of the EPR pair at the end of each teleportation is a nightmare that throws the entire company overboard. At present, there are several lines of research underway to overcome this delicate problem [31]. Notwithstanding what has been said, this is another open problem.

Showing up next, a setup with all the tools required to develop this work in depth is outlined in Section 2. In Section 3, we introduce the concept of quantum stretching and its projection on quantum information processing in general and quantum teleportation in particular. In Section 4, we present the technique to make quasi-copies of the same message (qubit) to be teleported through quantum repeaters on the quantum internet. Finally, Section 5 provides a conclusion and future work proposals.

2. Setup

In this section, we will explore the most relevant concepts of Quantum Information Processing [32], the No-Cloning Theorem [33], Quantum Entanglement [34-36] and Quantum Teleportation [1-5, 30, 37, 38] necessary for the subsequent development of this work.

2.1. A bit of Quantum Information Processing

All arbitrary qubit can be represented by the following wave-function [32]

$$|\psi\rangle = \alpha|0\rangle + \beta|1\rangle \tag{1}$$

where $\{|0\rangle, |1\rangle\}$ are the so-called Computational Basis States (CBS) and qubit basis states, which are located at the poles of the Bloch's sphere [32, 39, 40] of **Figure 1**

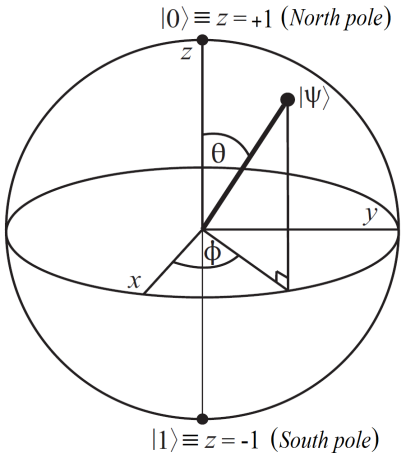

Figure 1 Bloch's Sphere.

while $\alpha \wedge \beta \in \mathbb{C}$ of Hilbert's space [32] with $|\alpha|^2 + |\beta|^2 = 1$. Specifically, in its most complete form, the wave-function will be

$$|\psi\rangle = e^{i\gamma}\left(\cos\frac{\theta}{2}|0\rangle + e^{i\phi}\sin\frac{\theta}{2}|1\rangle\right) = e^{i\gamma}\left(\cos\frac{\theta}{2}|0\rangle + (\cos\phi + i\sin\phi)\sin\frac{\theta}{2}|1\rangle\right) \tag{2}$$

where $0 \le \theta \le \pi$, $0 \le \phi < 2\pi$ [32]. However, we can ignore the factor $e^{i\gamma}$ of Eq.(2), because it has no observable effects [40], and for that reason we can effectively write,

$$|\psi\rangle = \cos\frac{\theta}{2}|0\rangle + e^{i\phi}\sin\frac{\theta}{2}|1\rangle \tag{3}$$

with $\alpha = \cos\left(\theta/2\right)$ and $\beta = e^{i\phi}\sin\left(\theta/2\right)$, being then Eq.(3) equivalent to Eq.(2). The numbers θ and ϕ define a point on the unit three-dimensional sphere, as shown in **Figure 1**. On the other hand, we can represent the mentioned poles in several different ways, i.e., based on the spin orientation {*spin up*, *spin down*}, the projection on the *z*-axis of Bloch's sphere {$z = -1$, $z = +1$}, among others:

$$\left(Spin\ up = |\uparrow\rangle = |0\rangle = \begin{bmatrix}1\\0\end{bmatrix} = North\ pole\right) \equiv (z = +1) \tag{4}$$

$$\left(Spin\ down = \left|\downarrow\right\rangle = \left|1\right\rangle = \begin{bmatrix} 0 \\ 1 \end{bmatrix} = South\ pole \right) \equiv \left(z = -1 \right) \tag{5}$$

Alternatives that will be very useful throughout the next analysis as well as those based on the Kronecker's product, would be as follow,

$$\left|0^A\right\rangle \otimes \left|0^B\right\rangle = \left|0^A\right\rangle\left|0^B\right\rangle = \left|0^A, 0^B\right\rangle = \left|0^A 0^B\right\rangle \tag{6a}$$

$$\left|1^A\right\rangle \otimes \left|1^B\right\rangle = \left|1^A\right\rangle\left|1^B\right\rangle = \left|1^A, 1^B\right\rangle = \left|1^A 1^B\right\rangle \tag{6b}$$

where $\otimes$ is the Kronecker's product [32]. Consequently with this, and being,

$$\left|00\right\rangle = \begin{bmatrix} 1 \\ 0 \end{bmatrix} \otimes \begin{bmatrix} 1 \\ 0 \end{bmatrix} = \begin{bmatrix} 1 \\ 0 \\ 0 \\ 0 \end{bmatrix}, \quad \left|11\right\rangle = \begin{bmatrix} 0 \\ 1 \end{bmatrix} \otimes \begin{bmatrix} 0 \\ 1 \end{bmatrix} = \begin{bmatrix} 0 \\ 0 \\ 0 \\ 1 \end{bmatrix}, \quad \left|01\right\rangle = \begin{bmatrix} 1 \\ 0 \end{bmatrix} \otimes \begin{bmatrix} 0 \\ 1 \end{bmatrix} = \begin{bmatrix} 0 \\ 0 \\ 1 \\ 0 \end{bmatrix}, \quad \left|10\right\rangle = \begin{bmatrix} 0 \\ 1 \end{bmatrix} \otimes \begin{bmatrix} 1 \\ 0 \end{bmatrix} = \begin{bmatrix} 0 \\ 1 \\ 0 \\ 0 \end{bmatrix} \tag{7}$$

we are going to use them to build the famous Bell's bases [34-36], with 2-qubit vectors, the combined Hilbert space will be $\mathrm{H}_4^{A\cup B} = \mathrm{H}_2^A \otimes \mathrm{H}_2^B$, and then we will have the following four vectors,

$$\begin{aligned} &\left|\beta_{00}\right\rangle = \left|\Phi^+\right\rangle = \frac{1}{\sqrt{2}}\left(\left|00\right\rangle + \left|11\right\rangle\right), \quad \left|\beta_{10}\right\rangle = \left|\Phi^-\right\rangle = \frac{1}{\sqrt{2}}\left(\left|00\right\rangle - \left|11\right\rangle\right), \\ &\left|\beta_{01}\right\rangle = \left|\Psi^+\right\rangle = \frac{1}{\sqrt{2}}\left(\left|01\right\rangle + \left|10\right\rangle\right), \quad \left|\beta_{11}\right\rangle = \left|\Psi^-\right\rangle = \frac{1}{\sqrt{2}}\left(\left|01\right\rangle - \left|10\right\rangle\right). \end{aligned} \tag{8}$$

Quantum teleportation protocol [1-5, 30, 37, 38], and therefore, the quantum internet [22-28] are based on the four vectors of Eq.(8), and constitute the very essence of entanglement.

2.2. No-Cloning Theorem

This theorem states that [33]:

There is no unitary operator U acting on $\mathrm{H}_4^{A\cup B} = \mathrm{H}_2^A \otimes \mathrm{H}_2^B$ *in such a way that for all the normalized states* $\left|\psi\right\rangle_A$ *and* $\left|e\right\rangle_B$ *in* **H** *comply with* $U\left(\left|\psi\right\rangle_A \left|e\right\rangle_B\right) = e^{i\alpha(\psi,e)}\left|\psi\right\rangle_A \left|\psi\right\rangle_B$ *for some real number* α *depending on* ψ *and* e.

To prove this theorem, an arbitrary pair of states $\left|\phi\right\rangle_A$ and $\left|\psi\right\rangle_A$ are selected in Hilbert's space **H**, then, since *U* is a unitary operator,

$$\begin{aligned} \left\langle\phi\middle|\psi\right\rangle\left\langle e\middle|e\right\rangle &\equiv \left\langle\phi\right|_A \left\langle e\right|_B \left|\psi\right\rangle_A \left|e\right\rangle_B = \left\langle\phi\right|_A \left\langle e\right|_B U^\dagger U \left|\psi\right\rangle_A \left|e\right\rangle_B \\ &= e^{-i(\alpha(\phi,e)-\alpha(\psi,e))} \left\langle\phi\right|_A \left\langle\phi\right|_B \left|\psi\right\rangle_A \left|\psi\right\rangle_B = e^{-i(\alpha(\phi,e)-\alpha(\psi,e))} \left\langle\phi\middle|\psi\right\rangle^2 \end{aligned} \tag{9}$$

Since the quantum state $\left|e\right\rangle$ is assumed to be normalized, then we get

$$\left|\left\langle\phi\middle|\psi\right\rangle\right|^2 = \left|\left\langle\phi\middle|\psi\right\rangle\right|, \tag{10}$$

This implies that either $\left|\left\langle\phi\middle|\psi\right\rangle\right| = 1$ or $\left|\left\langle\phi\middle|\psi\right\rangle\right| = 0$. Hence by the Cauchy–Schwarz inequality either

$\phi = e^{i\beta}\psi$ or ϕ is orthogonal to ψ. However, this cannot be the case for two arbitrary states. Therefore, a single universal U cannot clone a general quantum state. This proves the No-Cloning Theorem [33].

This theorem will have central importance in the development of the quantum stretching technique.

2.3. The avatars and the controlled quantum teleportation

In a recent work [30], it has been demonstrated in a theoretical and experimental way, that exactly in the middle of two entangled particles, which we will call originals and no matter how far away one is from the other, there are some reflexes, spectra, ghosts, shadows, projections, alter-egos or avatars that represent them entropically. In fact, the avatars are those that really communicate and each original will have its own avatar [30]. Since the distance between the avatars is zero, the length of the channel that lies between them will also be zero, therefore:

1. the avatars are mutually local to each other since they are together on a single point, and this is automatically equivalent to the non-locality of the originals (which coincides with the experimental results of the theorems of Bell [13] and CHSH [14]), i.e.:

   Non-locality of the originals ≡ *locality of the avatars*,

2. what a transmitter deposits at that point is perfect and exactly equal to what a receiver gets from that point, i.e., *what you put* at that point is equal to *what you get* from that point (WYPWYG), then, that channel has infinite bandwidth and null latency (anything that crosses it, will do it instantaneously). In the space of avatars, we are not talking about transmitting but about sharing information in that punctual channel,

3. there is no channel noise in a channel that does not exist, i.e., the link is robust [41],

4. a channel with infinite bandwidth and zero noise has an infinite channel capacity [41],

5. *it is impossible to attack, intercept or hack a channel that does not exist*, because it is impossible to attack the nothing,

6. there is no contradiction between Special Relativity and Quantum Mechanics because to instantly notify the result of a quantum measurement between entangled particles, a superluminal (or faster than light) speed is not necessary since the space to cross is zero. Therefore, Quantum Mechanics is automatically a complete theory. This disables the objections introduced by the EPR paradox [12] completely,

7. as a direct consequence of the previous item, we can deduce that all wormholes resulting from the entanglement between two black holes or a black hole and a white hole are traversable, because, what is it more traversable than something of zero length? This case implies two possibilities in relation to the mass of the avatars: a) they are particles without mass (massless), or b) they have immense masses and of opposite sign. We discard the first possibility because we know from Special Relativity that all massless particles must travel at the speed of light and the avatars are always fixed among the originals, therefore, the second option is correct, which implies antimatter and large volumes of energy, which are the ideal conditions to keep a wormhole open in a stable way,

8. the avatars act as a hinge between Special Relativity and Quantum Mechanics highlighting the relativistic nature of entanglement [30],

9. therefore, for entanglement, all the space is a point and all the time is an instant, for this reason, any technology that derives from it is a No-Channel technology, and

10. finally, everything said automatically leads to an instantaneous, robust and controlled version of quantum teleportation [30], which acts as a notary of the possibility of sending useful information instantaneously using a link based on entanglement [30]. Controlled quantum teleportation [30] exempts from the classic disambiguation channel needed in the original version of quantum teleportation [1] thus automatically raising the level of security and integrity of the information in the context of QKD [29] and the quantum internet [22-28]. Controlled quantum teleportation [30] will be developed in detail in Section 3.3.

Notwithstanding the foregoing, and in spite of all the advances presented in [30] and those developed in this work (i.e., the practicality of a technique that will help a quasi-replication and distribution from *1* to *N* of a qubit on the quantum Internet), the only problem of the redistribution of the EPR pairs at the end of each quantum teleportation (see Item 4, Section 1) tarnishes the achievements obtained thanks to the instantaneous quantum teleportation [30], always keeping in mind the possibility to take the quantum internet from Earth to Mars. However, if we see the positive side of the matter, if everything was resolved, then it would stop being interesting.

3. Quantum Stretching

In this section, we will present a complete description of this technique, as well as, a series of its most important applications, however, we will leave for Section 4 those applications particularly related to the quantum internet.

3.1. Stretched qubit or subit

Given a generic qubit in H_2 as that of Eq.(1)

$$|\psi\rangle = \alpha|0\rangle + \beta|1\rangle = \begin{bmatrix} \alpha \\ \beta \end{bmatrix}, \tag{11}$$

whose density matrix in $H_{2\times 2}$ is,

$$\rho_{|\psi\rangle} = |\psi\rangle\langle\psi^*| = \begin{bmatrix} \alpha \\ \beta \end{bmatrix}\begin{bmatrix} \alpha^* & \beta^* \end{bmatrix} = \begin{bmatrix} |\alpha|^2 & \alpha\beta^* \\ \beta\alpha^* & |\beta|^2 \end{bmatrix}, \tag{12}$$

where (•)* means complex conjugate of (•), thus, its stretched qubit or subit in H_4 is,

$$\|\psi\rangle = \alpha|00\rangle + \beta|11\rangle = \begin{bmatrix} \alpha \\ 0 \\ 0 \\ \beta \end{bmatrix}, \tag{13}$$

where $\|\psi\rangle$ means the subit of $|\psi\rangle$, and whose density matrix in $H_{4\times 4}$ is,

$$\rho_{\|\psi\rangle} = \|\psi\rangle\langle\psi^*\| = \begin{bmatrix} \alpha \\ 0 \\ 0 \\ \beta \end{bmatrix}\begin{bmatrix} \alpha^* & 0 & 0 & \beta^* \end{bmatrix} = \begin{bmatrix} |\alpha|^2 & 0 & 0 & \alpha\beta^* \\ 0 & 0 & 0 & 0 \\ 0 & 0 & 0 & 0 \\ \beta\alpha^* & 0 & 0 & |\beta|^2 \end{bmatrix}. \tag{14}$$

It is possible to obtain the subit of a subit with which the dimension of the subit is duplicated and therefore the dimension of its density matrix also is. In this case, we will have a subit in $H_{2^{k+1}}$ and its corresponding density matrix in $H_{2^{k+1}\times 2^{k+1}}$, where *k* represents the stretching degree.

As we can see, there is no loss of information in the subit in relation to the qubit from which the first one is derived, therefore, when we speak of quasi-copy via quantum stretching, in reality we refer basically to the subit losing the economy in size of the original qubit, which, as is logical, will be at least half the size of its corresponding subit. This has a direct impact on the dimension in the quantum internet host registries that use this technique to disseminate the same message to multiple destinations at the same time. However, given that the original idea is not to lose information in a broadcasting process of the same message on the quantum internet, then the attractiveness of this technique becomes evident. On the other hand, as the operator that takes us from the qubit to the corresponding subit must be reversible and unitary, then there must be an inverse and restoring process of the quantum stretching and that will be known as quantum shrinking, through which we pass from Eq.(13) to (11), i.e., thus recovering the original state.

Finally, and as we will see later, the resulting sparsity due to the zeros introduced by the technique does not complicate at all the implementations of quantum stretching on any quantum computing platform with cloud service, e.g., IBM Q [42] which is used in this work.

3.2. Quasi-Cloning Theorem

This theorem states that:

There is a unitary operator U acting on $\mathrm{H}_4^{A\cup B}=\mathrm{H}_2^A\otimes\mathrm{H}_2^B$ *in such a way that for all the normalized states* $|\psi\rangle_A$ *and* $|e\rangle_B$ *in* **H** *comply with* $U\left(|\psi\rangle_A|e\rangle_B\right)=e^{i\alpha(\psi,e)}\left[\|\psi\rangle_A,\|\psi\rangle_B\right]$ *for some real number* α *depending on* ψ *and* e.

To prove this theorem, an arbitrary pair of states $|\phi\rangle_A$ and $|\psi\rangle_A$ are selected in Hilbert's space **H**, then, since *U* is a unitary operator,

$$\begin{aligned}\langle\phi|\psi\rangle\langle e|e\rangle\equiv\langle\phi|_A\langle e|_B|\psi\rangle_A|e\rangle_B&=\langle\phi|_A\langle e|_B U^{\dagger}U|\psi\rangle_A|e\rangle_B\\&=e^{-i(\alpha(\phi,e)-\alpha(\psi,e))}\langle\phi\|_{A,B}\|\psi\rangle_{A,B}=e^{-i(\alpha(\phi,e)-\alpha(\psi,e))}\langle\phi\|\psi\rangle\end{aligned}\tag{15}$$

Since the quantum state $|e\rangle$ is assumed to be normalized, we thus get

$$\left|\langle\phi|\psi\rangle\right|=\left|\langle\phi\|\psi\rangle\right|,\tag{16}$$

being the case for two arbitrary states, such that if we resort to Eq.(11) and (13) and we recalculate for each case both terms of Eq.(16), we will have,

$$\left|\langle\phi|\psi\rangle\right|=\left|\begin{bmatrix}\alpha^*_{\langle\phi|} & \beta^*_{\langle\phi|}\end{bmatrix}\begin{bmatrix}\alpha_{|\psi\rangle}\\ \beta_{|\psi\rangle}\end{bmatrix}\right|=\left|\alpha^*_{\langle\phi|}\alpha_{|\psi\rangle}+\beta^*_{\langle\phi|}\beta_{|\psi\rangle}\right|\tag{17}$$

$$\left|\langle\phi\|\psi\rangle\right|=\left|\begin{bmatrix}\alpha^*_{\langle\phi|} & 0 & 0 & \beta^*_{\langle\phi|}\end{bmatrix}\begin{bmatrix}\alpha_{|\psi\rangle}\\ 0\\ 0\\ \beta_{|\psi\rangle}\end{bmatrix}\right|=\left|\alpha^*_{\langle\phi|}\alpha_{|\psi\rangle}+0+0+\beta^*_{\langle\phi|}\beta_{|\psi\rangle}\right|=\left|\alpha^*_{\langle\phi|}\alpha_{|\psi\rangle}+\beta^*_{\langle\phi|}\beta_{|\psi\rangle}\right|\tag{18}$$

Equal result of Eq.(17) and (18) proves the theorem. ■

The operator U will have two outputs, so the repetition, bilocation or splitting of the right side of the central equation of the theorem into two identical stretched elements, i.e., $\|\psi\rangle_A$ and $\|\psi\rangle_B$, will be,

$$U\left(|\psi\rangle_A|e\rangle_B\right)=e^{i\alpha(\psi,e)}\left[\|\psi\rangle_A,\|\psi\rangle_B\right] \tag{19}$$

Therefore, a single universal U can quasi-clone a general quantum state. This theorem represents, in itself, the centerpiece of the quantum stretching technique. It only remains to find an operator U and eventually another additional element that allows us to implement this technique in practice. Therefore, we are going to test an operator for two qubits widely used in practice, that is the *CNOT* gate, and an ancilla, that is, |0>, and we will replace them in Eq.(19) thanks to which we will obtain,

$$CNOT\left(|\psi\rangle_A|0\rangle_B\right)=\begin{bmatrix}1&0&0&0\\0&1&0&0\\0&0&0&1\\0&0&1&0\end{bmatrix}\left(\begin{bmatrix}\alpha\\\beta\end{bmatrix}\otimes\begin{bmatrix}1\\0\end{bmatrix}\right)=\begin{bmatrix}1&0&0&0\\0&1&0&0\\0&0&0&1\\0&0&1&0\end{bmatrix}\begin{bmatrix}\alpha\\0\\\beta\\0\end{bmatrix}=\begin{bmatrix}\alpha\\0\\0\\\beta\end{bmatrix}=\|\psi\rangle_{A,B} \tag{20}$$

The example of Eq.(20) shows that using a *CNOT* gate as the operator U and the ground state |0> instead of |*e*> perfectly satisfies the theorem and the requirements of the quantum stretching technique, therefore, we will use both from here on. In fact, we will perform a validation test of the elements involved in Eq.(20) thanks to the implementation on the IBM Q [42] platform, which allows us to choose between the following alternatives:

a) ibmqx4 in ibm-q/open/main: a Quantum Processing Unit (QPU) with 5 qubits,
b) ibmqx2 in ibm-q/open/main: a QPU with 5 qubits,
c) ibmq_16_melbourne in ibm-q/open/main: a QPU with 16 qubits, and
d) ibmq-qasm-simulator in ibm-q/open/main: a simulator, up to 32 qubits.

No other platform like this gives such an accurate notion of the dimension of the vectors involved. For this and other reasons, which we will explain throughout this section, we choose this platform, in particular, for all our implementations.

Let us start with the example of **Figure 2**, which consists in the generation of a simple qubit from a combination of gates of the type:

$$HTHT|0\rangle=\tfrac{1}{\sqrt{2}}\begin{bmatrix}1&1\\1&-1\end{bmatrix}\begin{bmatrix}1&0\\0&exp\left(\frac{i\pi}{4}\right)\end{bmatrix}\tfrac{1}{\sqrt{2}}\begin{bmatrix}1&1\\1&-1\end{bmatrix}\begin{bmatrix}1&0\\0&exp\left(\frac{i\pi}{4}\right)\end{bmatrix}\begin{bmatrix}1\\0\end{bmatrix} \tag{21}$$

Equation (21) results in what IBM Q calls statevector [(0.854+0.354j) (0.354-0.146j)]. This quantum circuit can be seen on the left of **Figure 2**. The height of the bar in the middle of **Figure 2** represents the complex modulus of the wavefunction, while the color of the bar is based on the complex argument or phase. The real part of the state is represented on the right of **Figure 2**, with 85.35534 % for |0> and 14.64466 % for |1>.

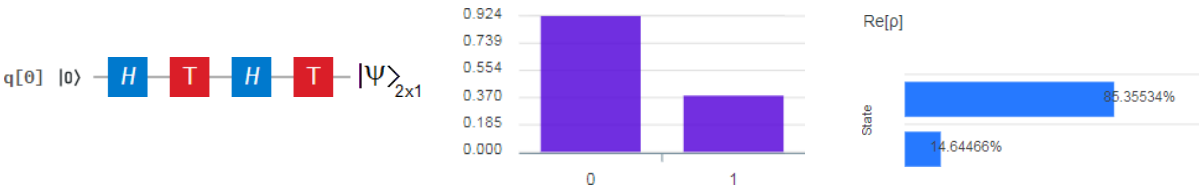

Figure 2 On the left is the quantum circuit for the qubit generation. In the middle, the height of the bar is the complex modulus of the wavefunction. Finally, on the right is the real part of the state.

The wavefunction will be,

$$|\psi\rangle = \begin{bmatrix} 0.9241 \\ 0.2706 + 0.2706\,j \end{bmatrix} \tag{22}$$

Then, resorting to Eq.(12), we will have the corresponding density matrix,

$$\rho_{|\psi\rangle} = \begin{bmatrix} 0.9241 \\ 0.2706 + 0.2706\,j \end{bmatrix} \begin{bmatrix} 0.9241 & 0.2706 - 0.2706\,j \end{bmatrix} = \begin{bmatrix} 0.854 & 0.25 + i0.25 \\ 0.25 - i0.25 & 0.146 \end{bmatrix}, \tag{23}$$

Figure 3 represents the complete density matrix of the wavefunction of Eq.(23): on the left, we have the real part, while, on the right, we dispose of the imaginary part. All these values obtained from **Figure 3** are absolutely consistent with those of **Figure 2**.

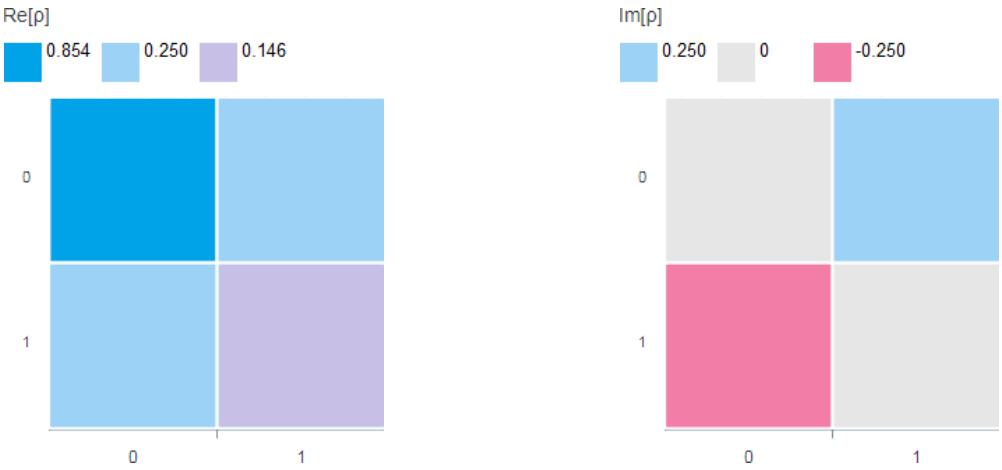

Figure 3 Wavefunction's density matrix: on the left, the real part, and on the right, the imaginary part.

Now, we will produce a quantum stretching based on the *CNOT* gate, that is, a quasi-copy without loss of information of the qubit generated in the previous example. The quantum circuit for this task is on the left side of **Figure 4**, which generates a replication and a one-dimensional stretching on the statevector of the previous example. Said stretching can be seen in **Figure 5**.

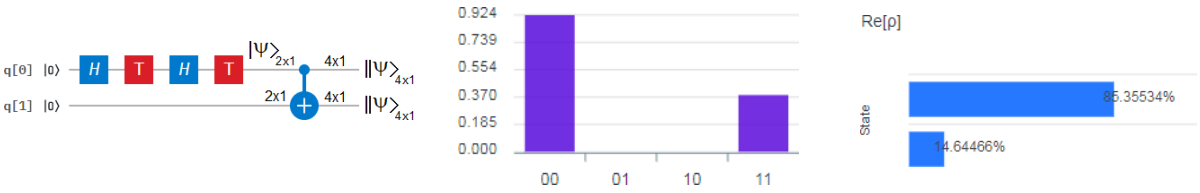

Figure 4 On the left is the quantum circuit for the qubit generation and *CNOT* gate which causes quasi-copy and stretching. In the middle, the height of the bar is the complex modulus of the wavefunction. Finally, on the right is the real part of the state.

We also see said stretching in the bar graph that is in the center of **Figure 4** representing the complex modulus of the wavefunction, with identical values to the previous example but clearly with horizontally separated bars, which constitutes the most conspicuous witness of the stretching. The real part of the state is represented on the right of **Figure 4** and is identical to that of **Figure 2**. Evidently, the stretching of the statevector is consistent with that of the wavefunction, as shown in **Figure 5** by the action of the *CNOT* gate. In this figure, we can see the statevector in the upper part and the

wavefunction in the lower part, where the subscript represents the size of wavefunction as a vector. Besides, we can clearly see both raise branches as a consequence of the *CNOT* gate action. That is, we have a replication (quasi-copy) with stretching and the conservation of information.

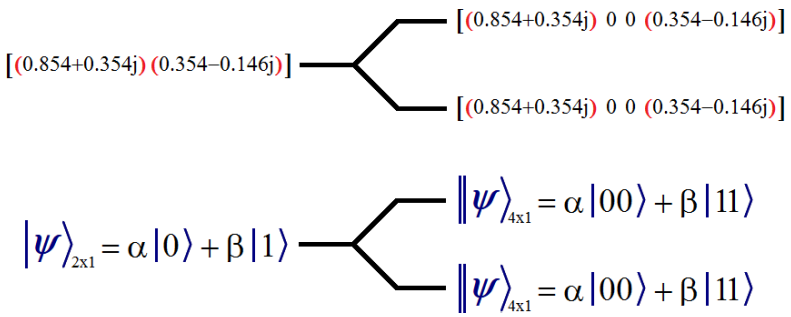

Figure 5 Stretching of statevector and wavefunction thanks to the action of *CNOT* gate.

Specifically, the stretched wavefunction will be,

$$\|\psi\rangle = \begin{bmatrix} 0.9241 \\ 0 \\ 0 \\ 0.2706 + 0.2706\,j \end{bmatrix} \tag{24}$$

in which stretching is evidenced if we compare it with that of Eq.(22). In fact, the stretching arises as a consequence of not violating the No-Cloning Theorem (NCT) [33], i.e., the wavefunction is stretched before violating the NCT.

Rule of inverse-of-the-sizes conservation: *before and after a stretching process the inverse of the sizes of the involved vectors must be conserved.*

Let us verify this rule with the example of **Figure 5**,

½ (*before CNOT*) = ¼ (*after CNOT, upper branch*) + ¼ (*after CNOT, lower branch*) (25)

Obviously, this rule is inexorably fulfilled in Eq.(25) and its application will be extremely useful in the verification of several types of configurations with many more ramifications.

On the other hand, from now on, and taking as an example the quantum circuit and the bars graph on the left and middle of **Figure 4**, respectively, the qubits q[0] (top line) and q[1] (bottom line) of the quantum circuit will be grouped as q[1]q[0] on the abscissa axis of the bar graph. That is, the qubit line that is lower in the quantum circuit corresponds to the qubit further to the left in the group of qubits that represents every value on the abscissa axis of the bar graph.

Obviously, stretching also occurs in the wavefunction density matrix in a two-dimensional way, then, resorting to Eq.(12), we will have the corresponding density matrix,

$$\rho_{\|\psi\rangle} = \begin{bmatrix} 0.9241 \\ 0 \\ 0 \\ 0.2706 + 0.2706\,j \end{bmatrix} \begin{bmatrix} 0.9241 & 0 & 0 & 0.2706 - 0.2706\,j \end{bmatrix} = \begin{bmatrix} 0.854 & 0 & 0 & 0.25 + i0.25 \\ 0 & 0 & 0 & 0 \\ 0 & 0 & 0 & 0 \\ 0.25 - i0.25 & 0 & 0 & 0.146 \end{bmatrix}. \tag{26}$$

This means that the wavefunction density matrix of **Figure 3** is two-dimensional stretched, resulting in the wavefunction density matrix of **Figure 6**, i.e., the same values but separated in two directions.

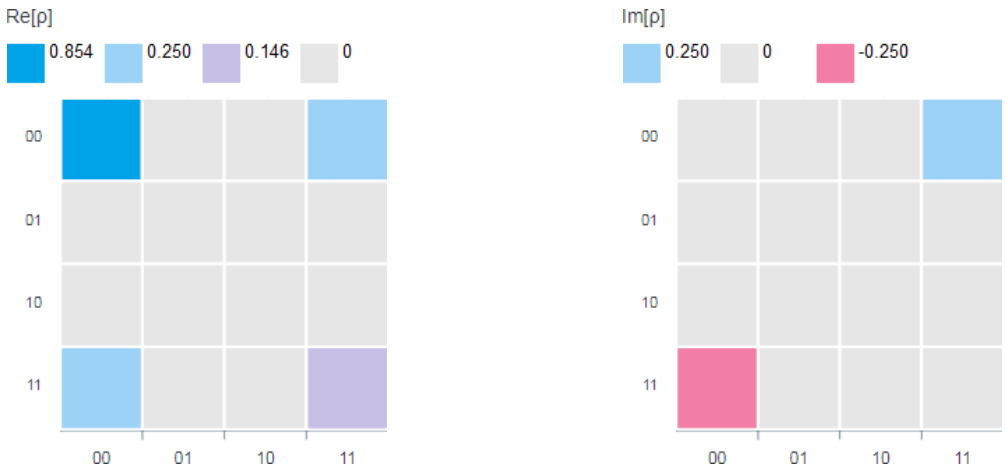

Figure 6 Wavefunction's density matrix: on the left, the real part, and on the right, the imaginary part.

Now, let us see a more complex example in which there is an important dimensional expansion based on a cascade of *CNOT* gates, as shown by the quantum circuit on the left of **Figure 7**. As a consequence of this, a statevector = [0.854+0.354j ←14-zeros→ 0.354-0.146j] arises, which will have a wavefunction,

$$\|\psi\rangle_{16\times1} = \begin{bmatrix} 0.9241 \\ \updownarrow 14\ zeros \\ 0.2706+0.2706\,j \end{bmatrix}. \tag{27}$$

Both statevector and wavefunction, also as a vector, will have a great level of sparsity: a big number of zeros inside them, between the elements of the original qubit stretched. This is the case of qubits, q[2] and q[3], on the right of the quantum circuit of **Figure 7** with 16 elements each. q[1] has 8 elements and q[0] has 4. Evidently, each quasi-copy becomes bigger and bigger, after each quantum stretching application, however, without loss of information.

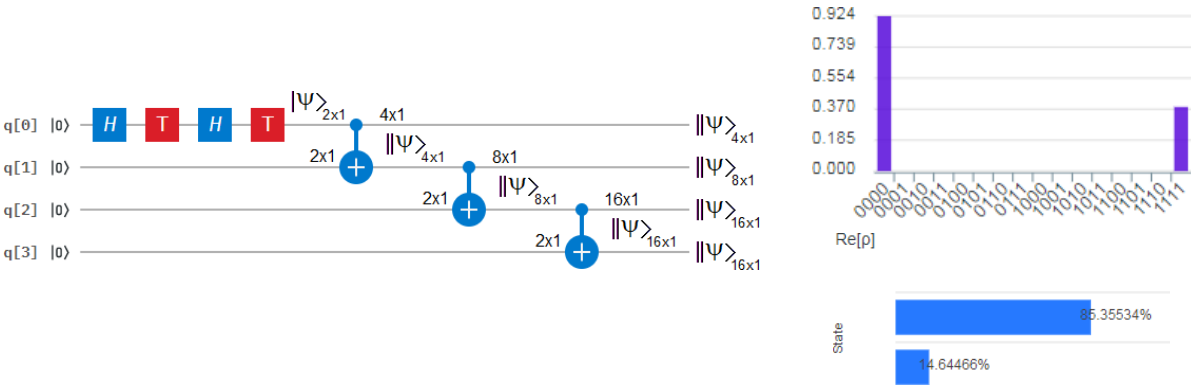

Figure 7 On the left is the quantum circuit for the qubit generation and the cascade of *CNOT* gates with four outcomes of different sizes. Before and after each *CNOT* gate we can see the size of the statevector and the wavefunctions as vectors. On the upper-right, the height of the bar is the complex modulus of the wavefunction. Finally, on the lower-right is the real part of the state.

The horizontal separation of the bars on the upper-right of **Figure 7** is clear evidence of the stretching process, which can be seen as a splitter procedure by octaves according to **Figure 8**,

1/2 (*before first CNOT*) = **1/4** (*after first CNOT, top branch*) + **1/8** (*after second CNOT, top branch*) + **1/16** (*after third CNOT, top branch*) + **1/16** (*after third CNOT, bottom branch*) (28)

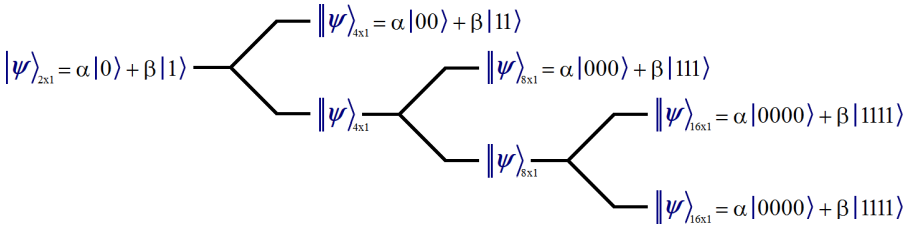

Figure 8 Stretching of the wavefunction by the action of a *CNOT* gate cascade.

Equation (28) represents an unequivocal verification of the rule of inverse-of-the-sizes conservation for the example of **Figure 7**. Finally, **Figure 9** shows us the wavefunction's density matrix, which shows a marked two-dimensional stretch compared to the two previous cases of **Figures 3** and **6**, however, without loss of information.

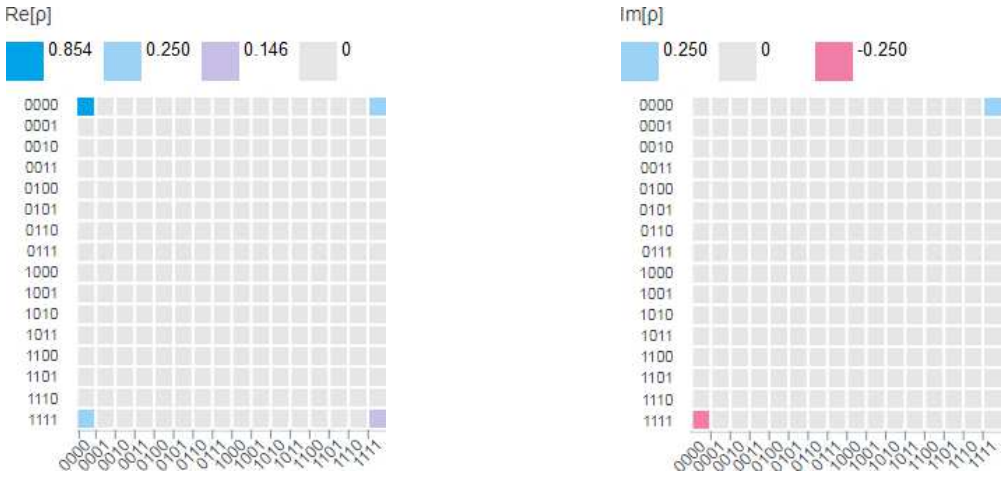

Figure 9 Wavefunction's density matrix: on the left, the real part, and on the right, the imaginary part.

Without any doubt, the most conspicuous case is represented by the state

$$|+\rangle = H|0\rangle = \frac{1}{\sqrt{2}}\begin{bmatrix}1 & 1\\ 1 & -1\end{bmatrix}\begin{bmatrix}1\\ 0\end{bmatrix} = \begin{bmatrix}\frac{1}{\sqrt{2}}\\ \frac{1}{\sqrt{2}}\end{bmatrix}, \tag{29}$$

where qubit $|+\rangle$ becomes $|\beta_{00}\rangle$ of Eq.(8) with a quantum stretching, i.e., $|\beta_{00}\rangle = \|+\rangle$. But, first, we start with the implementation of qubit $|+\rangle$ of Eq.(29) shown in **Figure 10**. On the left of this figure, we have the quantum circuit of Eq.(29). The bar graph in the middle of **Figure 10** shows the complex modulus of the wavefunction = [0.707 0.707] which, in this particular case, exactly coincides with the statevector. On the right of **Figure 10**, we have the real part of the state.

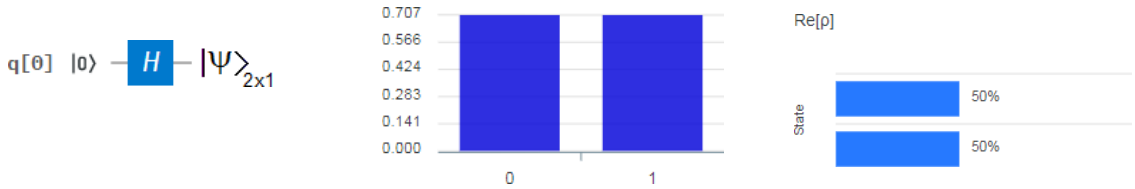

Figure 10 On the left is the quantum circuit for the qubit generation thanks to a Hadamard's gate. In the middle, the height of the bar is the complex modulus of the wavefunction, which, in this case, coincides with the wavefunction itself. Finally, on the right is the real part of the state.

Since in this case, the wavefunction is identical to the statevector (due to both elements of the wavefunction are real numbers), then, the wavefunction's density matrix will be that of **Figure 11**.

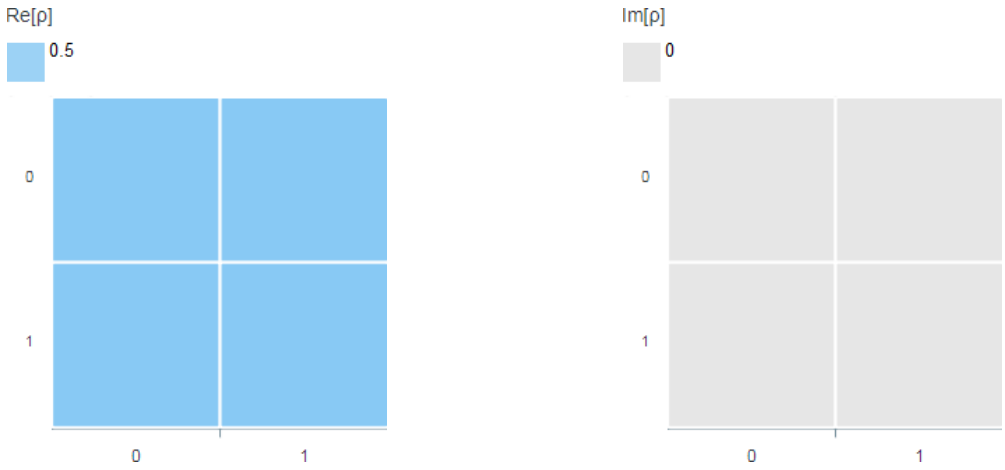

Figure 11 Wavefunction's density matrix: on the left, the real part, and on the right, the imaginary part.

If now, we perform stretching to the qubit of Eq.(29), it will result in a statevector and wavefunction equal to [0.707 0 0 0.707] thanks to the quantum circuit on the left of **Figure 12**. The bar graph in the middle of the figure is identical to that of **Figure 10** but clearly and horizontally separated, which evidences the action of the stretching process.

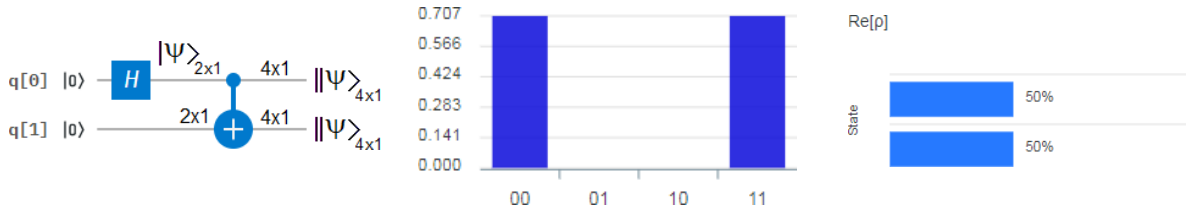

Figure 12 The quantum circuit for the qubit generation and *CNOT* gate which causes quasi-copy and stretching is on the left. In the middle, the height of the bar is the complex modulus of the wavefunction, which, in this case, also coincides with the wavefunction itself. Finally, the real part of the state is on the right.

A two-dimensional stretching occurs between the wavefunction's density matrix of **Figures 11** and **13**. Evidently, it is the same graph where the light blue squares are separated between them.

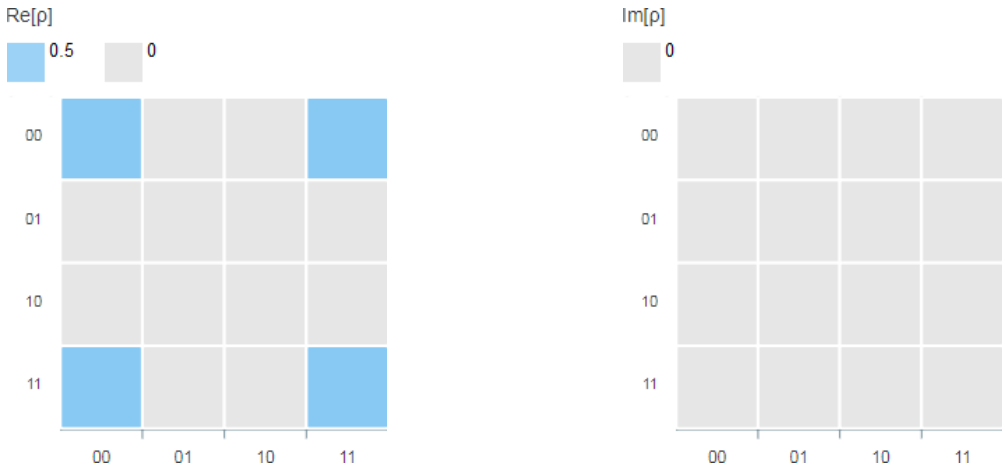

Figure 13 Wavefunction's density matrix: on the left, the real part, and on the right, the imaginary part.

All these examples contribute in a clear way to the verification of the Quasi-Cloning Theorem. On the other hand, it is also evident that when the two theorems, i.e., the Quasi-Cloning Theorem and the No-Cloning Theorem, are brought together, some conclusions immediately emerge:

1) it is **impossible** to copy an arbitrary **qubit**,
2) it is **possible** to quasi-copy an arbitrary **qubit**,
3) it is **possible** to copy an arbitrary **subit**, in fact, the stretching process itself generates a couple,
4) it is **possible** to quasi-copy an arbitrary **subit**.

On the other hand, the literature says that the Computational Basis States (CBS), i.e., {|0>, |1>} can be copied and compared [43], but, why that rare privilege? The answer is separability [32, 34-36], i.e., the ability to factorize a vector in its two or more constitutive vectors. If in Eq.(20), we replace $|\psi\rangle$ with |0> and then with |1>, then we will have,

$$CNOT\left(|0\rangle_A|0\rangle_B\right)=\begin{bmatrix}1&0&0&0\\0&1&0&0\\0&0&0&1\\0&0&1&0\end{bmatrix}\left(\begin{bmatrix}1\\0\end{bmatrix}\otimes\begin{bmatrix}1\\0\end{bmatrix}\right)=\begin{bmatrix}1&0&0&0\\0&1&0&0\\0&0&0&1\\0&0&1&0\end{bmatrix}\begin{bmatrix}1\\0\\0\\0\end{bmatrix}=\begin{bmatrix}1\\0\\0\\0\end{bmatrix}=|00\rangle=|0\rangle|0\rangle, \quad (30a)$$

$$CNOT\left(|1\rangle_A|0\rangle_B\right)=\begin{bmatrix}1&0&0&0\\0&1&0&0\\0&0&0&1\\0&0&1&0\end{bmatrix}\left(\begin{bmatrix}0\\1\end{bmatrix}\otimes\begin{bmatrix}1\\0\end{bmatrix}\right)=\begin{bmatrix}1&0&0&0\\0&1&0&0\\0&0&0&1\\0&0&1&0\end{bmatrix}\begin{bmatrix}0\\0\\1\\0\end{bmatrix}=\begin{bmatrix}0\\0\\0\\1\end{bmatrix}=|11\rangle=|1\rangle|1\rangle. \quad (30b)$$

As we can see from Eq.(30), there is a stretching of the CBS where the results are two vectors of 4x1 and each can be factored into two identical vectors of 2x1 each, that is, each resulting vector can be separated into two identical subvectors of the half of its size. In other words, it is because of separability that the quasi-copy and copy coincide for the CBS case. This is because the CBS are a particular type of qubits on the Bloch's sphere in which the wavefunction (see Eq.1) only has one of its components (i.e., α or β) different to zero, in this case, equal to 1. This simple fact activates the separability, allowing the factorization. Finally, the CBS are the only exception to the No-Cloning Theorems, thanks to separability, and that we have verified thanks to quantum stretching.

3.3. Drawing some conclusions

By focusing on the Eq.(19), we will have

$$U\left(|\psi\rangle_{2x1}|a\rangle_{2x1}\right)=\left[\|\psi\rangle_{4x1},\|\psi\rangle_{4x1}\right] \quad (31)$$

where $|a\rangle$ is the ancilla. In this case, we have a quantum stretching based on a universal *U* operator with and without separability, therefore, we will have a quasi-copy with 2 stretched wavefuncions with a size equal to 2 in respect to the original. Specifically, if we replace the operator *U* by the *CNOT* gate and the generic ancilla $|a\rangle$ by the ground state $|0\rangle$, yields

$$CNOT\left(|\psi\rangle_{2x1}|0\rangle_{2x1}\right)=\left[\|\psi\rangle_{4x1},\|\psi\rangle_{4x1}\right]=\left[\alpha|00\rangle_{4x1}+\beta|11\rangle_{4x1},\alpha|00\rangle_{4x1}+\beta|11\rangle_{4x1}\right], \quad (32)$$

which represents a case like the example in **Figure 4**. Now, if we turn to the example of **Figure 12** which results from the state |+> of **Figure 10**, we will have,

$$CNOT\left(|+\rangle_{2x1}|0\rangle_{2x1}\right)=\left[\|+\rangle_{4x1},\|+\rangle_{4x1}\right]=\left[|\beta_{00}\rangle_{4x1},|\beta_{00}\rangle_{4x1}\right]$$
$$=\left[{}^{1}\!/\!_{\sqrt{2}}|00\rangle_{4x1}+{}^{1}\!/\!_{\sqrt{2}}|11\rangle_{4x1},{}^{1}\!/\!_{\sqrt{2}}|00\rangle_{4x1}+{}^{1}\!/\!_{\sqrt{2}}|11\rangle_{4x1}\right], \quad (33)$$

which is the typical case of generating an EPR pair from a state |+>. If we now compare Eq.(32) with Eq.(33), we see that in Eq.(33), $\alpha=\beta={}^{1}\!/\!_{\sqrt{2}}$. Taking into account the condition seen in Subsection 2.1 which states that $|\alpha|^2+|\beta|^2=1$, therefore, Eq.(32) will be equivalent to:

$$\left[\alpha|00\rangle+\beta|11\rangle,\alpha|00\rangle+\beta|11\rangle\right]=\left[\eta|00\rangle+e^{i\phi}\sqrt{1-|\eta|^2}\,|11\rangle,\eta|00\rangle+e^{i\phi}\sqrt{1-|\eta|^2}\,|11\rangle\right], \quad (34)$$

with $\alpha=\eta$ and ϕ can be seen in **Figure 1** on the Bloch's sphere. The result of Eq.(34) tells us that Eq.(33) represents the case maximally entangled, while Eq.(32) represents a generic not maximally entangled case. In other words, what these equations show is that quantum entanglement is part of a broader process: quantum stretching, therefore, *quantum entanglement is a particular case of quantum stretching*. In Subsection 4.2, this affirmation will be put to the test.

Finally, and for the sole purpose of analyzing the dimensional aspect of Eq.(30), we repeat it below,

$$CNOT\left(|0\rangle_{2x1}|0\rangle_{2x1}\right)=\left[|0\rangle_{2x1},|0\rangle_{2x1}\right]=|00\rangle_{4x1}=|0\rangle_{2x1}|0\rangle_{2x1}, \quad (35a)$$

$$CNOT\left(|1\rangle_{2x1}|0\rangle_{2x1}\right)=\left[|1\rangle_{2x1},|1\rangle_{2x1}\right]=|11\rangle_{4x1}=|1\rangle_{2x1}|1\rangle_{2x1}, \quad (35b)$$

As we can see from Eq.(35), there is stretching and separability, therefore, in addition to the doubling in the size of the outcomes with quasi-copy, we will also have copy.

3.4. Relevant cases

In this subsection, we will show the most conspicuous examples that will allow us to understand in which cases quantum stretching occurs and in which cases it is canceled.

Case 1:

Although it seems simple, the case of **Figure 14** gives us a lot of information about how IBM Q [42] presents the outcomes from a set of tools typically used in Quantum Information Processing [32]. Unlike the case of **Figure 2**, the thread belonging to the qubit q[1] in the quantum circuit to the left of **Figure 14** modifies the bar graph as can be seen by comparing the central graphics of **Figures 2** and **14**. In this case, the statevector is $\left[(0.854+0.354j)\quad(0.354-0.146j)\quad 0\quad 0\right]^T=|0\rangle|\psi\rangle$, where $(\bullet)^T$ means transpose of (•), and although this seems to be a case of stretching with respect to the case of **Figure 2**, its two components (i.e., $|0\rangle$ and $|\psi\rangle$) are separable, due to both branches are independents.

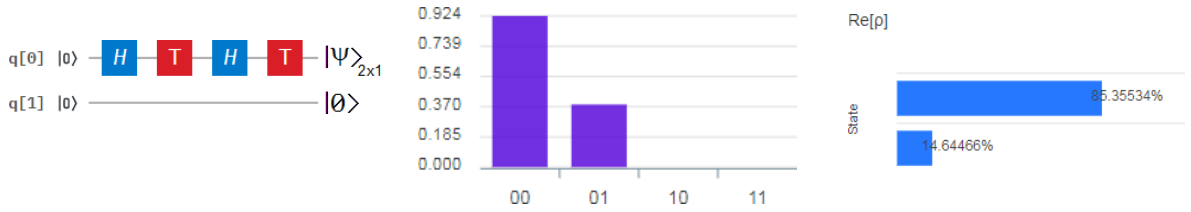

Figure 14 On the left is the quantum circuit for the qubit generation in q[0] and an additional alone line from q[1] = |0>. In the middle, the height of the bar is the complex modulus of the wavefunction, which, in this case, also coincides with the wavefunction itself. Finally, on the right is the real part of the state.

Figure 14 is completed with the real part of the state. **Figure 15** shows the real and imaginary parts of the wavefunction's density matrix, which allows us to appreciate the two-dimensional expansion of the configuration of **Figure 3** without stretching and therefore quasi-copies.

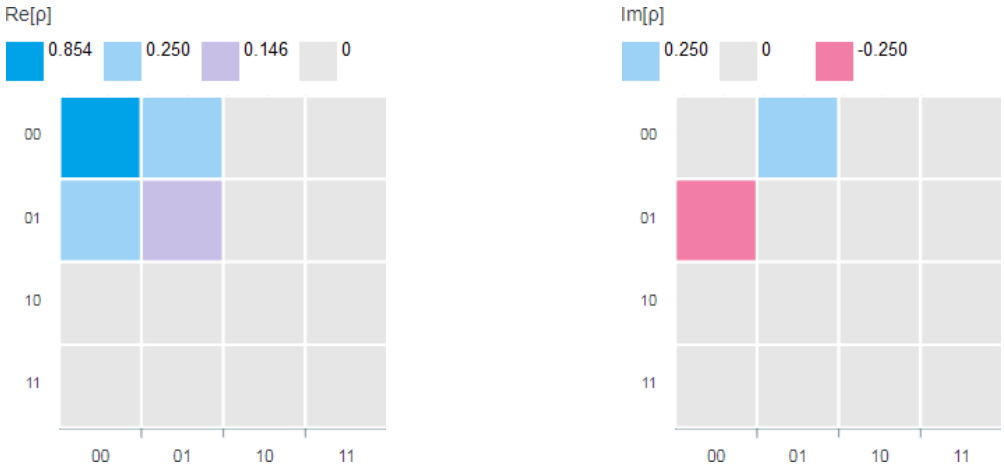

Figure 15 Wavefunction's density matrix: on the left, the real part, and on the right, the imaginary part.

Case 2:

This case is represented in **Figure 4**, where we could see a stretching without separability and with a statevector as in $\left[(0.854+0.354j)\quad 0\quad 0\quad (0.354-0.146j)\right]^T = CNOT\left(|\psi\rangle|0\rangle\right)$. This example represents a typical case of quantum stretching.

Case 3:

This configuration yields a result similar to ***Case 1***, i.e., there is no stretching or quasi-copy, instead $|0\rangle$ and $|\psi\rangle$ are separable, being the statevector: $\left[(0.854+0.354j)\quad (0.354-0.146j)\quad 0\quad 0\right]^T = |0\rangle|\psi\rangle$.

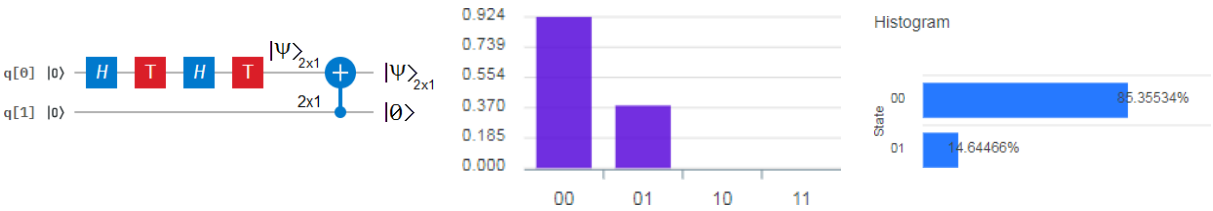

Figure 16 On the left is the quantum circuit for the qubit generation and a *CNOT* gate from q[1] to q[0]. In the middle, the height of the bar is the complex modulus of the wavefunction, which, in this case, also coincides with the wavefunction itself. On the right is the real part of the state (histogram o measurement probabilities).

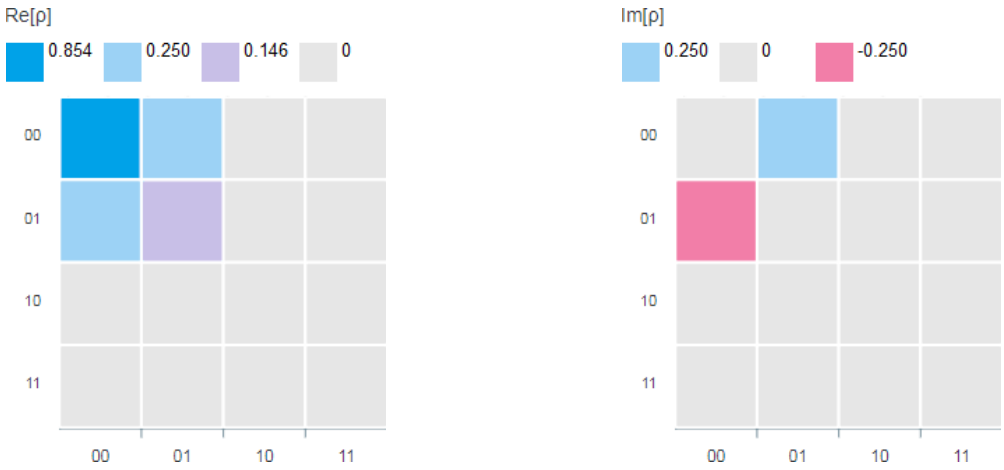

Figure 17 Wavefunction's density matrix: on the left, the real part, and on the right, the imaginary part.

Figure 16 shows on the left the quantum circuit with a simple variant, where, unlike the previous case, the *CNOT* gate is upside-down. However, this apparent insignificant change modifies everything, because this fact cancels stretching and then, separability acts directly. Therefore, the rest of **Figure 16** and the complete **Figure 17** are similar to those of ***Case 1***.

Case 4:

This is another case similar to 1 and 3. The results are based on the fact that the operator U of the Quasi-Cloning Theorem, Eq.(19), must be unitary and reversible, as the *CNOT* gate, actually, is. Therefore, if we start from the original state of **Figure 2**, $\left[(0.854+0.354j)\quad(0.354-0.146j)\right]^T=|\psi\rangle$, and then we apply the *CNOT* gate twice as indicated by the top-left graph of **Figure 18**, we obtain the last state vector $\left[(0.854+0.354j)\quad(0.354-0.146j)\quad 0\quad 0\right]^T=|0\rangle|\psi\rangle$ without stretching and therefore quasi-copies, being $|0\rangle$ and $|\psi\rangle$ separable, i.e., it is like if both *CNOT* did not exist. In short, we have $|\psi\rangle$ in the upper branch (i.e., the thread of q[0]) and $|0\rangle$ in the lower branch (i.e., the thread of q[1]).

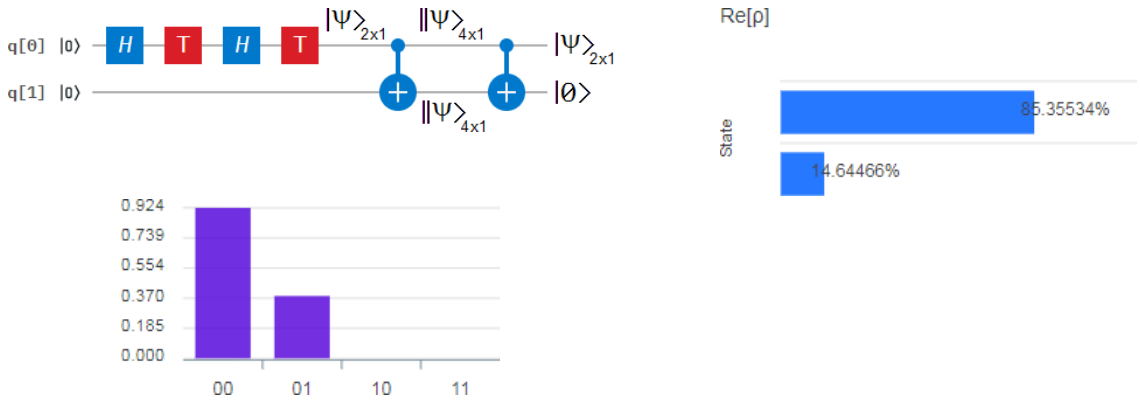

Figure 18 On the top-left is the quantum circuit for the qubit generation and the cascade of two *CNOT* gates with two outcomes: the original state and the ground state. Before and after each *CNOT* gate we can see the size of the statevector and the wavefunctions as vectors. On the bottom-left, the height of the bar is the complex modulus of the wavefunction. Finally, on the right is the real part of the state.

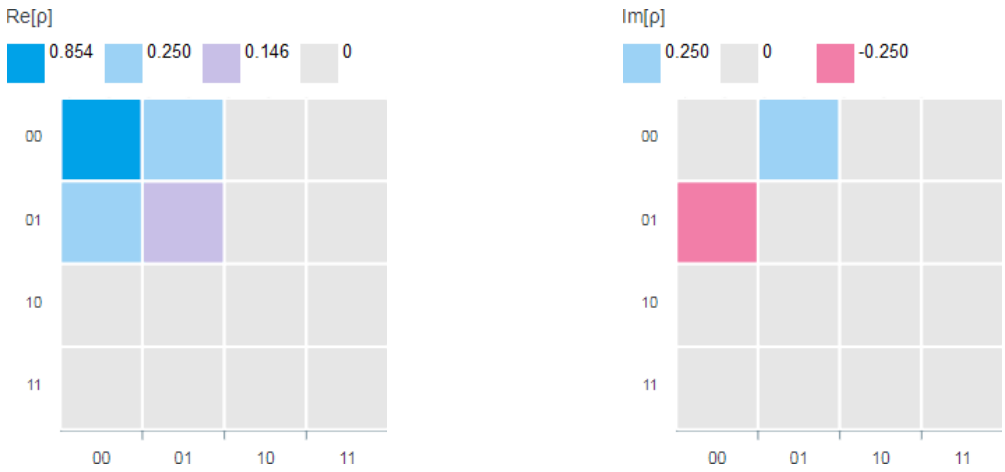

Figure 19 Wavefunction's density matrix: on the left, the real part, and on the right, the imaginary part.

Finally, the set of graphics of **Figures 18** and **19** is composed of those of ***Cases* 1** and **3** with exactly the same outcomes.

Cases 5, 6 and 7:

These three cases are generated by alternating *CNOT* gates in a direct and upside-down way, thus we obtain three versions of the so-called *SWAP* gates. These three versions can be seen on the left of **Figure 20** and give rise to a statevector: $\left[(0.854+0.354j)\quad 0\quad (0.354-0.146j)\quad 0\right]^T=|\psi\rangle|0\rangle$, which does not register stretching, being the two constituent qubits of the statevector (i.e., $|0\rangle$ and $|\psi\rangle$) separable. **Figure 20** is completed with a bar graph and the real part of the histogram or the measurement probabilities. **Figure 21** shows the complete wavefunction's density matrix for this experiment.

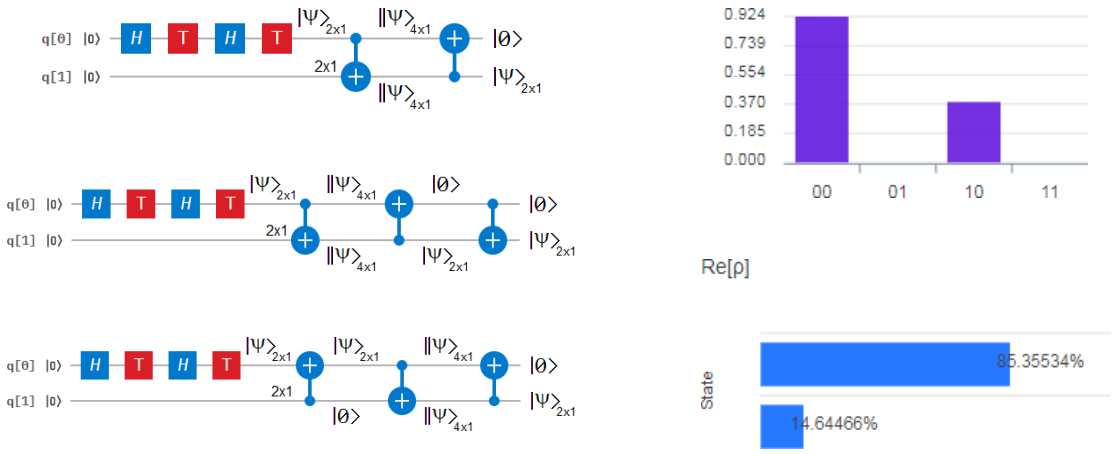

Figure 20 On the left are three quantum circuit to provoke a *SWAP* action. On the top-right, the height of the bar is the complex modulus of the wavefunction, which, in this case, also coincides with the wavefunction itself. Finally, on the bottom-right is the real part of the state.

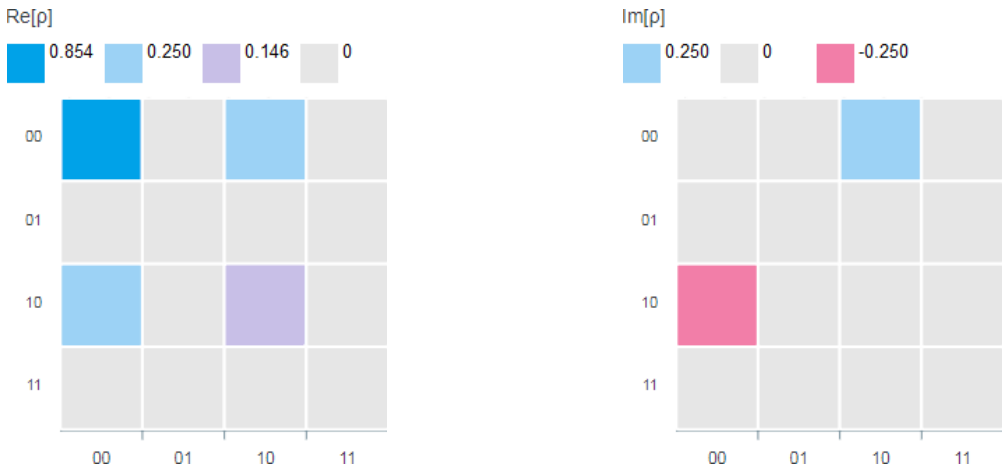

Figure 21 Wavefunction's density matrix: on the left, the real part, and on the right, the imaginary part.

Case 8:

Although this case, prima facie, could seem similar to the previous ones (i.e., **5**, **6**, and **7**), it is noticeably different, given that in this case there is stretching without separability of the qubits involved, i.e., $|0\rangle$ and $|\psi\rangle$, with a statevector $\left[(0.854+0.354j)\quad 0\quad 0\quad (0.354-0.146j)\right]^T=CNOT\left(|\psi\rangle|0\rangle\right)$ being similar to **Case 2** and **Figure 4**. **Figure 22** shows this configuration, which begins with an upside-down *CNOT* gate and finishes with another one but applied in a direct way. The rest of **Figure 22** as well as the complete **Figure 23** are identical to those of ***Case 2***.

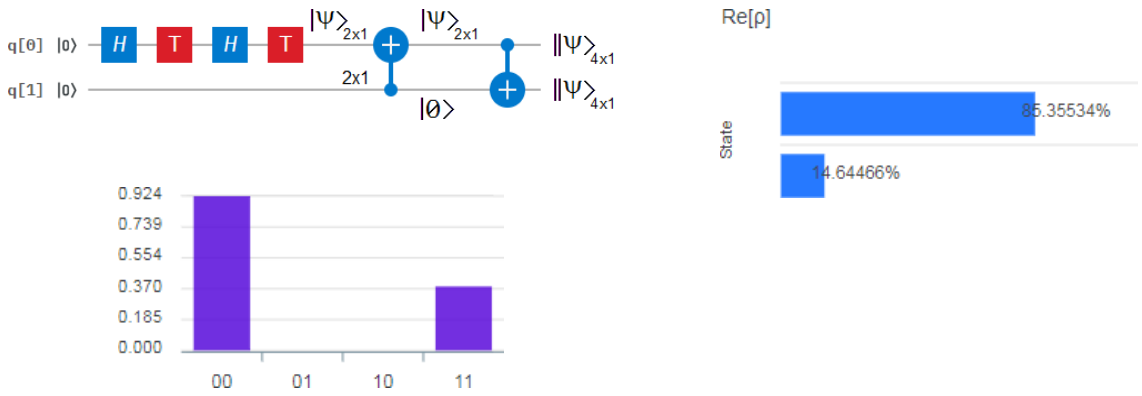

Figure 22 On the top-left is the quantum circuit for the qubit generation and the cascade of two *CNOT* gates in opposition with two outcomes: both stretched. Before and after each *CNOT* gate we can see the size of the statevector and the wavefunctions as vectors. On the bottom-left, the height of the bar is the complex modulus of the wavefunction. Finally, on the right is the real part of the state.

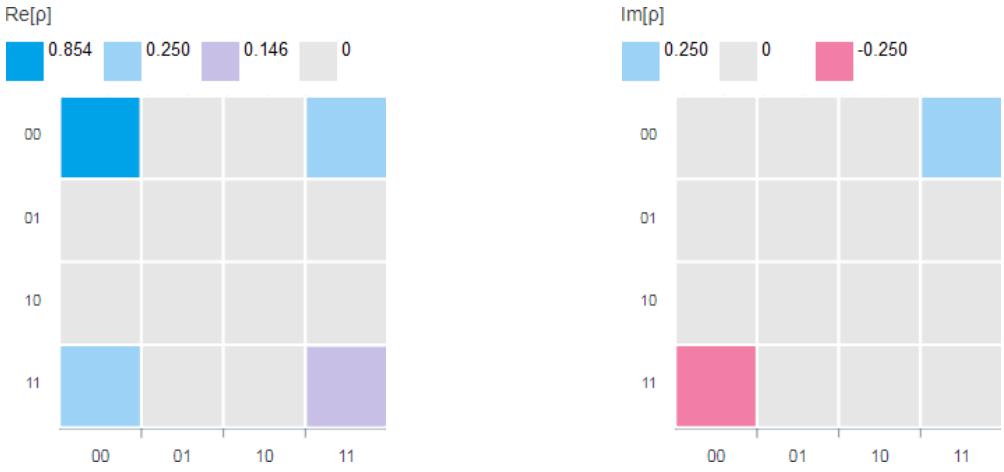

Figure 23 Wavefunction's density matrix: on the left, the real part, and on the right, the imaginary part.

3.5. Multiple entanglements

Although within the arsenal of Quantum Information Processing [32, 39, 40] we have configurations of type GHZ (Greenberger–Horne–Zeilinger) and W [34], only GHZ_2 (which we have used as an EPR pair so far) has a practical purpose in quantum teleportation, and therefore, in quantum networking for the quantum internet [22-28], the rest: GHZ_3, GHZ_4, or GHZ_N are not useful to make a distribution of the same message without violating the No-Cloning Theorem [33]. Therefore, we will analyze multiple entanglement alternatives based on quantum stretching.

Case 1:

This is the case of **Figure 12** based on the state $|+\rangle$ of **Figure 10**. It has stretching with quasi-copy, i.e., two identical nonseparable states like $CNOT(|+\rangle|0\rangle) = [1/\sqrt{2} \quad 0 \quad 0 \quad 1/\sqrt{2}]^T \sim [0.707 \quad 0 \quad 0 \quad 0.707]^T$.

Case 2:

This case corresponds to the configuration of **Figure 24**, in which the incorporation of a second *CNOT* gate deepens the stretching by generating one statevector $[0.707 \; 0 \; 0 \; 0.707]^T$ and two statevectors $[0.707 \quad 0 \quad 0 \quad 0 \quad 0 \quad 0 \quad 0 \quad 0.707]^T$ where all the resulting states continue to be non-separable.

The rest of **Figure 24** as well as **Figure 25** show characteristics of an entanglement presence. In this case, we can also verify the fulfillment of the *rule of inverse-of-the-sizes conservation*:

1/2 (*before first CNOT*) = **1/4** (*after first CNOT, top branch*) + **1/8** (*after second CNOT, middle branch*)
+ **1/8** (*after second CNOT, bottom branch*), (36)

which can be observed in **Figure 26**, where the stretched outcomes ($\|\psi\rangle_{4\times1}$, $\|\psi\rangle_{8\times1}$, $\|\psi\rangle_{8\times1}$) do not lose information regarding the original wavefunction $|\psi\rangle_{2\times1}$, simply, they only increase in size.

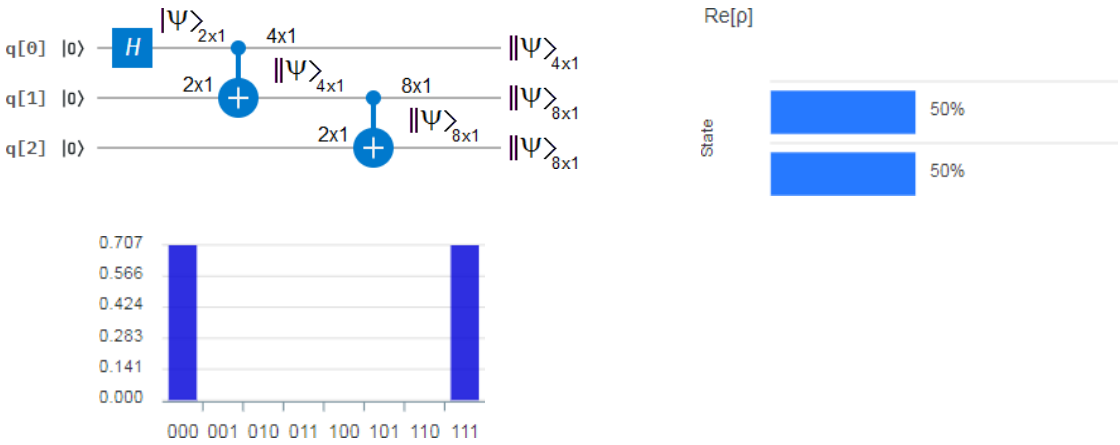

Figure 24 On the top-left is the quantum circuit for multiple entanglement generation thanks to two *CNOT* gates in cascade which produces three wavefunctions. Before and after each *CNOT* gate we can see the size of the statevector and the wavefunctions as vectors. On the bottom-left, the height of the bar is the complex modulus of the wavefunction. Finally, on the right is the real part of the state.

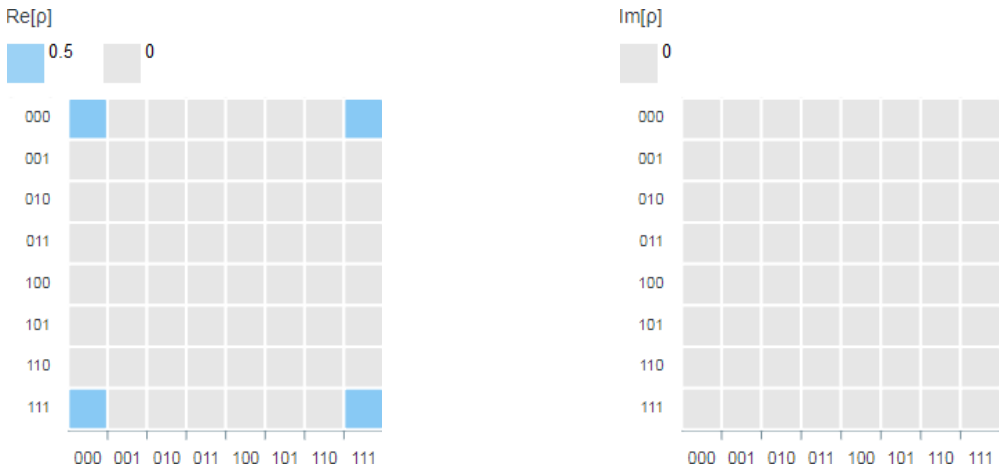

Figure 25 Wavefunction's density matrix: on the left, the real part, and on the right, the imaginary part.

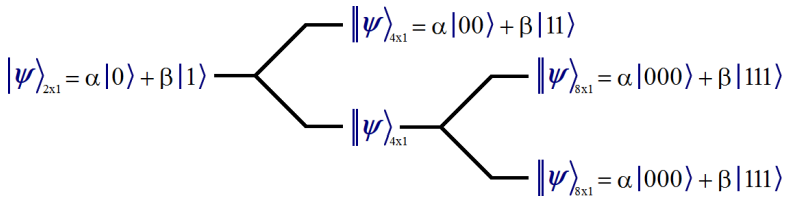

Figure 26 Stretching of the wavefunction by the action of a cascade of *CNOT* gates.

Case 3:

In this case, a third *CNOT* gate is added according to **Figure 27**, obtaining the following four outcomes:

$$\left\|\psi\right\rangle_{4\times1} = 0.707\left|00\right\rangle + 0.707\left|11\right\rangle = \left|\beta_{00}\right\rangle \tag{37a}$$

$$\left\|\psi\right\rangle_{8\times1} = 0.707\left|000\right\rangle + 0.707\left|111\right\rangle \tag{37b}$$

$$\left\|\psi\right\rangle_{16\times1} = 0.707\left|0000\right\rangle + 0.707\left|1111\right\rangle (\times 2) \tag{37c}$$

All the elements of the Eq.(37) are the result of a stretching and the four outcomes are non-separable. Obviously, in this experiment the *rule of inverse-of-the-sizes conservation* is also fulfilled:

1/2 (*before first CNOT*) = **1/4** (*after first CNOT, q[0]*) + **1/8** (*after second CNOT, q[1]*)
+ **1/16** (*after third CNOT, q[2]*) + **1/16** (*after third CNOT, q[3]*) (38)

The metrics exposed in **Figure 27** show typical characteristics of an entanglement presence although with additional stretching. We can make identical considerations of an additional two-dimensional stretching process present in the wavefunction's density matrix of **Figure 28**.

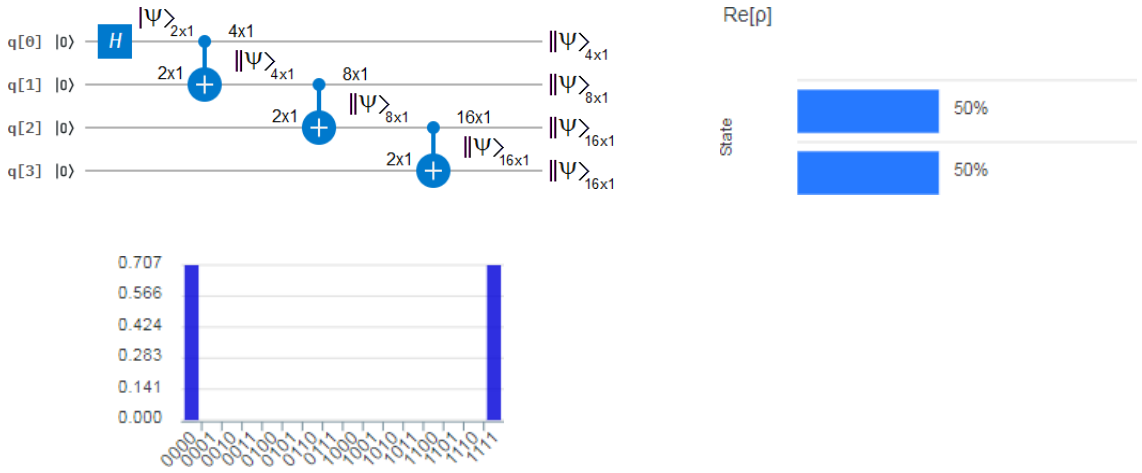

Figure 27 On the top-left is the quantum circuit for a multiple entanglement generation thanks to three *CNOT* gates in cascade, which produces four wavefunctions. Before and after each *CNOT* gate, we can see the size of the statevector and the wavefunctions as vectors. On the bottom-left, the height of the bar is the complex modulus of the wavefunction. Finally, on the right is the real part of the state.

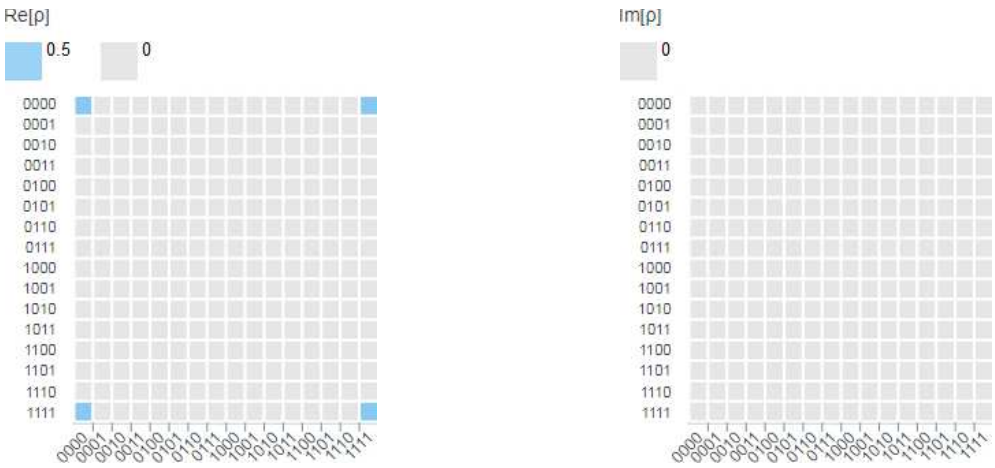

Figure 28 Wavefunction's density matrix: on the left, the real part, and on the right, the imaginary part.

4. Copying messages on the quantum internet

The copying of messages, that is, the dissemination, broadcasting or simultaneous distribution of the same qubits to multiple destinations without violating the No-Cloning Theorem is one of the problems that has most delayed the development and implementation of the quantum internet because of its dissemination to long distances, in particular, we refer to the colossal task of bringing this version of the Internet from Earth to Mars. Therefore, using everything seen so far in this work, we will try solutions to amend this serious problem.

4.1. Quantum Stretching and Teleportation

4.1.1. Theoretical focusing

Figure 29 represents the original version of quantum teleportation of Bennett *et al* [1] which put in a much broader and more exhaustive context is known as uncontrolled quantum teleportation [1-5]. We will present a procedural version of this protocol for a better understanding of it.

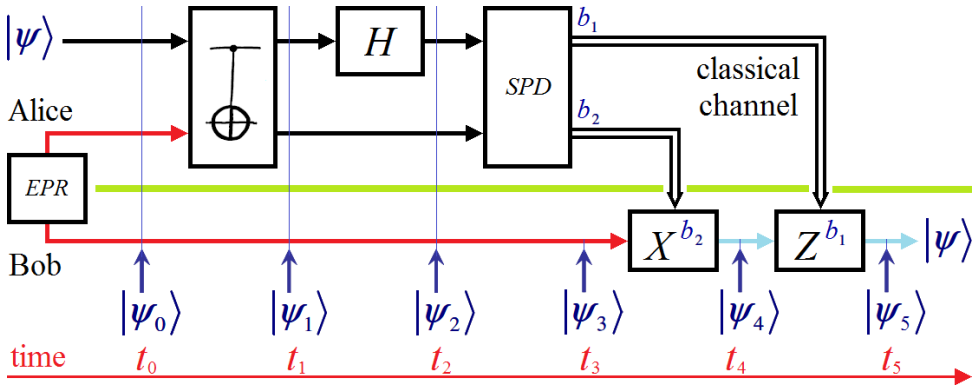

Figure 29 Uncontrolled (original) quantum teleportation. EPR means EPR pair generation procedure, *X* and *Z* are the corresponding Pauli's matrices, *H* is a Hadamard's gate, SPD is the *single-photon detector* module, while, b_1 and b_2 are the classical bits of disambiguation that travel via the classical channel from Alice to Bob.

An EPR pair like that of Eq.(8), i.e., $|\beta_{00}\rangle = |\Phi^+\rangle$, is distributed between Alice and Bob.

1) In t_0, Alice gets an arbitrary and unknown state to be teleported $|\psi\rangle$ like the one of Eq.(1) and (11). Before the *CNOT* gate, $|\psi\rangle$ and $|\beta_{00}\rangle$ are involved in a Kronecker's product between them, thus obtaining a 3-partite state result,

$$\begin{aligned}|\psi_0\rangle &= |\psi\rangle \otimes |\beta_{00}\rangle = |\psi\rangle|\beta_{00}\rangle = (\alpha|0\rangle + \beta|1\rangle)\,{}^{1}\!/_{\sqrt{2}}(|00\rangle + |11\rangle) \\ &= {}^{1}\!/_{\sqrt{2}}\left[\alpha|0\rangle(|00\rangle + |11\rangle) + \beta|1\rangle(|00\rangle + |11\rangle)\right] = {}^{1}\!/_{\sqrt{2}}\left[\alpha|000\rangle + \alpha|011\rangle + \beta|100\rangle + \beta|111\rangle\right] \\ &= \left[{}^{\alpha}\!/_{\sqrt{2}} \quad {}^{\beta}\!/_{\sqrt{2}} \quad 0 \quad 0 \quad 0 \quad 0 \quad {}^{\alpha}\!/_{\sqrt{2}} \quad {}^{\beta}\!/_{\sqrt{2}}\right]^T\end{aligned} \tag{39}$$

2) In t_1, Alice gets the result of applying a *CNOT* gate on $|\psi_0\rangle$, being this gate the first module of the Bell State Measurement (BSM) block [1-5],

$$|\psi_1\rangle = \frac{1}{\sqrt{2}}\left[\alpha|000\rangle + \alpha|011\rangle + \beta|110\rangle + \beta|101\rangle\right] = \left[{}^{\alpha}\!/_{\sqrt{2}} \quad 0 \quad 0 \quad {}^{\beta}\!/_{\sqrt{2}} \quad 0 \quad {}^{\beta}\!/_{\sqrt{2}} \quad {}^{\alpha}\!/_{\sqrt{2}} \quad 0\right]^T \tag{40}$$

3) In t_2, Alice gets the result of applying a Hadamard's gate (H) on $|\psi_1\rangle$, being this gate the second module of the BSM block [1-5],

$$
\begin{aligned}
|\psi_2\rangle &= \frac{1}{2}\left[|00\rangle X^0 Z^0 |\psi\rangle + |01\rangle X^1 Z^0 |\psi\rangle + |10\rangle X^0 Z^1 |\psi\rangle + |11\rangle X^1 Z^1 |\psi\rangle\right] \\
&= \frac{1}{2}\left[|\Phi^+\rangle X^0 Z^0 |\psi\rangle + |\Phi^-\rangle X^1 Z^0 |\psi\rangle + |\Psi^+\rangle X^0 Z^1 |\psi\rangle + |\Psi^-\rangle X^1 Z^1 |\psi\rangle\right] \\
&= \left[\alpha/2 \quad \alpha/2 \quad \beta/2 \quad -\beta/2 \quad \beta/2 \quad -\beta/2 \quad \alpha/2 \quad \alpha/2\right]^T \\
&= \left[\alpha/2 \quad 0 \quad \beta/2 \quad 0 \quad 0 \quad 0 \quad 0 \quad 0\right]^T \rightarrow |\Phi^+\rangle \rightarrow |00\rangle \rightarrow 00 \rightarrow X^0 Z^0 \\
&+ \left[0 \quad \alpha/2 \quad 0 \quad -\beta/2 \quad 0 \quad 0 \quad 0 \quad 0\right]^T \rightarrow |\Psi^+\rangle \rightarrow |10\rangle \rightarrow 10 \rightarrow X^0 Z^1 \\
&+ \left[0 \quad 0 \quad 0 \quad 0 \quad \beta/2 \quad 0 \quad \alpha/2 \quad 0\right]^T \rightarrow |\Phi^-\rangle \rightarrow |01\rangle \rightarrow 01 \rightarrow X^1 Z^0 \\
&+ \left[0 \quad 0 \quad 0 \quad 0 \quad 0 \quad -\beta/2 \quad 0 \quad \alpha/2\right]^T \rightarrow |\Psi^-\rangle \rightarrow |11\rangle \rightarrow 11 \rightarrow X^1 Z^1
\end{aligned}
\tag{41}
$$

4) Before t_3, Alice measures on Eq.(41), where the last four rows have the same probability to be chosen, i.e., ¼. This action is performed on the third module of BSM, i.e., the SPD. Alice measures and then randomly obtains two classical bits $\{b_2, b_1\}$. Finally, she transmits this pair to Bob via a classical channel like that shown in **Figure 29** with a double line. Therefore, on Bob's side the following and not ambiguous state results,

$$|\psi_3\rangle = X^{b_2} Z^{b_1} |\psi\rangle \tag{42}$$

5) Before t_4, Bob applies a Pauli's matrix X to $|\psi_3\rangle$ depending on the value of the bit b_2,

$$|\psi_4\rangle = X^{b_2} |\psi_3\rangle = X^{b_2} X^{b_2} Z^{b_1} |\psi\rangle = Z^{b_1} |\psi\rangle \tag{43}$$

6) Before t_5, Bob applies a Pauli's matrix Z to $|\psi_4\rangle$ depending on the value of the bit b_1,

$$|\psi_5\rangle = Z^{b_1} |\psi_4\rangle = Z^{b_1} Z^{b_1} |\psi\rangle = |\psi\rangle \tag{44}$$

In this way, we retrieve the teleported state from Bob's side without violating the No-Cloning Theorem because on Alice's side the measurement carried out on the *SPD* module destroyed the original state. As we mentioned above, in a more general context [30], this protocol is known as *uncontrolled quantum teleportation protocol*, because the result of the measurement carried out by Alice in the *SPD* is absolutely random, without any control on the part of the experimenter, in this case Alice, who should only transmit the coordinates of the projected base as a result of the measurement in order to disambiguate the state from the linear combination in which it is located in Eq.(41).

This version of quantum teleportation could never be instantaneous, as a direct consequence of the use of a classic channel for the transmission of the classical bits of disambiguation between Alice and Bob, since it is subject to the postulates of the Special Relativity [17]. This has deeper implications for the superior task of carrying the quantum internet from Earth to Mars, i.e., we would have a delay of, at least, 8 minutes in each transmission.

Therefore, the mere idea of a version of this protocol that does not require such a classic channel is extremely attractive. This protocol exists and is known as a *controlled quantum teleportation protocol* [30] and can be seen in **Figure 30**.

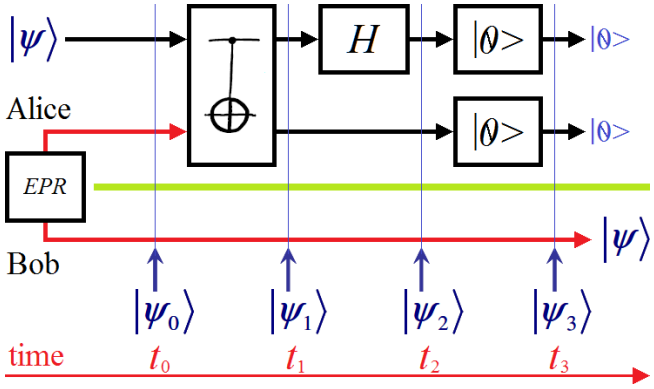

Figure 30 Controlled quantum teleportation protocol.

Specifically, the difference between this protocol and the previous one is in the *BSM*, in fact, in this protocol the *BSM* does not have an *SPD* but a pair of qubit reset gates [|0>] [30], which are located at the exit of the Hadamard's gate (*H*) and carry these states to the ground state |0>, thus blocking the entanglement. Therefore, we are not talking about *BSM* but Bell State Control (BSC) [30]. The impact of this block on Eq.(41) is dramatic since it causes the elimination *per se* of ambiguity by selecting *in pectore* a state like the following,

$$|\psi_3\rangle = X^0 Z^0 |\psi\rangle = |\psi\rangle, \tag{45}$$

without the need for:

a) Alice to transmit something,
b) a classic channel,
c) Bob to apply a unitary operator.

The qubit reset gates [|0>] exert complete control over the state of Eq.(41) eliminating ambiguity and entanglement in a single step. As we will see later, if we only block the upper branch of Alice (at the exit of Hadamard's gate *H*) with a qubit reset gate [|0>], there would be quasi-copy and stretching between the lower branch of Alice (without qubit reset gate [|0>]) and the branch of Bob.

Next, we present a robust version of the uncontrolled quantum teleportation protocol based on **Figure 31** [30]. Here, we return to the use of *BSM*, however, there is a *SWAP* between both branches of Alice in comparison to the protocol of **Figure 29**. This single fact will cause a huge change in the results that Alice will get at the exit of the *SPD* module.

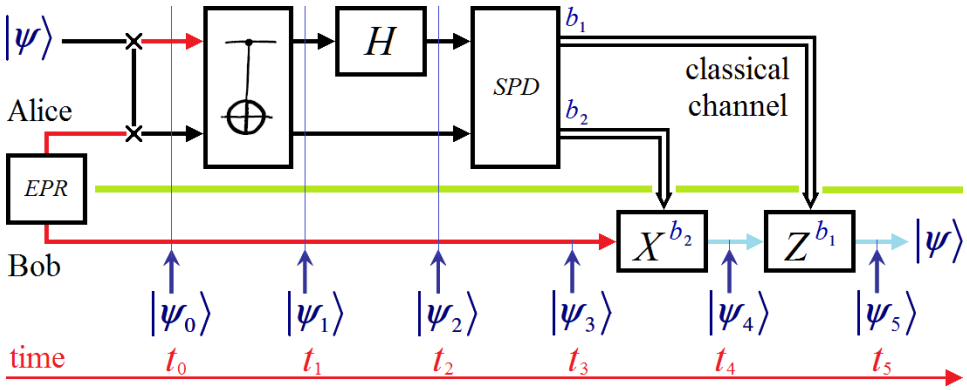

Figure 31 Robust and uncontrolled quantum teleportation. Although the constituent elements are the same as those in **Figure 29**, both Alice branches are completely inverted, i.e., swapped.

1) In t_0, the main difference between the protocols of **Figures 29** and **31** can be interpreted as a *SWAP* gate before the Kronecker's product of Eq.(39) on Alice's side, thus obtaining in here a 3-partite state result again,

$$\begin{aligned}|\psi_0\rangle = |\beta_{00}\rangle|\psi\rangle &= \frac{1}{\sqrt{2}}\big(|00\rangle+|11\rangle\big)\big(\alpha|0\rangle+\beta|1\rangle\big)\\ &= \frac{1}{\sqrt{2}}\big[\alpha|000\rangle+\beta|001\rangle+\alpha|110\rangle+\beta|111\rangle\big]\\ &= \left[\alpha/\sqrt{2}\quad 0\quad 0\quad \alpha/\sqrt{2}\quad \beta/\sqrt{2}\quad 0\quad 0\quad \beta/\sqrt{2}\right]^T\end{aligned} \tag{46}$$

2) In t_1, Alice gets the result of applying a *CNOT* gate on $|\psi_0\rangle$ (being this gate the first module of the BSM block [30]) in her lower branch because in her upper branch is $|\beta_{00}\rangle$,

$$\begin{aligned}|\psi_1\rangle &= \frac{1}{\sqrt{2}}\big[\alpha|000\rangle+\beta|001\rangle+\alpha|100\rangle+\beta|101\rangle\big] = \frac{1}{\sqrt{2}}\big[|00\rangle\big(\alpha|0\rangle+\beta|1\rangle\big)+|10\rangle\big(\alpha|0\rangle+\beta|1\rangle\big)\big]\\ &= \frac{1}{\sqrt{2}}\big(\alpha|0\rangle+\beta|1\rangle\big)\big[|00\rangle+|10\rangle\big] = \big(\alpha|0\rangle+\beta|1\rangle\big)\left[\frac{1}{\sqrt{2}}\big(|0\rangle+|1\rangle\big)\right]|0\rangle = |\psi\rangle|+\rangle|0\rangle\end{aligned} \tag{47}$$

3) In t_2, Alice gets the result of applying a Hadamard's gate (H) on $|\beta_{00}\rangle$ in her upper branch, being this gate the second module of the BSM block [30],

$$\begin{aligned}(I\otimes H)|\beta_{00}\rangle &= \left(\begin{bmatrix}1 & 0\\ 0 & 1\end{bmatrix}\otimes\frac{1}{\sqrt{2}}\begin{bmatrix}1 & 1\\ 1 & -1\end{bmatrix}\right)\frac{1}{\sqrt{2}}\big(|00\rangle+|11\rangle\big)\\ &= \frac{1}{2}\big(|00\rangle+|10\rangle+|01\rangle-|11\rangle\big)\end{aligned} \tag{48}$$

As we can see in Eq.(47), the *SWAP* in t_0 eliminated the ambiguity and the randomness at the root because the projection on the base $|+\rangle|0\rangle$ will always take 100% of the projection probability, while any other base will be at zero. In order for Bob to reconstruct the teleported state, Alice must measure to eliminate the entanglement and not violate the No-Cloning Theorem [33], however always transmitting the pair $\{b_2 = 0, b_1 = 0\}$ for the classic channel to the effects that Bob does the following task,

$$|\psi_3\rangle = X^0 Z^0|\psi\rangle = |\psi\rangle \tag{49}$$

The protocol in **Figure 31** is noticeably more noise-tolerant (i.e., robust) than that in **Figure 29** [30], although both are equally subject to the restrictions imposed by the Special Relativity [17]. However, we present below the controlled version of the protocol of **Figure 31**, which can be seen in **Figure 32**. Like the protocol in **Figure 30**, this version also does not use a *BSM* but a *BSC*. Therefore, until the Eq.(48) the protocols of **Figures 31** and **32** coincide, but then, the action of the qubit reset gates blocks the entanglement on Alice's side, therefore, on Bob's side we will have,

$$|\psi_3\rangle = |\psi\rangle. \tag{50}$$

That is, Bob automatically receives the teleported state directly and without the need to perform any additional unitary operation [30], and perhaps most importantly, without Alice transmitting anything to him through a classic channel. In other words, this last version gathers all the advantages that can be required of a protocol of quantum teleportation for the quantum internet: instantaneity, robustness, and simplicity of implementation. Either of the two versions, i.e., those of **Figures 30** or **32** can be used interchangeably for the implementations on IBM Q [42] that we will see next.

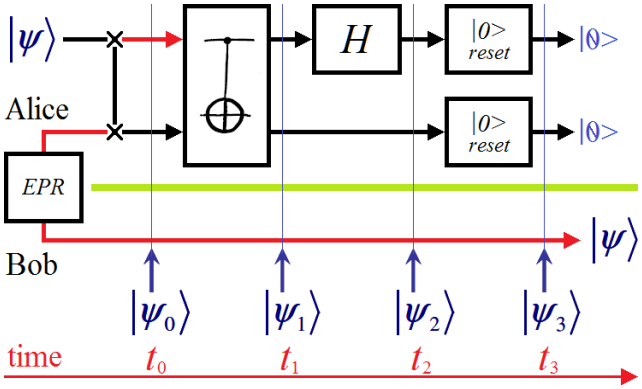

Figure 32 Robust and controlled quantum teleportation protocol.

4.1.2. Experimental verification

We implement here the protocol of **Figure 29** on IBM Q [42]. **Figure 33** shows the quantum circuit, the complex modulus of the wavefunction, and the real part of the state, where the state vector will be: [0.177-0.073j, -0.177+0.073j, 0.427+0.177j, 0.427+0.177j, -0.427-0.177j, -0.427-0.177j, -0.177+0.073j, 0.177-0.073j].

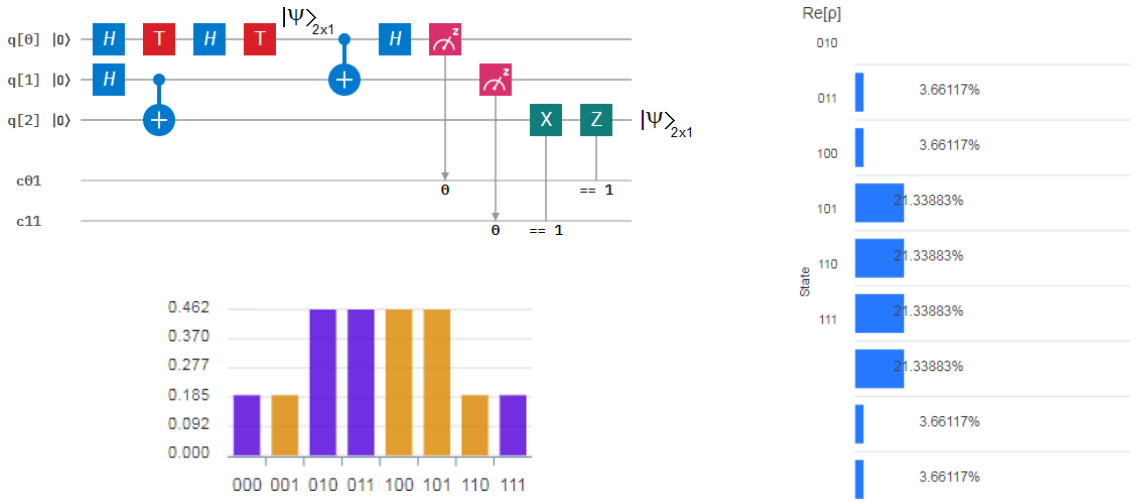

Figure 33 On the top-left is the quantum circuit for uncontrolled quantum teleportation protocol. On the bottom-left, the height of the bar is the wavefunction's complex modulus. Finally, on the right is the real part of the state.

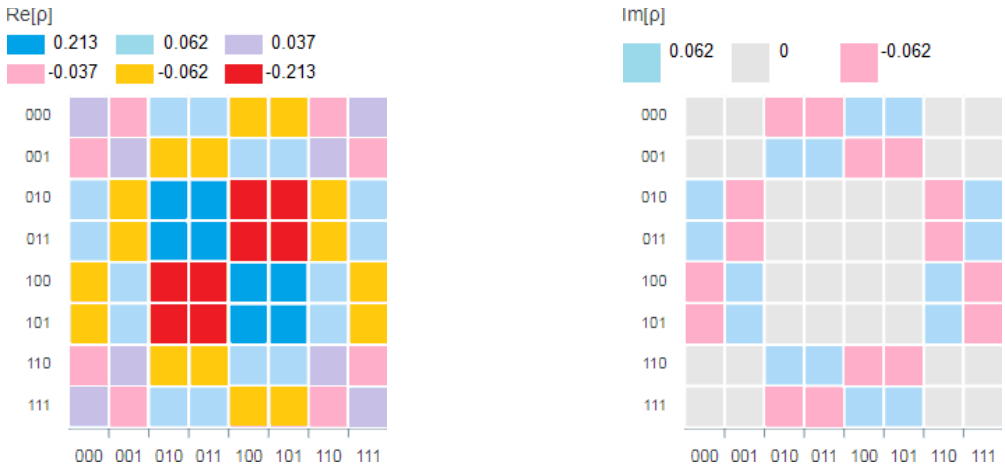

Figure 34 Wavefunction's density matrix: on the left, the real part, and on the right, the imaginary part.

It is evident that the procedure to check the results is a bit uncomfortable since we need to make an addition of different parts of the statevector to reach the final outcomes, e.g., we can add the following values of the wavefunction's complex modulus for q[2] = 0 in **Table 1**, and q[2] = 1 in **Table 2**.

Table 1. Reconstruction of the teleported qubit for q[2] = 0.

allocation in the wavefunction's complex modulus q[2]q[1]q[0]	*value of the wavefunction's complex modulus* (addition)
0 0 0	0.177-0.073j
0 0 1	-0.177+0.073j
0 1 0	0.427+0.177j
0 1 1	0.427+0.177j
Total	0.854+0.354j

Table 2. Reconstruction of the teleported qubit for q[2] = 1.

allocation in the wavefunction's complex modulus q[2]q[1]q[0]	*value of the wavefunction's complex modulus* (addition)
0 0 0	-0.427-0.177j
0 0 1	-0.427-0.177j
0 1 0	-0.177+0.073j
0 1 1	0.177-0.073j
Total	-0.854-0.354j

Table 1 shows the correct value of a part of the teleported qubit, i.e., for q[2] = 0, but **Table 2** shows a result that has nothing to do with the statevector of Eq.(21) for q[2] = 1. Then, in order to fully recover the teleported state, we must return to **Table 2** and consider that when q[0] = 0, we must change the sign of the value of the wavefunction's complex modulus and again perform the addition in the right column, therefore we will have:

$$-(-0.427-0.177j) + (-0.427-0.177j) - (-0.177+0.073j) + (0.177-0.073j) = 0.354-0.146j, \quad (51)$$

which is the correct result that matches that of the statevector of Eq.(21) for q[2] = 1. Finally, **Figure 34** shows the wavefunction's density matrix: on the left, the real part, and on the right, the imaginary part. The richness of colors is another evidence of complexity when interpreting the correct values from the byproducts of the outcomes of both tables and figures.

Next, we will implement the protocol of **Figure 31** on IBM Q [42], i.e., the robust and uncontrolled quantum teleportation protocol [30]. This implementation is presented in **Figure 35** with a statevector [0.177-0.073j, 0.427+0.177j, -0.177+0.073j, -0.427-0.177j, -0.427-0.177j, -0.177+0.073j, -0.427-0.177j, -0.177+0.073j], which is very similar to that of the previous case, with which we will build **Tables 3** and **4**.

Table 3. Reconstruction of the teleported qubit for q[2] = 0.

allocation in the wavefunction's complex modulus q[2]q[1]q[0]	*value of the wavefunction's complex modulus* (addition)
0 0 0	0.177-0.073j
0 0 1	0.427+0.177j
0 1 0	-0.177+0.073j
0 1 1	-0.427-0.177j
Total	0+0j

Table 4. Reconstruction of the teleported qubit for q[2] = 1.

allocation in the wavefunction's complex modulus q[2]q[1]q[0]	*value of the wavefunction's complex modulus* (addition)
0 0 0	-0.427-0.177j
0 0 1	-0.177+0.073j
0 1 0	-0.427-0.177j
0 1 1	-0.177+0.073j
Total	-1.208-0.208j

As we can see, prima facie, both tables give values that do not correspond to the value of the qubit that we expected to be teleported. Therefore, and taking into account that in this case a *SWAP* was carried out between both branches on Alice's side, we must change the sign of the values of the column on the right of **Table 3** when q[1] ∧ q[0] = 1,

$$+ (0.177\text{-}0.073j) + (0.427\text{+}0.177j) + (\text{-}0.177\text{+}0.073j) - (\text{-}0.427\text{-}0.177j) = 0.854\text{+}0.354j, \quad (52)$$

while in the case of **Table 4**, we must change the sign of the values of the column on the right when q[1] ∨ q[0] = 1,

$$+ (\text{-}0.427\text{-}0.177j) - (\text{-}0.177\text{+}0.073j) - (\text{-}0.427\text{-}0.177j) - (\text{-}0.177\text{+}0.073j) = 0.354\text{-}0.146j. \quad (53)$$

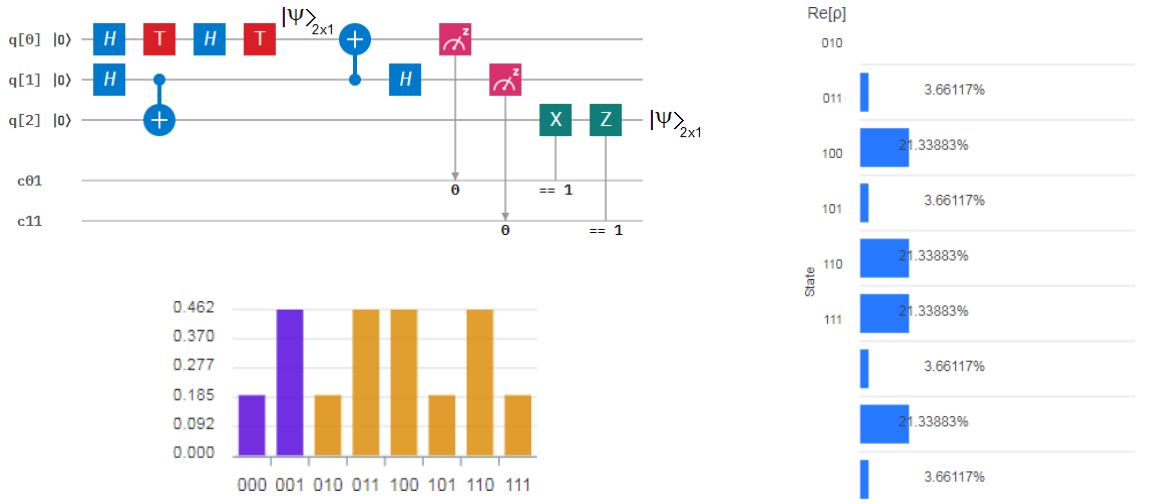

Figure 35 On the top-left is the quantum circuit for robust and uncontrolled quantum teleportation. On the bottom-left, the height of the bar is the complex modulus of the wavefunction. Finally, on the right is the real part of the state.

Now, both Eq.(52) and (53) give the correct values of the teleported qubit. Obviously, this type of protocol (i.e., those known as uncontrolled) causes a segmentation on all the metrics that evaluate their performance, which makes the evaluation and the analysis of the teleportation performance extremely uncomfortable.

Figure 35 is completed with the wavefunction's complex modulus and the real part of the state. Both graphs show that the values that constitute the parts of the teleported qubit are extremely scattered throughout the range of the metrics, where in the case of the wavefunction's complex modulus, the color blue means positive values, while, the beige means negative values.

Finally, **Figure 36** shows the wavefunction's density matrix: on the left, the real part, and on the right, the imaginary part. Here too, the great number of colors evidences a big scattering of values.

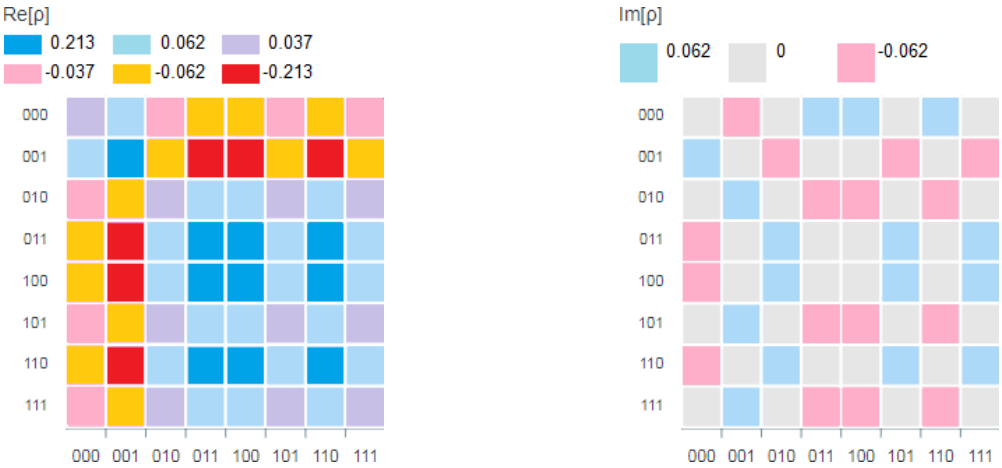

Figure 36 Wavefunction's density matrix: on the left, the real part, and on the right, the imaginary part.

Next, we will implement a simplified version of the protocol of **Figure 33** in **Figure 37**. Specifically, the main modification is in the *BSM*, where we have eliminated the Hadamard's gate (*H*) and half of the detectors of the *SPD*. However, Bob also reduces the number of gates of his unitary transform, i.e., he will use the *X* gate exclusively. As a direct consequence of this, we will obtain a quasi-cloning of the original state, where, the resulting state appears in two places at the same time: on Alice's upper branch and on Bob's side. Therefore, the only possibility of not violating the No-Cloning Theorem is that both of these states are stretched states, what actually happens. Then, if the statevector delivered by IBM Q [42] is one like [0 0.25-0.104j 0.604+0.25j 0 0.604+0.25j 0 0 0.25-0.104j], the two resulting outcomes that we will obtain by making a series of linear combinations will be:

$$q[0] = q[2] = [\ 0.854+0.354j \ \ 0 \ \ 0 \ \ 0.354-0.146j\ ]^T. \tag{54}$$

The only thing that justifies the quasi-cloning of Eq.(54) is stretching. This protocol will make Alice conserve a stretched vector and teleport the other to Bob. Here the entanglement does not completely die, precisely because there is stretching, and therefore, quasi-copies. The question is: can the EPR pair be reused for the next teleportation? The answer to this question exceeds the scope of this work, however, it will be explored in the following one.

On the other hand, **Figure 37** is completed with the wavefunction's complex modulus and the real part of the state (histogram o measurement probabilities).

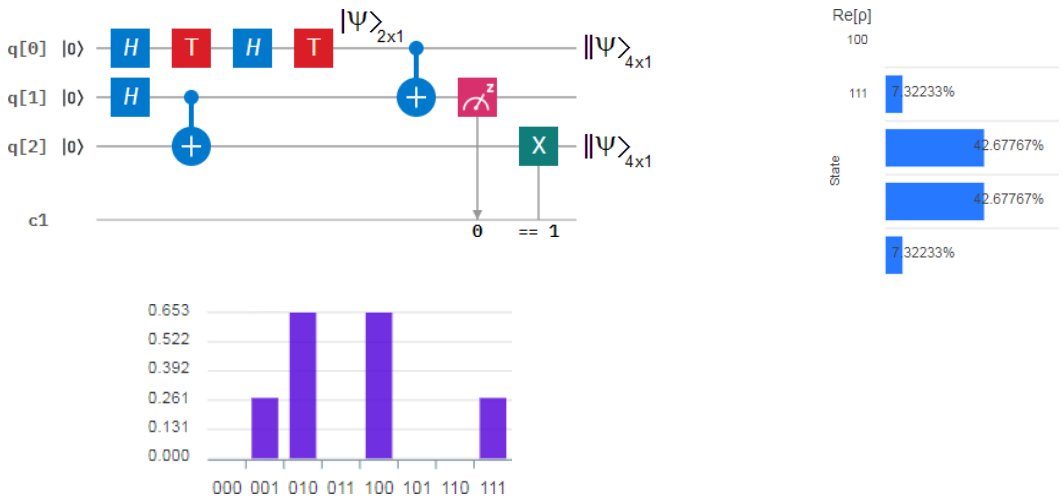

Figure 37 On the top-left is the quantum circuit for simplified and uncontrolled quantum teleportation. On the bottom-left, the height of the bar is the complex modulus of the wavefunction. Finally, on the right is the real part of the state.

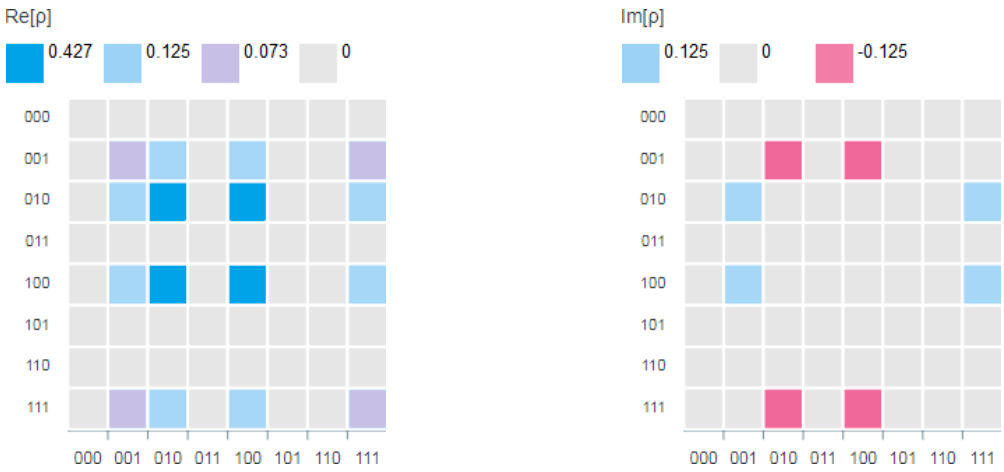

Figure 38 Wavefunction's density matrix: on the left, the real part, and on the right, the imaginary part.

Finally, **Figure 38** shows the wavefunction's density matrix of the experiment of **Figure 37**. Next, we will implement a simplified version of the protocol of **Figure 35** in **Figure 39** with a statevector like [0 0 0.25-0.104j 0.604+0.25j 0.604+0.25j 0.25-0.104j 0 0]. By similar considerations to the previous case, the outcomes are the same but in q[1] and q[2]. **Figures 39** and **40** complete the set of metrics.

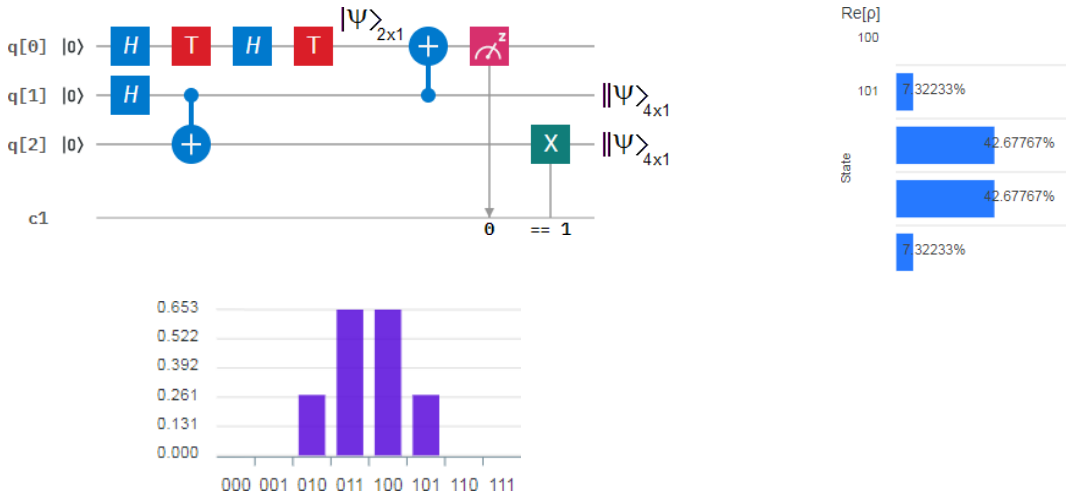

Figure 39 On the top-left is the quantum circuit for simplified and uncontrolled quantum teleportation. On the bottom-left, the height of the bar is the complex modulus of the wavefunction. Finally, on the right is the real part of the state.

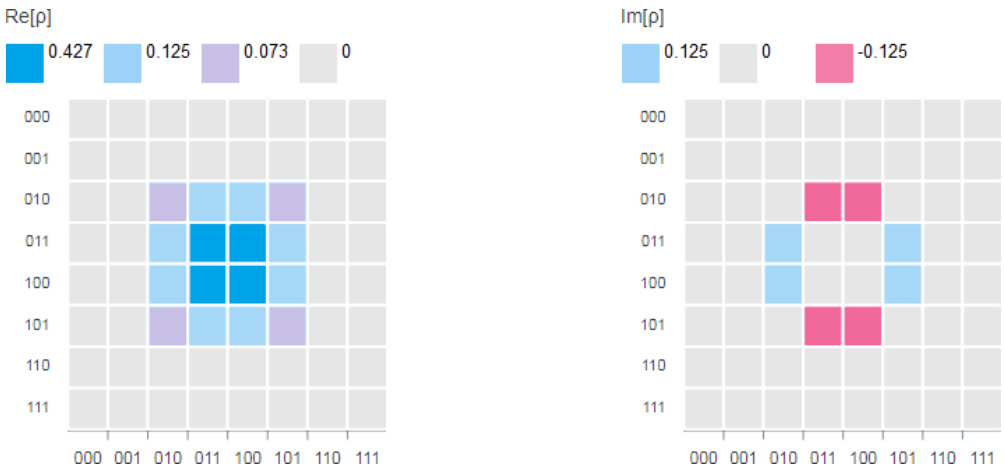

Figure 40 Wavefunction's density matrix: on the left, the real part, and on the right, the imaginary part.

At this point, it is important to highlight that any protocol which uses a *qubit reset gate* (i.e., a gate that converts any generic state into a ground state |0>) or an *if gate* (i.e., the if-then-else statement) can only be implemented on the IBM Q simulator for the time being, because these gates have not been implemented in its premium QPU yet. All the other protocols can be implemented on IBM Q QPUs depending on the number of qubits required (NQR), if:

a) NQR ≤ 5: Yorktown or Tenerife, and if
b) 5 < NQR ≤ 16: Melbourne.

In **Figure 41**, we implement the protocol of **Figure 30**. If we compare the outcomes of **Figure 33** and **34** (including the columns of **Tables 1** and **2**) with those of Figures **41** and **42** we will see that those in the former pair are illegible. The outcomes in **Figure 41** are read directly without the need for any type of arithmetic operation. In fact, the statevector recovered by Bob thanks to this protocol in q[2] is $[0.854+0.354j\ 0\ 0\ 0\ 0.354-0.146j\ 0\ 0\ 0]^T = [0.854+0.354j\ 0.354-0.146j]^T |0\rangle|0\rangle$, i.e., it is directly the correct result for a right quantum teleportation and all thanks to the control granted by the qubit reset gate [|0>] and the *BSC* over the *BSM* of traditional or uncontrolled teleportation [30]. **Figures 41** and **42** are completed with the main metrics of this experiment.

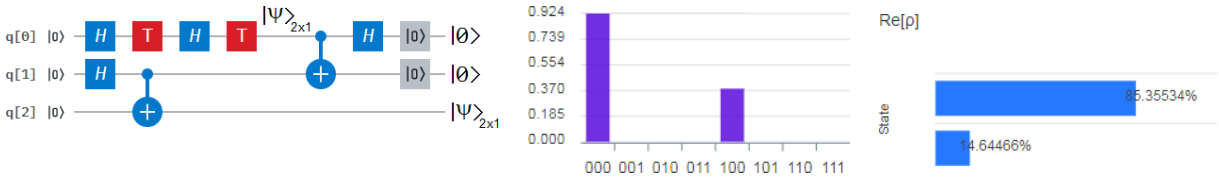

Figure 41 On the left is the quantum circuit for the qubit generation in q[0] and the *BSC* in q[0] and q[1]. In the middle, the height of the bar is the complex modulus of the wavefunction. On the right is the real part of the state (histogram o measurement probabilities).

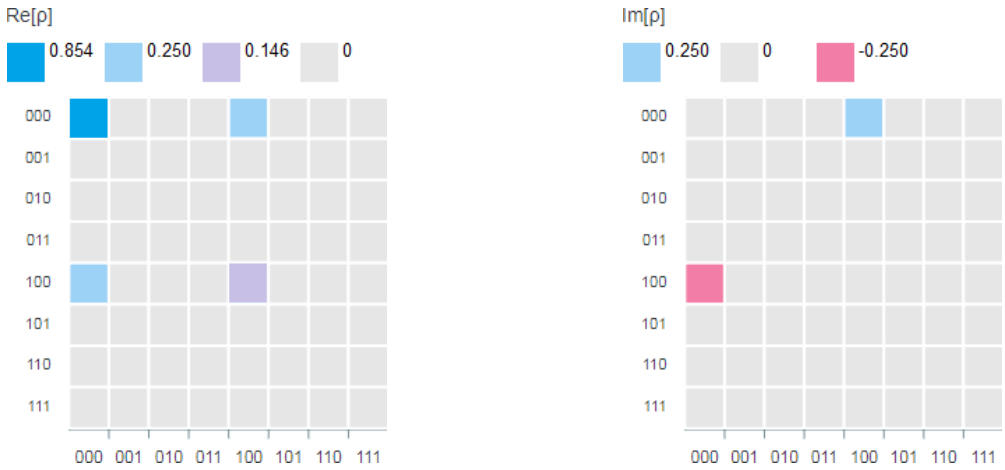

Figure 42 Wavefunction's density matrix: on the left, the real part, and on the right, the imaginary part.

Figures 43 and **44** represent the IBM Q [42] implementation of the protocol in **Figure 32**. Both the statevector and all the metrics give us identical results to those of the previous experiment.

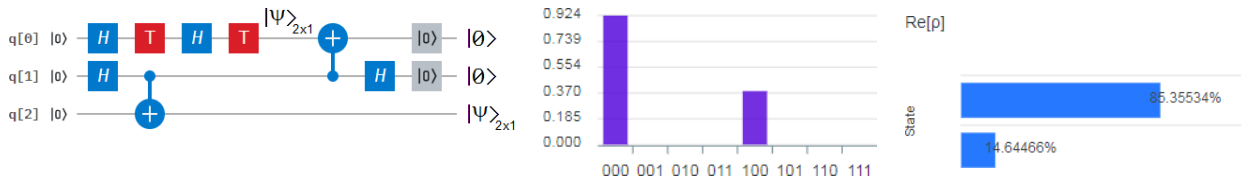

Figure 43 On the left is the quantum circuit for the qubit generation and the swapped *BSC* between q[0] and q[1]. In the middle, the height of the bar is the complex modulus of the wavefunction. On the right is the real part of the state (histogram o measurement probabilities).

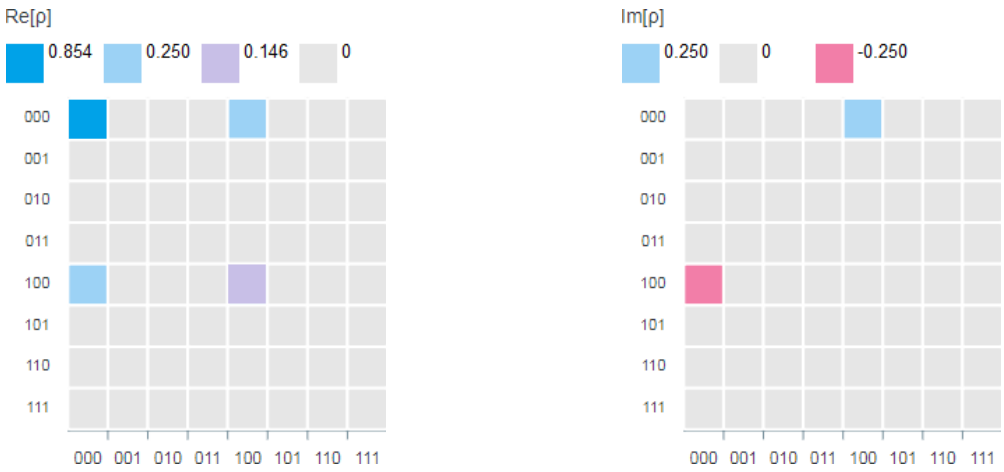

Figure 44 Wavefunction's density matrix: on the left, the real part, and on the right, the imaginary part.

Figure 45 and **46** show the outcomes belong to the controlled version of the protocol in **Figure 37**. [0 0.354-0.146j 0 0 0.854+0.354j 0 0 0]$^T \rightarrow \left[|0\rangle\|\psi\rangle_{4x1}, |0\rangle\|\psi\rangle_{4x1}\right]_{q[0],q[2]}$ (i.e., with a circular shift to the right) is the statevector, which is clearly more explicit and direct than that of **Figure 37**. However, both outcomes are stretched and are mutual quasi-copies with identical values to Eq.(54).

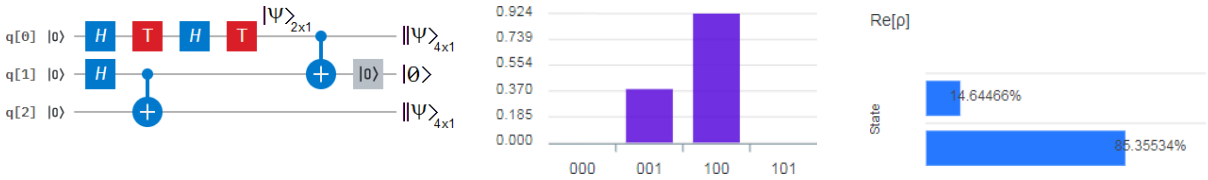

Figure 45 On the left is the quantum circuit for the qubit generation in q[0] and the simplified *BSC* in q[0] and q[1]. In the middle, the height of the bar is the complex modulus of the wavefunction. On the right is the real part of the state (histogram o measurement probabilities).

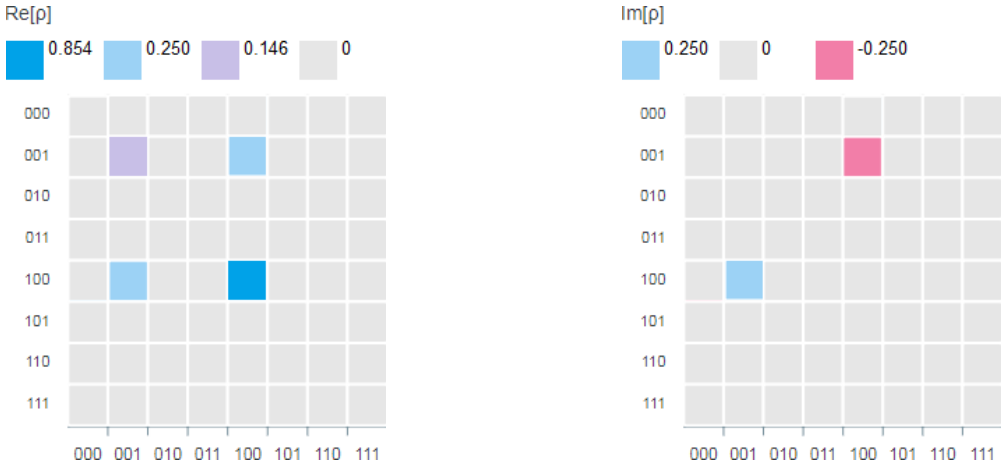

Figure 46 Wavefunction's density matrix: on the left, the real part, and on the right, the imaginary part.

Finally, in **Figures 47** and **48** we implement a simplified version of the protocol in **Figure 32** with a statevector [0.854+0.354j 0 0 0 0 0 0.354-0.146j 0]$^T = \left[\|\psi\rangle_{4x1}|0\rangle, \|\psi\rangle_{4x1}|0\rangle\right]_{q[1],q[2]}$. This result implies a couple of stretched outcomes in the qubits q[1] and q[2], which are mutual quasi-copies with identical values to those of Eq.(54). This is a direct consequence of avoiding the violation of the No-Cloning Theorem [33].

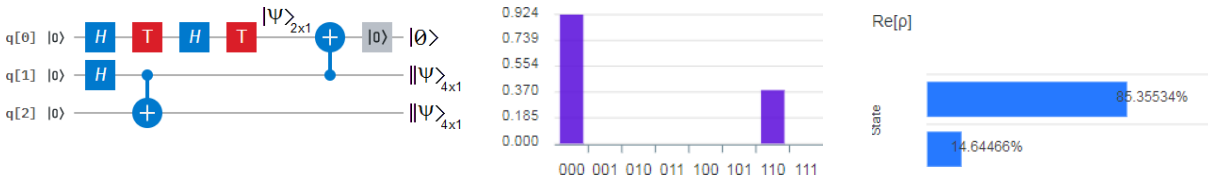

Figure 47 On the left is the quantum circuit for the qubit generation in q[0] and the swapped simplified *BSC* in q[1] and q[0]. In the middle, the height of the bar is the complex modulus of the wavefunction. On the right is the real part of the state (histogram o measurement probabilities).

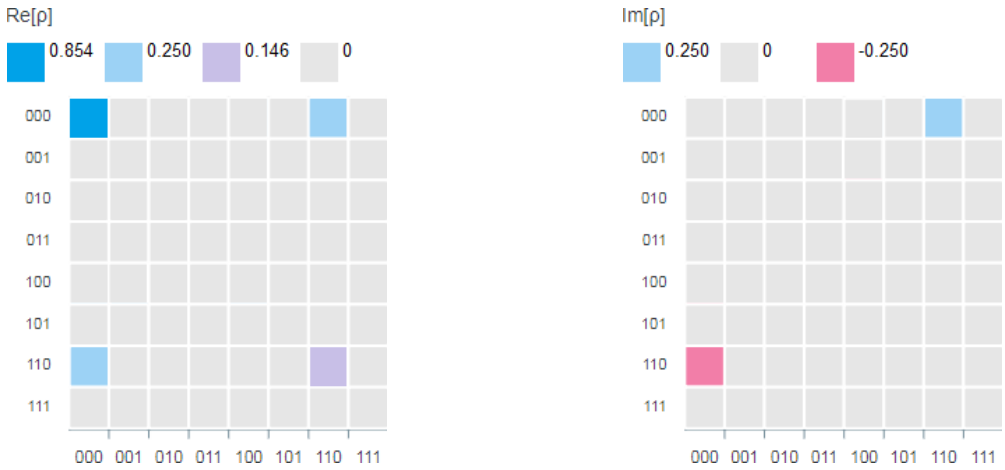

Figure 48 Wavefunction's density matrix: on the left, the real part, and on the right, the imaginary part.

4.2. Quantum teleporting without maximally entangled states

In this subsection, we will compare those relevant cases where the elements of the EPR pair to be distributed, in order to generate the quantum channel, are maximally or not maximally entangled [34-36], even including an innovative alternative to the maximally entangled case of **Figures 12** and **13**. In fact, starting with this alternative, if in the Eq.(29) we replace the Hadamard's gate (*H*) by R_y gate of IBM Q [42], we will have,

$$|+\rangle = R_y\left(\theta = \pi/2\right)|0\rangle = 1/\sqrt{2}\begin{bmatrix}1 & -1\\ 1 & 1\end{bmatrix}\begin{bmatrix}1\\ 0\end{bmatrix} = \begin{bmatrix}1/\sqrt{2}\\ 1/\sqrt{2}\end{bmatrix}. \tag{55}$$

As we can see, Eq.(29) and (55) have similar results, i.e., the |+> state. Therefore, **Figures 10** and **11** have identical metrics to those of **Figures 49** and **50**, where a simple stretching on Eq.(55) will generate a maximally entangled state. Since we have replaced *H* by R_y and even though the effect is the same, we confirm what has been mentioned in Subsection 3.3 that entanglement is part of a broader process, and therefore, is a particular case of stretching. As a direct consequence of what has been said, the statevector delivered by IBM Q [42] will be [0.707 0.707].

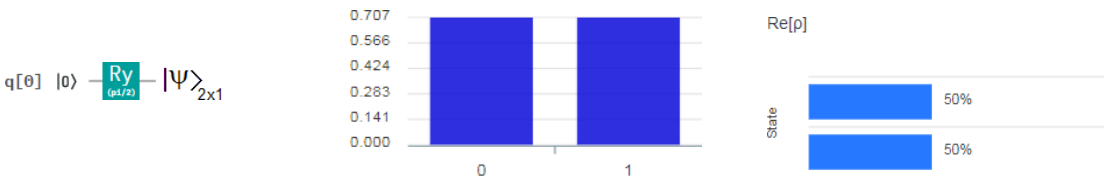

Figure 49 On the left is the quantum circuit for the qubit generation in q[0]. In the middle, the height of the bar is the complex modulus of the wavefunction, which is typical of a |+> state. On the right is the real part of the state, also typical of a |+> state.

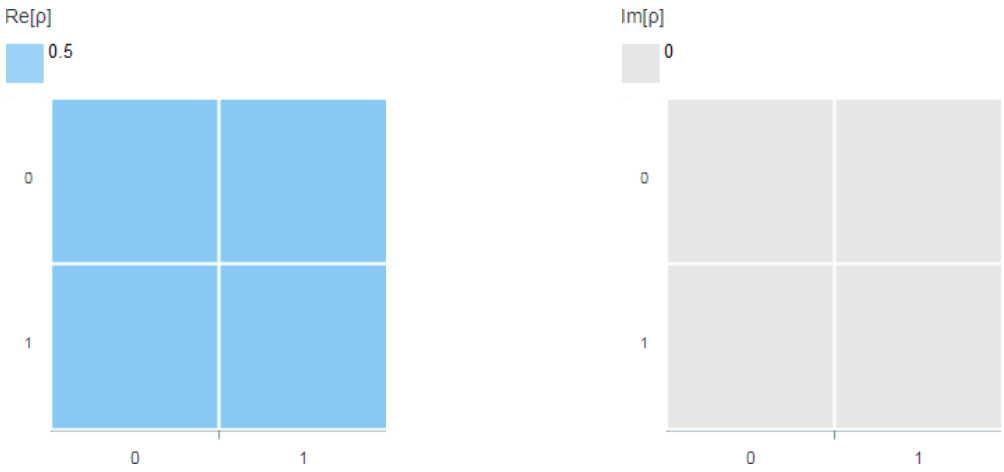

Figure 50 Wavefunction's density matrix: on the left, the real part, and on the right, the imaginary part.

In the next experiment, a maximally entangled pair is generated based on the state of the previous example to distribute it between Alice and Bob as part of the protocol of **Figure 30**. **Figures 51** and **52** imply a statevector [0.854+0.354j 0 0 0 0.354-0.146j 0 0 0]^T = $|\psi\rangle|0\rangle|0\rangle$. As we can see, the outcomes are absolutely equal to those of **Figures 41** and **42** using H to generate the EPR pair instead of R_y. Therefore, we are in the presence of another maximally entangled case.

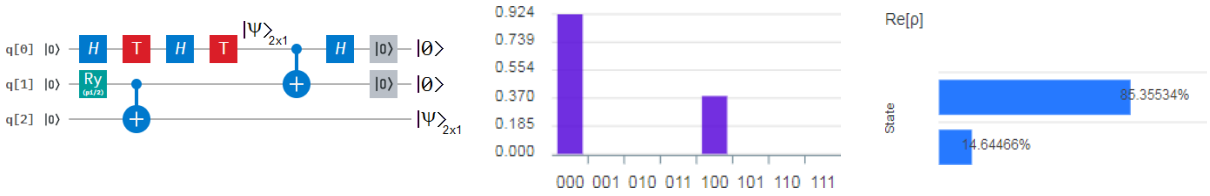

Figure 51 On the left is the quantum circuit for controlled quantum teleportation. In the middle, the height of the bar is the complex modulus of the wavefunction, which is identical to that of **Figure 41**. On the right is the real part of the state, also identical to that of **Figure 41**.

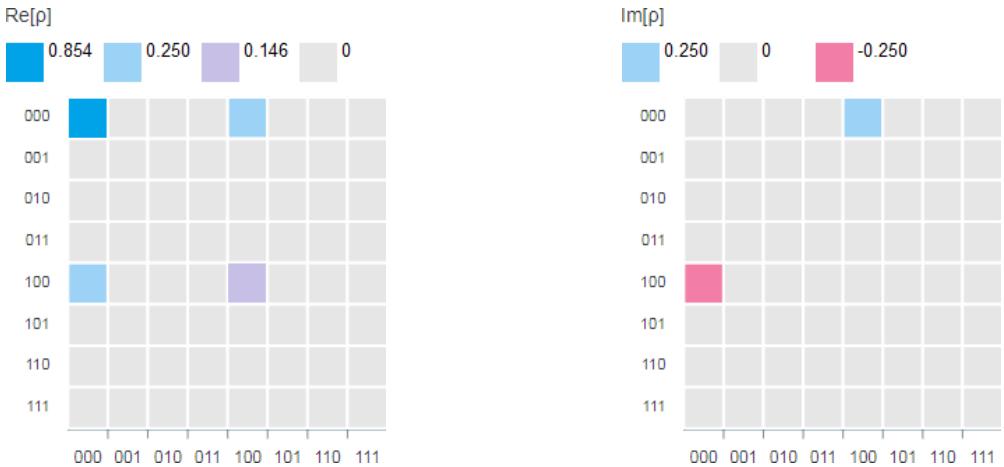

Figure 52 Wavefunction's density matrix: on the left, the real part, and on the right, the imaginary part.

Next, we will test a witness case of a not balanced state, where the combination of the five gates of **Figure 53** gives a statevector [0.854-0.354j 0.354-0.146j]^T, which is different from the typical case of the experiment in **Figure 49**, i.e., |+> = [0.707 0.707]^T, because this case presents an imbalance between the component of |0> and that of |1>. **Figure 54** completes the set of metrics.

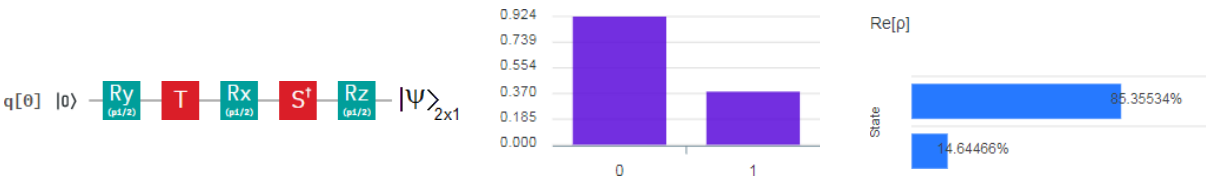

Figure 53 On the left is the quantum circuit for the qubit generation in q[0]. In the middle, the height of the bar is the complex modulus of the wavefunction, which is different from that of **Figure 49**. On the right is the real part of the state, also it is different from that of **Figure 49**.

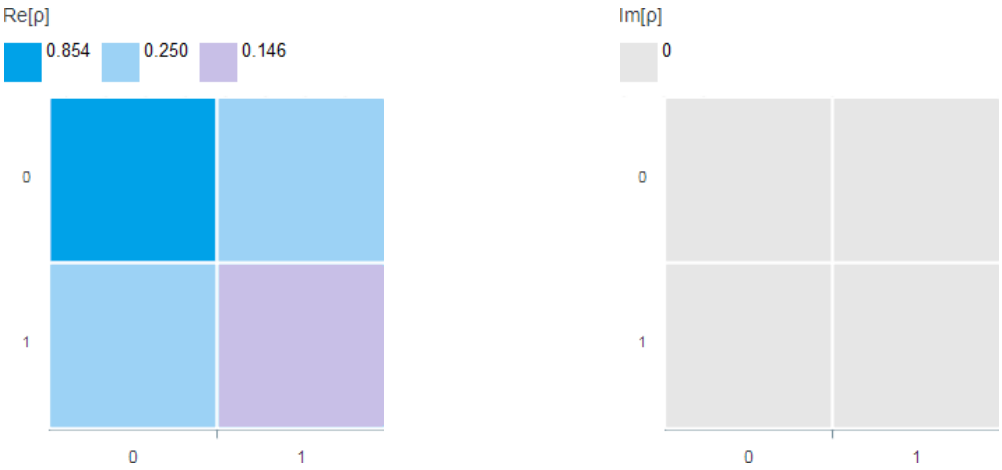

Figure 54 Wavefunction's density matrix: on the left, the real part, and on the right, the imaginary part.

In the experiment of **Figures 55** to **57**, we will use the state of the previous example to generate a not maximally entangled pair, which inherits the imbalance between the components of |0> and |1> of the state of **Figure 53**, so that it can be distributed between Alice and Bob, the results of **Figure 55** will experience this imbalance.

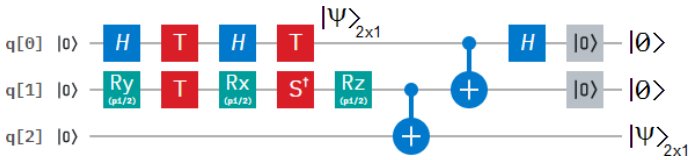

Figure 55 Controlled quantum teleportation protocol with a not maximally entangled pair.

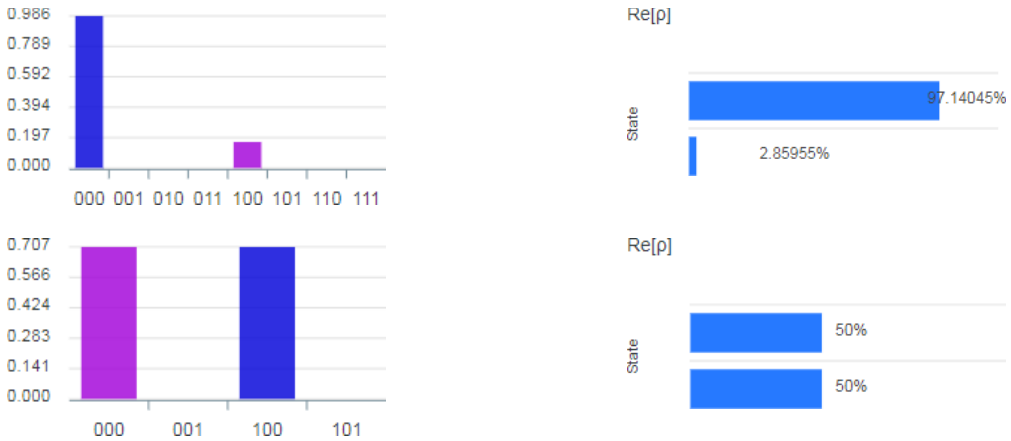

Figure 56 IBM Q delivers two types of outcomes in a randomly way, at the top: the wavefunction's complex modulus and the real part of the state with different values from those expected, and, at the bottom: wavefunction's complex modulus and the real part of the state, but with different values from those expected again.

Thus, the protocol of **Figure 55** (in fact, as well as any other protocol of quantum teleportation used) will teleport depending on the imbalance of the base, i.e., Bob receives two distorted versions of the state to be teleported, which will have for the:

a) top version of **Figures 56** and **57** a statevector = [0.986 0 0 0 0.12-0.12j 0 0 0],
b) bottom version of **Figures 56** and **57** a statevector = [0.5-0.5j 0 0 0 0.707 0 0 0].

Evidently, these two possible outcomes that IBM Q [42] gives us have little or nothing to do with the qubit to be teleported, i.e., that of the Eq.(21).

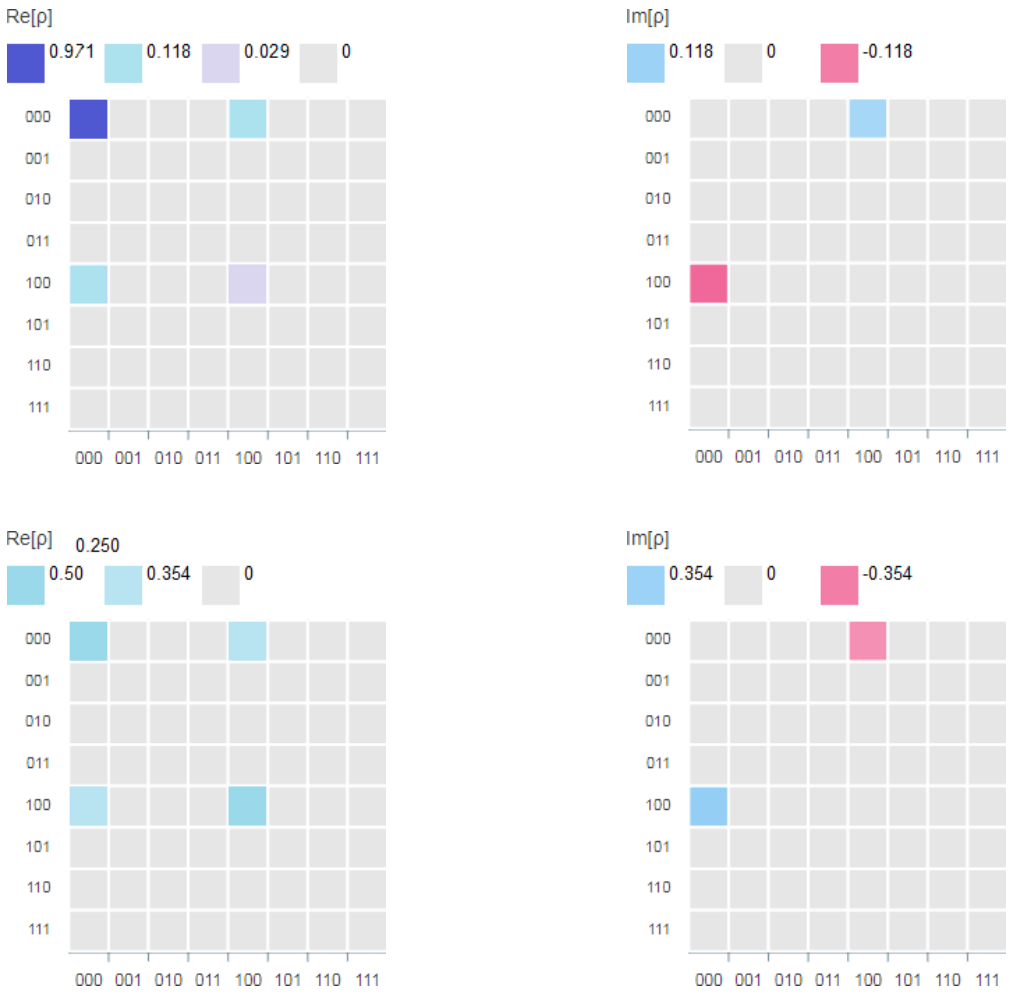

Figure 57 Top: wavefunction's density matrix for the first type of statevector, and, bottom: wavefunction's density matrix for the second type of statevector delivered by IBM Q [42].

In the only case in which the result of teleportation via a not maximally entangled pair is identical to the original state to be teleported is when we want to teleport CBS = {|0>, |1>} states. For this reason, we will test two similar experiments, one for the case of teleporting the |0> state (**Figures 58** and **59**) and another one for |1> (**Figures 60** and **61**). Then, the first statevector obtained thanks to **Figure 58** is

statevector #1 = [0.924-0.383j 0 0 0 0 0 0 0], while the second one is

statevector #2 = [-0.924+0.383j 0 0 0 0 0 0 0] thanks to **Figure 60**.

As it is visually obvious from both statevectors, the second one is the negative version of the first one, i.e., statevector #1 = - statevector #2, therefore, statevector #1 → |0>, while, statevector #2 → |1>.

In other words, if Bob receives the statevector #1 said outcomes will be interpreted as the teleportation of the |0> state, instead, if Bob receives the statevector #2 said outcomes will be interpreted as the teleportation of the |1> state.

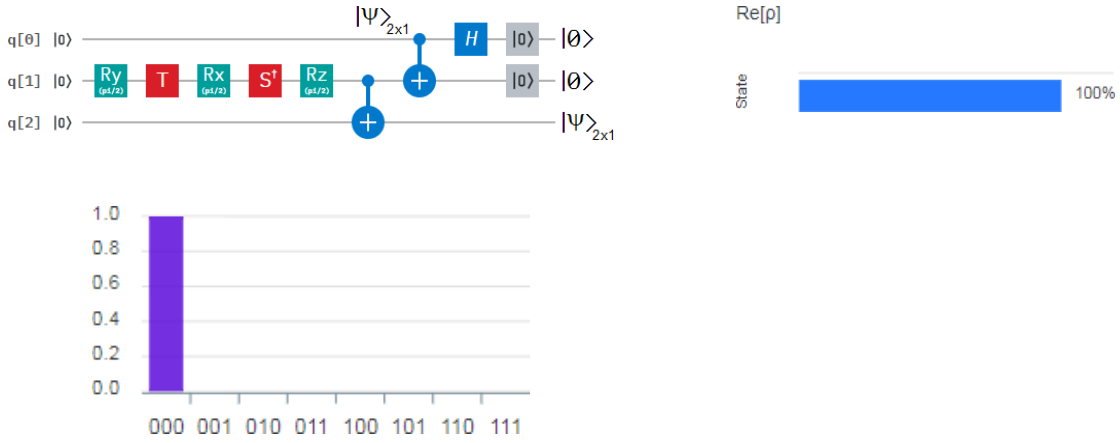

Figure 58 On the top-left is the quantum circuit for controlled quantum teleportation of |0> via a not maximally entangled pair. On the bottom-left, the height of the bar is the complex modulus of the wavefunction. Finally, on the right is the real part of the state.

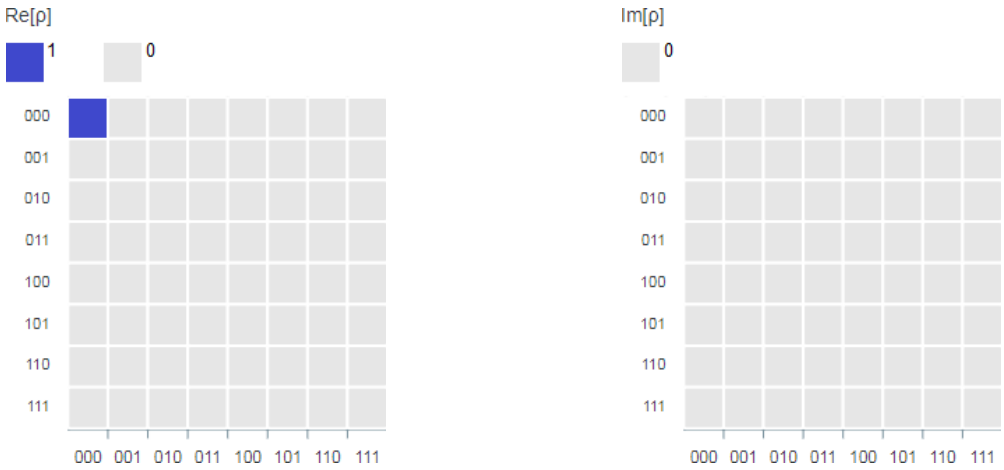

Figure 59 Wavefunction's density matrix: on the left, the real part, and on the right, the imaginary part.

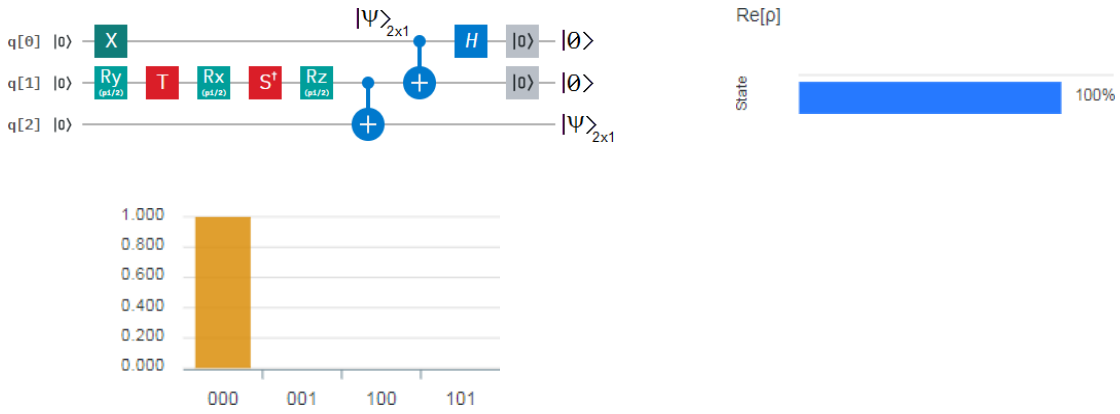

Figure 60 On the top-left is the quantum circuit for controlled quantum teleportation of |1> via a not maximally entangled pair. On the bottom-left, the height of the bar is the complex modulus of the wavefunction. Finally, on the right is the real part of the state.

This proves that any qubit with α and β simultaneously nonzero via quantum stretching can carry quantum teleportation, at least of CBS. For this reason, we say in Subsection 3.3 that the quantum entanglement is a particular case of quantum stretching.

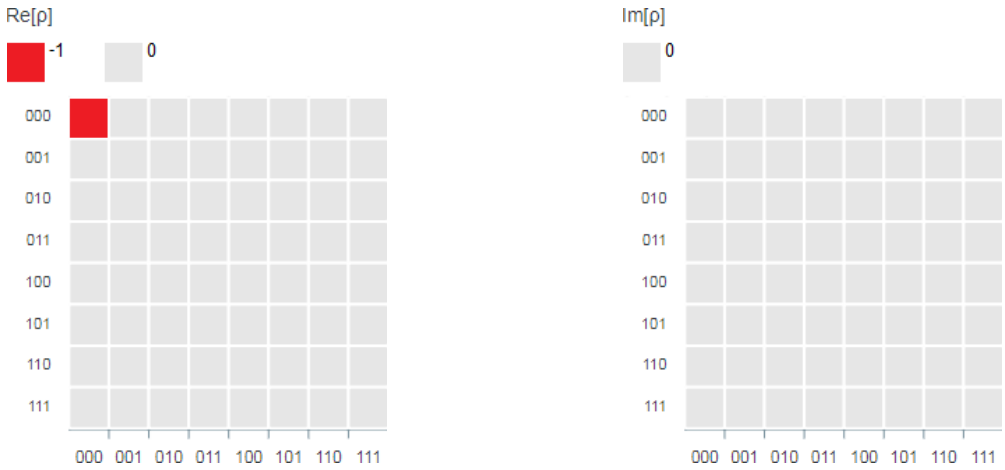

Figure 61 Wavefunction's density matrix: on the left, the real part, and on the right, the imaginary part.

4.3. Quantum Stretching, Networking, Wormholes and Multiple Teleporting

In **Figure 62**, we can see the controlled quantum teleportation protocol of **Figure 30**. The evolution of this protocol along **Figure 62** from left to right shows that it behaves like a big *SWAP*.

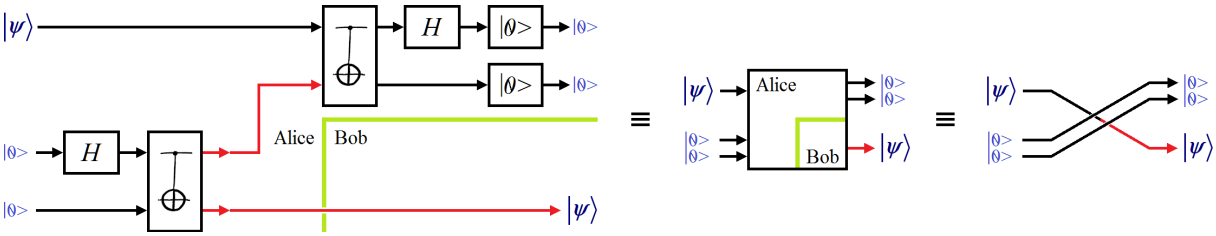

Figure 62 The controlled quantum teleportation ends up in a big *SWAP* or cross.

In **Figures 41** and **42**, we can see the outcomes of this protocol for a specific qubit to be teleported. **Figure 63** shows a wormhole resulting from the entanglement of two black holes or a black hole and a white hole. The trip of the state to be teleported $|\psi\rangle$ through the equivalent wormhole is precisely seen as the controlled quantum teleportation protocol of **Figure 62**. From two previous works [30, 44], we know that two entangled things are represented entropically by their respective avatars [30], which are in an intermediate location between the entangled things and are the ones who actually communicate. Besides, since the distance between the avatars is null the channel that they define also is, therefore, all wormholes resulting from the entanglement of two black holes (or a black hole and a white hole) are traversable, confirming that the information inside a black hole is not lost. Thanks to the avatars, what was said becomes evident, given that, what is more traversable than something of zero length?

The wormhole to the left of **Figure 63** is equivalent to two black holes without a body on top of each other, which can be seen to the right of the figure represented as two rings, superimposed. Since the rings are so close together (i.e., with no distance between them), superluminal speed is not necessary to pass from one to the other instantaneously. In fact, a turtle walking at 3 km/h would go through that wormhole instantaneously being its speed 10^5 times slower than that of light.

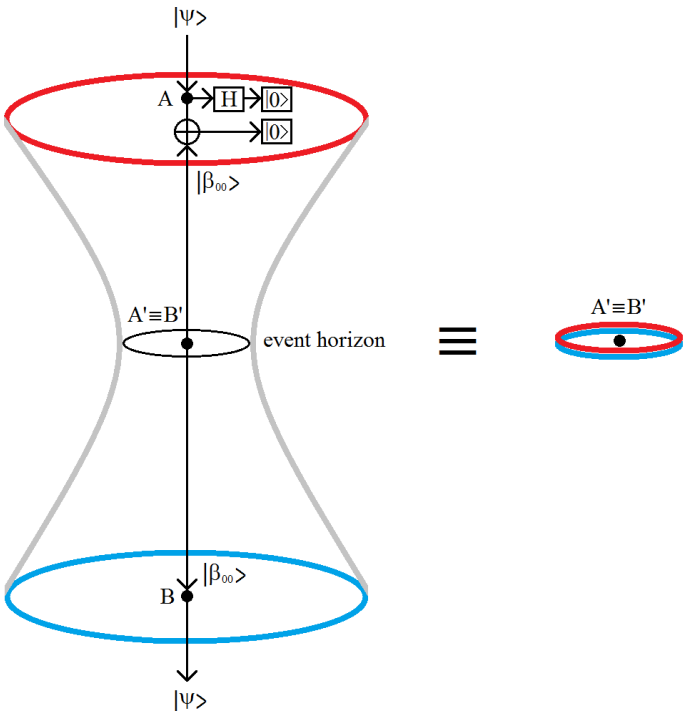

Figure 63 Wormhole resulting from the entanglement of two black holes or a black hole and a white hole. The trip of the state $|\psi\rangle$, through the wormhole, is equivalent to a teleportation thanks to the controlled quantum teleportation protocol without a classical channel for disambiguation. From avatars, we know that this type of wormhole is equivalent to a pair of rings, one on top of the other, therefore, it is perfectly traversable.

Next, we will implement the controlled quantum teleportation protocol, where we have performed a stretching on the lower branch of the entangled pair that generates the quantum channel between Alice and Bob, so that in addition to Bob there could be a second recipient of the stretched version of the teleported state. The statevector [0.854+0.354j "11 zeros" 0.354-0.146j "3 zeros"]^T = $\|\psi\rangle_{4x1}|0\rangle|0\rangle$ has 16 elements, however, this indicates that we have two identical outcomes represented to the right of the quantum circuit of **Figure 64** as $\|\psi\rangle_{4x1}$ = [0.854+0.354j 0 0 0.344-0.146j]^T. Obviously, both outcomes will have the double size of the original qubit to be teleported.

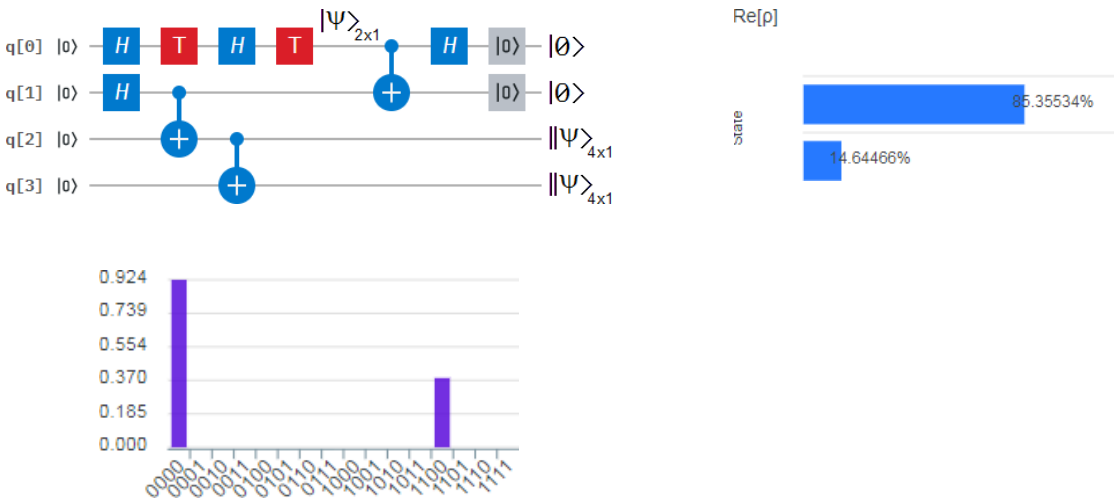

Figure 64 On the top-left is the quantum circuit for controlled quantum teleportation where the lower branch of the EPR pair is stretched allowing another receiver additional to Bob. On the bottom-left, the height of the bar is the complex modulus of the wavefunction. Finally, on the right is the real part of the state.

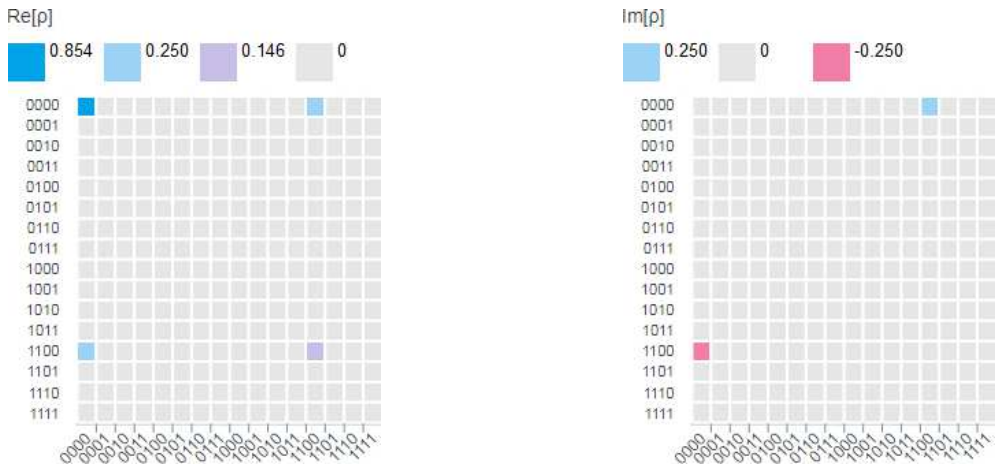

Figure 65 Wavefunction's density matrix: on the left, the real part, and on the right, the imaginary part.

Figure 65 shows us the wavefunction's density matrix for this experiment. Besides, the protocol of **Figure 64** has its own interpretation in the wormhole context. **Figure 66** shows that it will have a very similar shape to a pair of wide trousers. In other words, the quantum stretching causes, simultaneously, a bifurcation and dilation in the equivalent wormhole. As a consequence of this, the two receiving black holes will be increasingly larger in dimension since their size grows with each quasi-copy.

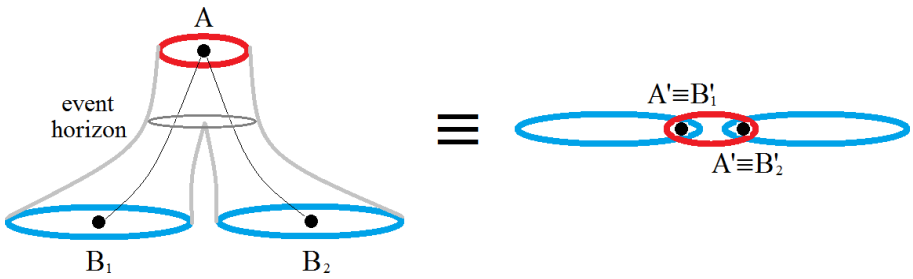

Figure 66 Wormhole equivalent to a controlled quantum teleportation with stretching as that of **Figure 64**. The stretched quasi-copies of the state to be teleported travel by both branches of the wormhole. From avatars, this wormhole is equivalent to three overlapped rings, being perfectly traversable.

Next, we will implement the controlled quantum teleportation protocol of **Figure 67**, which presents a double process of quantum stretching, in a cascade way, in the lower branch of the entangled pair. The statevector delivered by IBM Q [42] is [0.854+0.354j "27 zeros" 0.354-0.146j 0 0 0]$^T = \|\psi\rangle_{8\times1}|0\rangle|0\rangle$, which can be interpreted as three outcomes, one by each output of the quantum circuit of **Figure 67**,

$$\|\psi\rangle_{4\times1} = [0.854+0.354j \quad 0 \quad 0 \quad 0.354-0.146j]^T,$$
$$\|\psi\rangle_{8\times1} = [0.854+0.354j \quad 0 \quad 0 \quad 0 \quad 0 \quad 0 \quad 0 \quad 0.354-0.146j]^T \quad (\times 2).$$

All the involved states must comply with the rule of inverse-of-the-sizes conservation:

$$\tfrac{1}{2}\left(from\,|\psi\rangle_{2\times1}\right) = \tfrac{1}{4}\left(from\,\|\psi\rangle_{4\times1}\right) + \tfrac{1}{8}\left(from\,\|\psi\rangle_{8\times1}\right) + \tfrac{1}{8}\left(from\,\|\psi\rangle_{8\times1}\right). \quad (56)$$

Figures 67 and **68** complete the set of metrics for this experiment, while **Figure 69** shows the graphic representation of the rule of inverse-of-the-sizes conservation for the states involved in Eq.(56), and finally, **Figure 70** shows the equivalent wormhole with three branches of different widths.

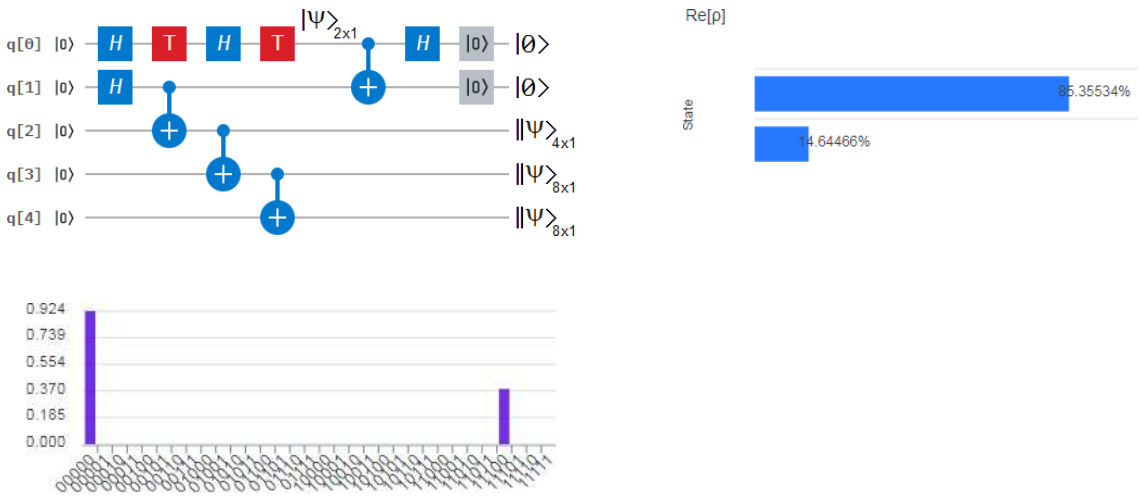

Figure 67 On the top-left is the quantum circuit for controlled quantum teleportation where the lower branch of the EPR pair is stretched allowing another receiver additional to Bob. On the bottom-left, the height of the bar is the complex modulus of the wavefunction. Finally, on the right is the real part of the state.

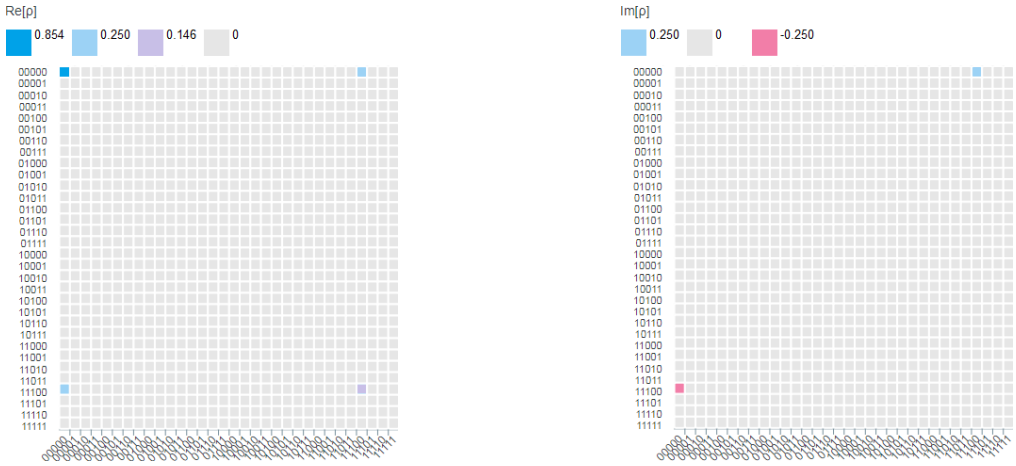

Figure 68 Wavefunction's density matrix: on the left, the real part, and on the right, the imaginary part.

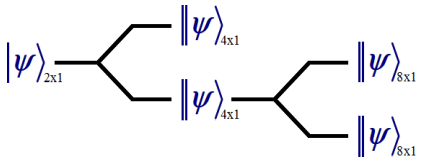

Figure 69 Graphic representation of the rule of inverse-of-the-sizes conservation for this experiment.

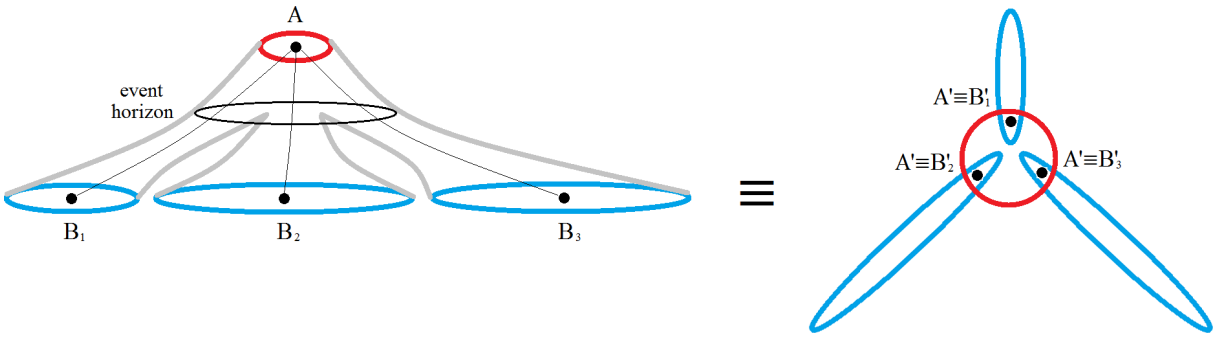

Figure 70 Equivalent wormhole for the experiment of **Figure 67** with three branches of different sizes.

The equivalent wormhole is composed, at the same time, by three simultaneous sub-wormholes resulting from successive quasi-copies and stretching, thus getting bigger and bigger, which makes it even more traversable.

Finally, the experiment of **Figure 71** represents a controlled quantum teleportation protocol with an EPR pair which suffers two successive stretchings and shrinkings. Therefore the qubit q[2] on the right of the quantum circuit of **Figure 71** is the host of the teleported state, which is identical to the qubit to be teleported in value and size, beyond the fact that the statevector delivered by IBM Q is extremely large: [0.854+0.354j 0 0 0 0.354-0.146j "27 zeros"]^T = $|0\rangle|0\rangle|\psi\rangle|0\rangle|0\rangle$, with [0.854+0.354j 0.354-0.146j] = q[2] = $|\psi\rangle$, which represents exactly the waited state, confirming a perfect teleportation.

The two shrinkings after the two stretchings have a restorative effect on the experiment as a whole, obtaining identical results to those of the experiment in **Figure 41**, which does not use stretching or shrinking.

Figures 71 and **72** complete the set of metrics for this experiment. The outcome delivered by IBM Q [42] is $|0\rangle|0\rangle|\psi\rangle|0\rangle|0\rangle$, which evidences the presence of separability and the correct recovery of the teleported state, regardless of the large size of the statevector.

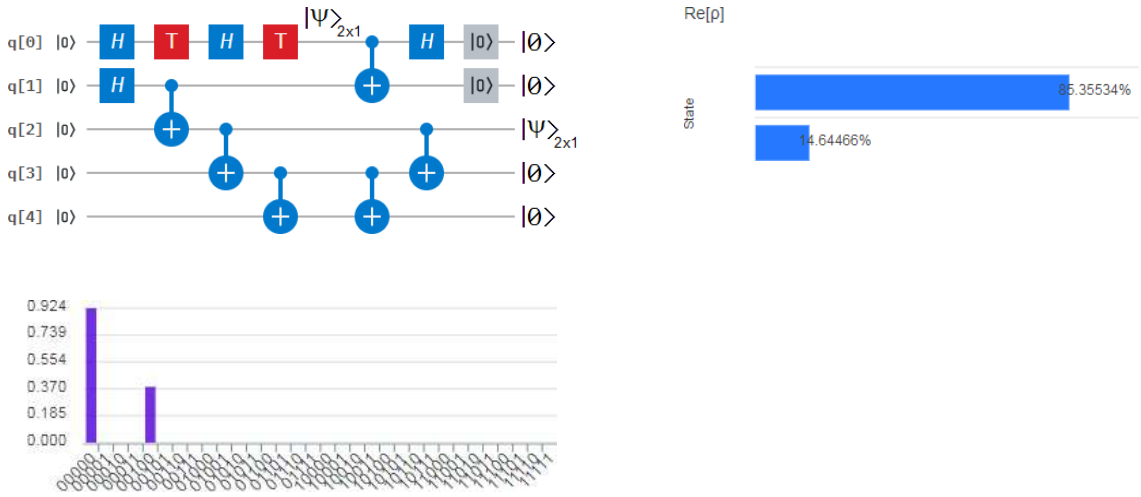

Figure 71 On the top-left is the quantum circuit for controlled quantum teleportation where the lower branch of the EPR pair is stretched twice and shrunk twice, annulling their effects mutually. On the bottom-left, the height of the bar is the complex modulus of the wavefunction. Finally, on the right is the real part of the state.

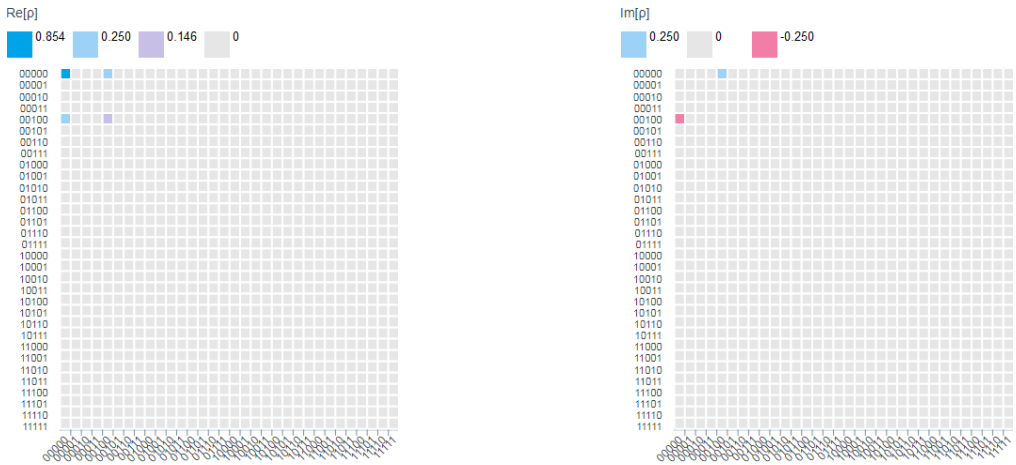

Figure 72 Wavefunction's density matrix: on the left, the real part, and on the right, the imaginary part.

4.4. Entanglement and quasi-entanglement blocker

In this subsection, we will present some conspicuous examples, which are absolutely extrapolated to any situation in which the qubit reset gate [|0>] is used as an entanglement and a quasi-entanglement (i.e., with a not maximally entangled pair) blocker.

Case 1:

We analyze here, the cases of **Figure 73**, where we apply the qubit reset gate [|0>] in an alternative way (i.e., first in the lower branch and then in the upper branch) to the output of a quantum stretching process which acts as a quasi-entanglement generator. Being the original qubit generated before the *CNOT* gate, $|\psi\rangle_{2\times1}=[0.854+0.354j \quad 0.354-0.146j]^T$, the quantum stretching process will generate two, $\|\psi\rangle_{4\times1}=[0.854+0.354j \quad 0 \quad 0 \quad 0.354-0.146j]^T$ at the output of the *CNOT* gate, however, the qubit reset gate will produce a statevector, $[0.924+0.383j \quad 0 \quad 0 \quad 0]^T \sim |00\rangle=|0\rangle|0\rangle$, i.e., we obtain a double and separable $|0\rangle$. This result, according to IBM Q [42], confirms the destruction of stretching. But, what is the origin of such a strange statevector? The answer is very simple, because if the original qubit is $|\psi\rangle_{2\times1}=[0.854+0.354j \quad 0.354-0.146j]^T=[\alpha \quad \beta]^T$, then, the statevector will be the next, $[0.924+0.383j \quad 0 \quad 0 \quad 0]^T=[|\alpha|+|\beta|j \quad 0 \quad 0 \quad 0]^T=[|0.854+0.354j|+|0.354-0.146j|j \quad 0 \quad 0 \quad 0]^T$. **Figures 73** and **74** complete the set of metrics. An interesting attribute that will be repeated in all cases

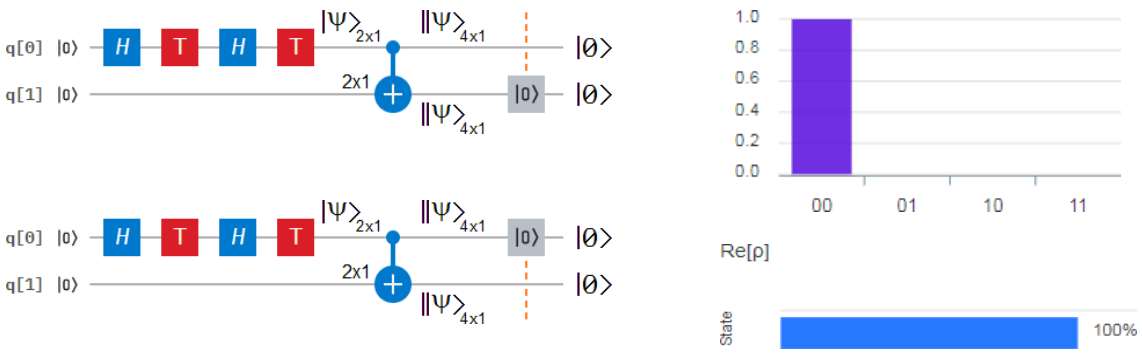

Figure 73 On the left, both versions for a blocking via qubit reset gate in one of the two branches at the output of the *CNOT* gate. On the top-right is the unitary wavefunction's complex modulus, and on the bottom-right is the real part of the state, which is unitary too.

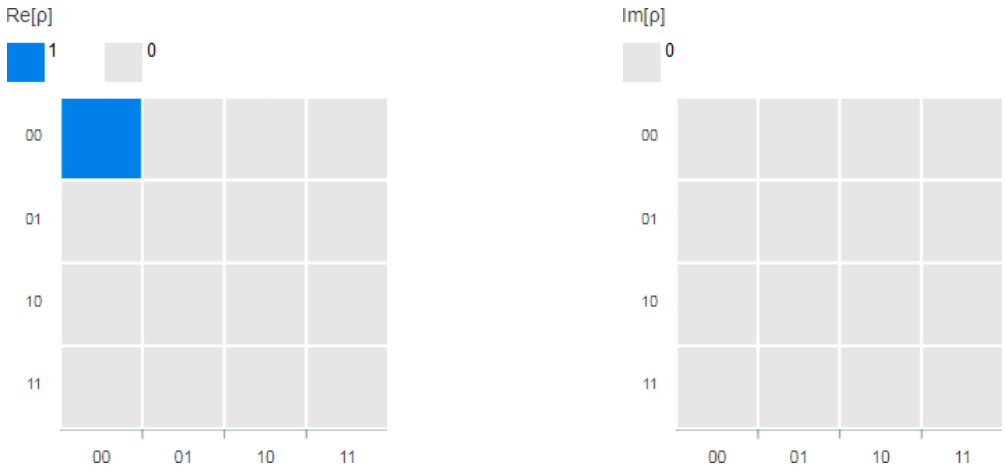

Figure 74 Wavefunction's density matrix: on the left, the real part, and on the right, the imaginary part.

consists in that both wavefunction's complex modulus and the real part of the state, are unique and unitary, in fact, $\sqrt{|\alpha|^2+|\beta|^2}=\sqrt{|0.924|^2+|0.383|^2}=1$, which, as it should be, complies with what was seen in Section 2.1 for the Bloch's sphere.

Case 2:

The case of **Figure 75** represents a multiple stretching in cascade, however, it shows that by blocking the most distant and remote branch of that configuration, all the branches, without exception, collapse to the ground state |0>. The statevector is [1 "15 zeros"] = |0000>. In fact, we start with the famous state |+> = *H* |0> in the top branch of the configuration, then, the first stretching via a *CNOT* gate produces an EPR pair. The following *CNOT* gates produce successive stretchings, with quasi-copies increasing in size, but, the qubit reset gate in the lowest branch generates a collective collapse of the whole configuration. **Figures 75** and **76** complete the set of metrics.

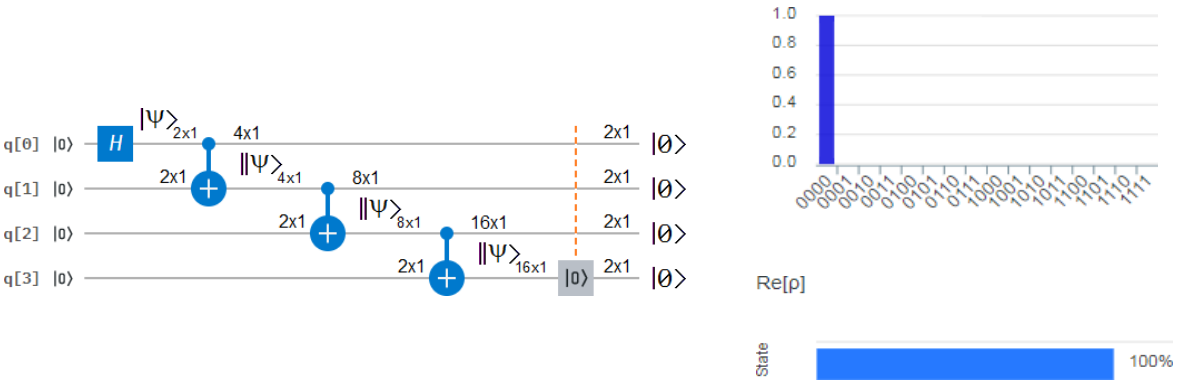

Figure 75 On the left, the configuration starts with the generation of the |+> state, the first *CNOT* gate generates an EPR pair, while the following ones produce successive stretchings of the pair. The qubit reset gate in the lowest branch put all the output to ground state |0>. On the top-right is the unitary wavefunction's complex modulus, and on the bottom-right is the real part of the state, which is unitary too.

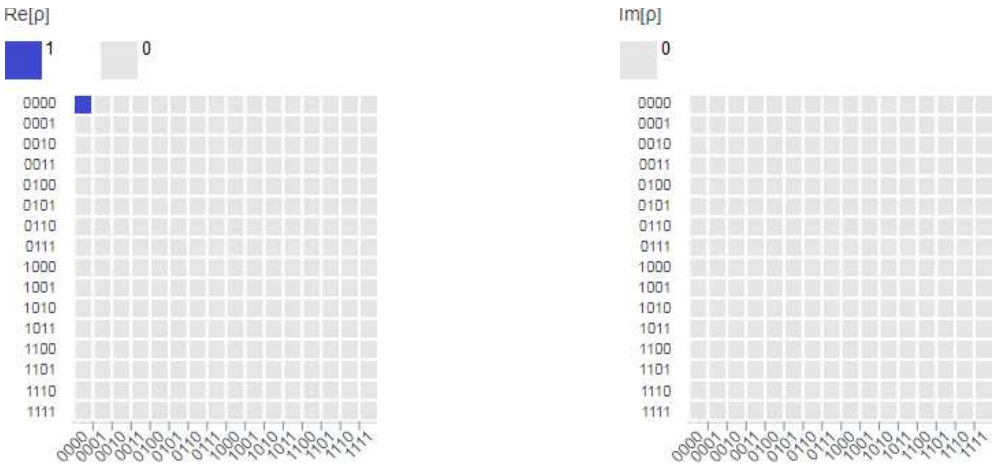

Figure 76 Wavefunction's density matrix: on the left, the real part, and on the right, the imaginary part.

Case 3:

Figure 77 shows a configuration with characteristics of the two preceding cases, i.e., begins with a not maximally entangled pair as **Case 1**, but then it continues with a cascade of two *CNOT* gates that

produce successive stretchings as **Case 2**. The configuration of **Figure 77** begins with the generation of the qubit $|\psi\rangle_{2x1} = R_y T R_x S^{\dagger} R_z |0\rangle = [0.854 + 0.354\,j \quad 0.354 - 0.146\,j]^T$ in the top branch corresponding to q[0], where the statevector is [0.924-0.383j "15 zeros"]^T ~ |0000> . Similar to the previous case, the presence of the qubit reset gate [|0>] in the lowest branch of this configuration simultaneously put all the outputs to |0>, destroying, at the same time, the stretching and the quasi-entanglement. **Figures 77** and **78** complete the set of metrics, which have an undoubted unitary nature.

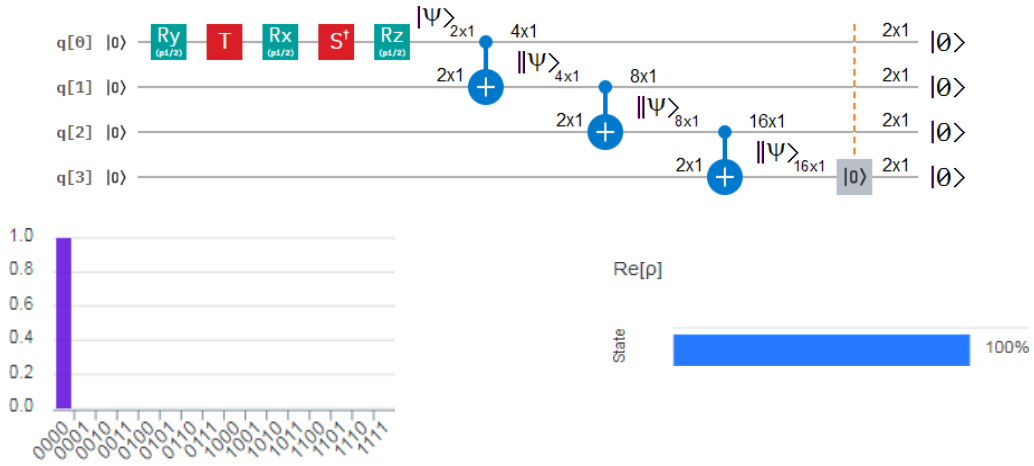

Figure 77 On the top, the generation of a not maximally entangled pair, then, two successive *CNOT* gates appear in cascade. The presence of a qubit reset gate [|0>] in the lowest branch simultaneously produces an automatic collapse of all the outputs to the ground state |0>, destroying the stretching and the quasi-entanglement. Finally, the bottom-left, shows a unitary wavefunction's complex modulus, while, bottom-right, shows the real part of the state, which is unitary too.

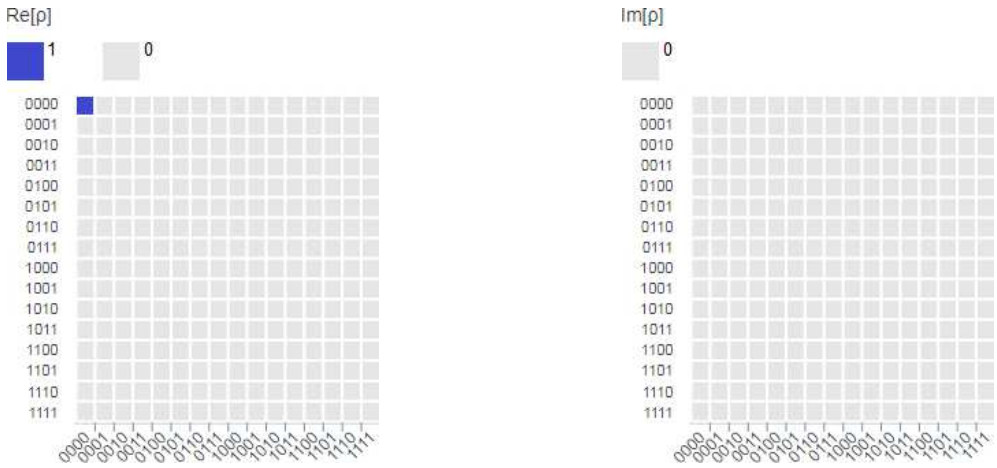

Figure 78 Wavefunction's density matrix: on the left, the real part, and on the right, the imaginary part.

Case 4:

Figure 79 represents a controlled quantum teleportation protocol, where the lowest branch of the EPR pair is stretched. At the same time, the lowest branch of the stretched EPR pair is blocked thanks to a qubit reset gate, then, the resulting statevector [0.924+0.383j "15 zeros"] is a clear evidence of: a perturbation in the teleportation process, the death of the entanglement, and the complete collapse of the stretching, where all the output of the quantum circuit ends up in |0> simultaneously. The rest of **Figure 79** and all of **Figure 80** complete the set of metrics, with a purely unitary character.

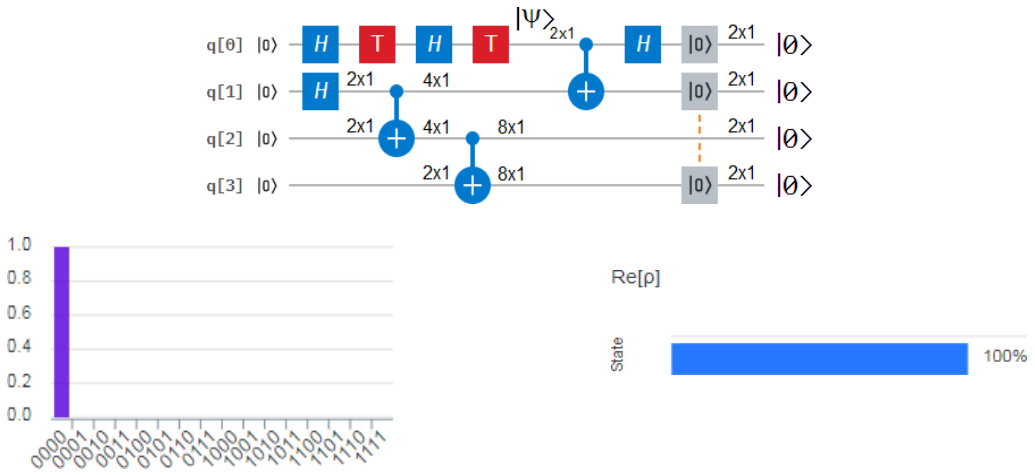

Figure 79 On the top, a controlled quantum teleportation protocol with stretching on the lowest branch of the EPR pair generation module with blocking on one of its two stretched branches. The bottom-left shows a unitary wavefunction's complex modulus. The bottom-right shows the real part of the state, which is unitary too.

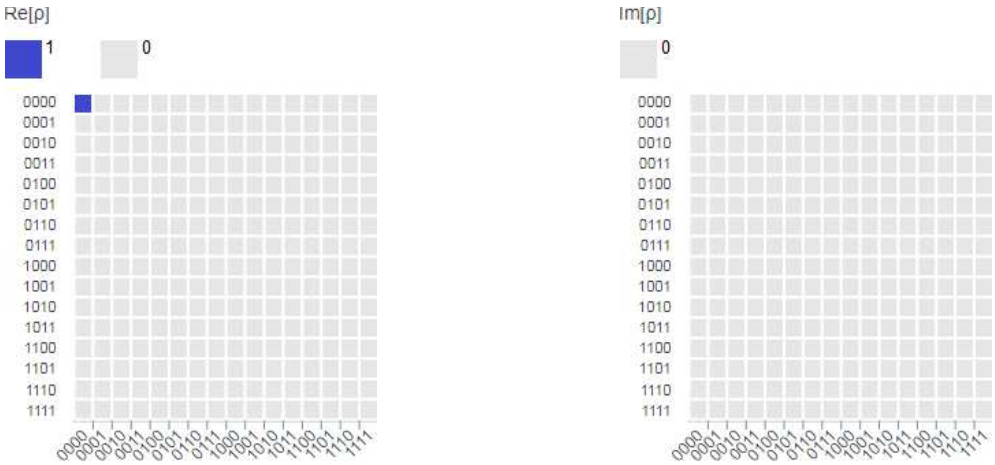

Figure 80 Wavefunction's density matrix: on the left, the real part, and on the right, the imaginary part.

Case 5:

Figure 81 shows an identical configuration to the previous case, but, with a not maximally entangled

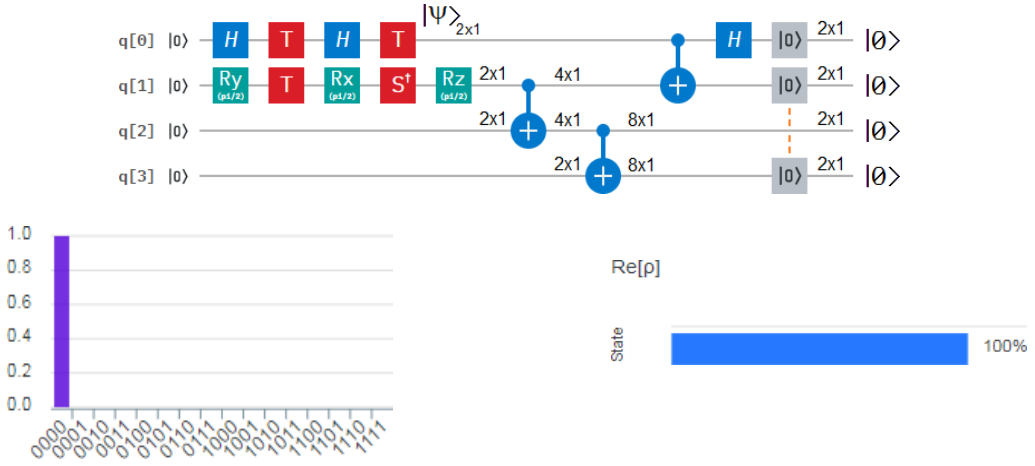

Figure 81 Idem to the previous case, with identical results, but using a not maximally entangled pair.

EPR pair, where the statevector is [1 “15 zeros”]. All of the metrics of **Figures 81** and **82** are exactly equal to those of the previous case.

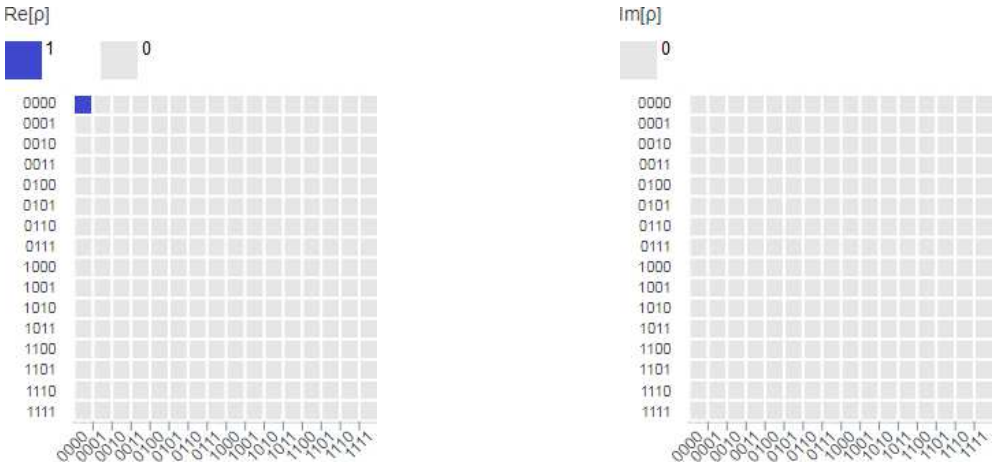

Figure 82 Wavefunction’s density matrix: on the left, the real part, and on the right, the imaginary part.

4.5. Metrics between Alice and Bob

Quantum stretching allows evaluating the teleportation quality of any type of protocol in a way never seen before thanks to the possibility of having simultaneously quasi-copies of both: the qubit to be teleported and the one finally received by Bob.

4.5.1. Case 1

Figure 83 represents a controlled quantum teleportation protocol with stretching on the qubit to be teleported: a quasi-copy goes to the BSC and the other directly to the output of the qubit q[3]. The result of the teleportation is received at the output of the protocol in qubit q[2]. For the first time in the history of quantum teleportation, both elements (that qubit to be teleported and the teleported qubit) are able to meet simultaneously in a direct metric.

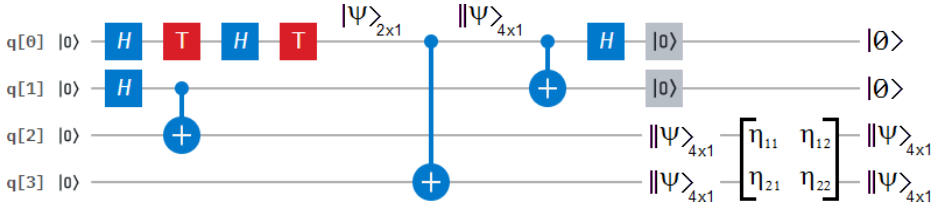

Figure 83 All begins with a stretching (from which we obtain two quasi-copies) of the qubit to be teleported, one quasi-copy goes to the BSC, while the other one goes directly to the output: to the qubit q[3]. The controlled quantum teleportation protocol teleports the upper quasi-copy, which appears to the output: in the qubit q[2]. Then, we have, for the first time, both: a version of the qubit to teleported and a version of the teleported qubit which allows us to apply any metric to evaluate the fidelity of teleportation.

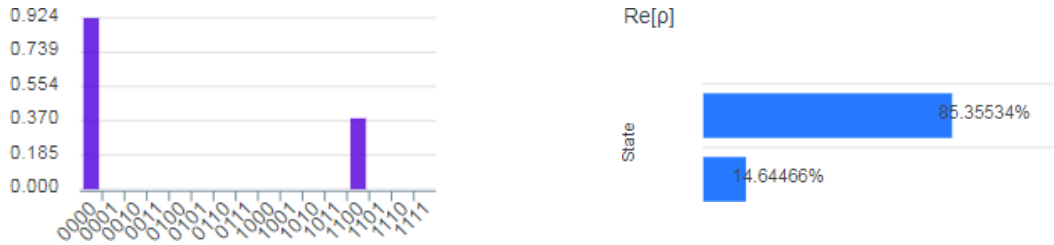

Figure 84 On the left, the wavefunction’s complex modulus. On the right, the real part of the state.

The statevector delivered by IBM Q [42] is [0.854+0.354j "11 zeros" 0.354-0.146j 0 0 0]^T = [0.854+0.354j 0 0 0.354-0.146j]$^T |0\rangle|0\rangle = \|\psi\rangle_{4\times1}|0\rangle|0\rangle$, with, [0.854+0.354j 0 0 0.354-0.146j]^T = q[2] = q[3] = $\|\psi\rangle_{4\times1}$, where, they are identical and with the same information inside as that of the qubit to be teleported, i.e., q[0] = [0.854+0.354j 0.354-0.146j]^T = $|\psi\rangle_{2\times1}$. In other words, since the qubit to be teleported does not lose information in the stretching itself or during the teleportation, this experiment is an excellent evaluator of the teleportation performance of the protocol used.

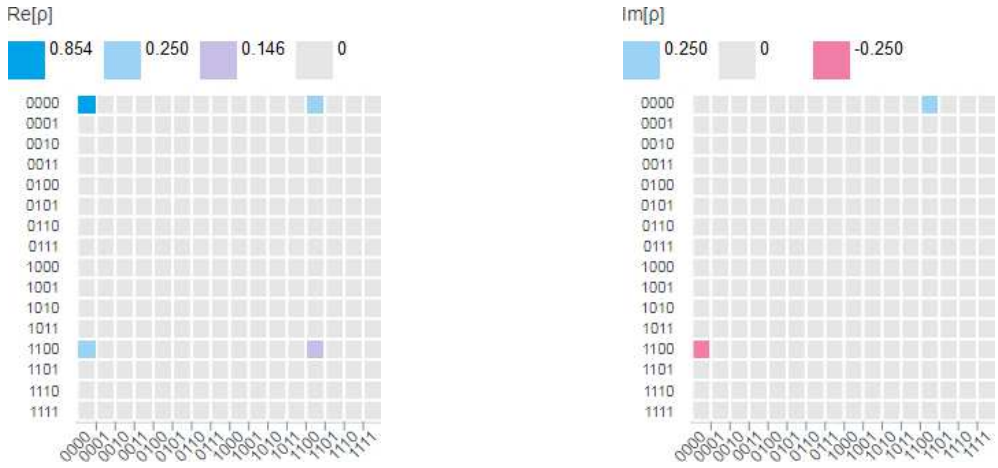

Figure 85 Wavefunction's density matrix: on the left, the real part, and on the right, the imaginary part.

Figures 84 and **Figure 85** complete the metrics of this experiment, however, the matrix at the output of **Figure 83**, among qubits q[2] and q[3], evidently represents a cross-correlation between these qubits, i.e., a cross-correlation between input and output, which is exactly what we need to be able to evaluate teleportation performance directly. In fact, such a matrix will be,

$$\eta = \begin{bmatrix} 0.854632 & 0 & 0 & 0.250632 \\ 0 & 0 & 0 & 0 \\ 0 & 0 & 0 & 0 \\ 0.250632 & 0 & 0 & 0.146632 \end{bmatrix} + \begin{bmatrix} 0 & 0 & 0 & 0.25 \\ 0 & 0 & 0 & 0 \\ 0 & 0 & 0 & 0 \\ -0.25 & 0 & 0 & 0 \end{bmatrix} j, \tag{57}$$

which is identical to the outcomes of **Figure 85**, i.e., the cross-correlation between q[2] and q[3] is identical to the wavefunction's density matrix of outcomes delivered by IBM Q, which represents a clear symptom of a perfect teleportation.

This metric is much higher than that commonly used in teleportation known as fidelity [45] and average fidelity [45], since in the presence of No-Cloning Theorem [33], i.e., leaving the stretching aside completely, fidelity and average fidelity can only be calculated in an estimated form, while thanks to the stretching, we can perform cross-correlations between input and output in a direct way, which represents a clearly superlative advantage.

4.5.2. Caso 2

In this case, featured in **Figure 86**, we will replace the cross-correlation matrix between the qubits q[2] and q[3] at the output of **Figure 83** by a *CNOT* gate, which, as we will see below, will have a restorative task. That is to say, before that last *CNOT* gate we will have the same statevector of the previous case: [0.854+0.354j "11 zeros" 0.354-0.146j 0 0 0]^T, but after such *CNOT* gate the statevector will be,

$$[0.854+0.354j \quad 0 \quad 0 \quad 0 \quad 0.354-0.146j \quad 0 \quad 0 \quad 0 \quad 0 \quad 0 \quad 0 \quad 0 \quad 0 \quad 0 \quad 0 \quad 0] = |0\rangle|\psi\rangle_{2\times1}|00\rangle, \tag{58}$$

which implies separability between $|\psi\rangle_{2\times1}$ in q[2] and $|0\rangle$ in q[3]. Therefore, if in the lowest branch, q[3], we recover a perfect $|0\rangle$, which can be measured without the slightest alteration [43], then, this is an unambiguous symptom that in the higher branch, q[2], we will have the exact version of the original qubit to be teleported, which we will know indirectly, without measuring it so as not to alter it, but still in a totally exact way. For the rest, **Figures 87** and **88** complete the set of metrics by highlighting the aforementioned separability.

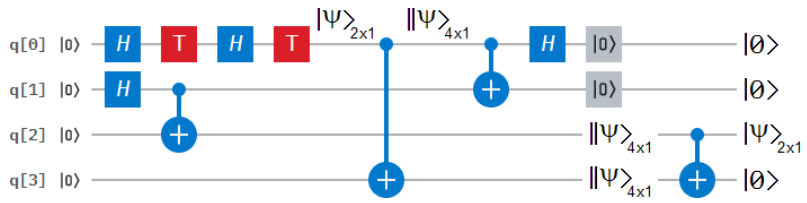

Figure 86 With a similar scheme to the previous case, the final *CNOT* gate at the output between qubits q[2] and q[3] restores the original qubit to be teleported, without the need to measure it so as not to alter it, instead, we measure q[3] and depending on how similar it is to a |0>, it is indirectly but with total accuracy that we evaluate the quality of teleportation.

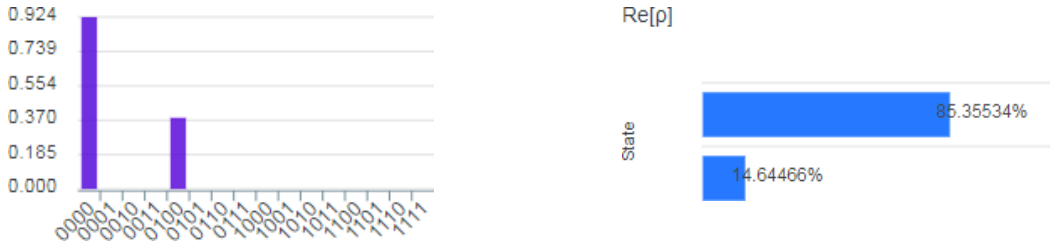

Figure 87 On the left, the wavefunction's complex modulus. On the right, the real part of the state.

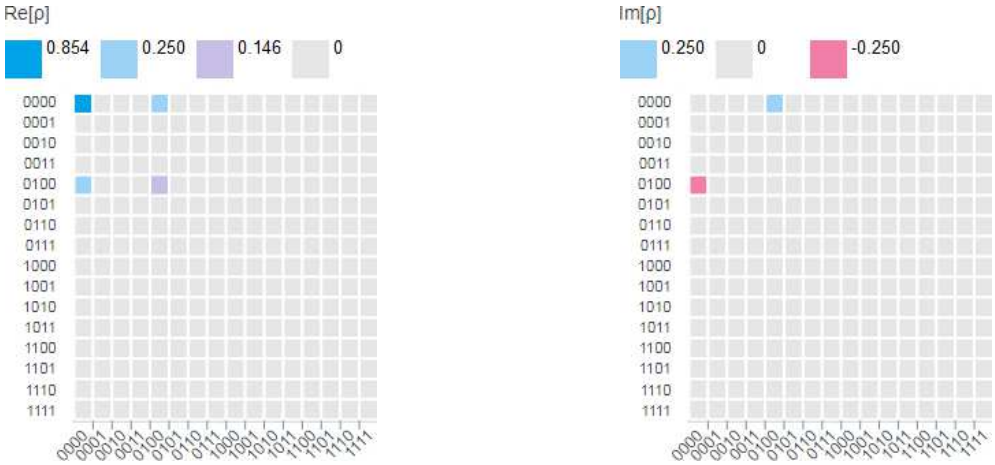

Figure 88 Wavefunction's density matrix: on the left, the real part, and on the right, the imaginary part.

4.6. Quantum splitters

Figure 89 shows the configuration for the distribution of a message to two recipients allocated in different places of the space, at the same time. **Figure 89** uses two controlled quantum teleporters to transmit both quasi-copies resulting from the stretching process. Although, the statevector delivered by IBM Q is [0.854+0.354j "35 zeros" -0.354+0.146j "27 zeros"]^T, q[2] and q[5] at the output of the configuration are [0.854+0.354j 0 0 -0.354+0.146j]^T.

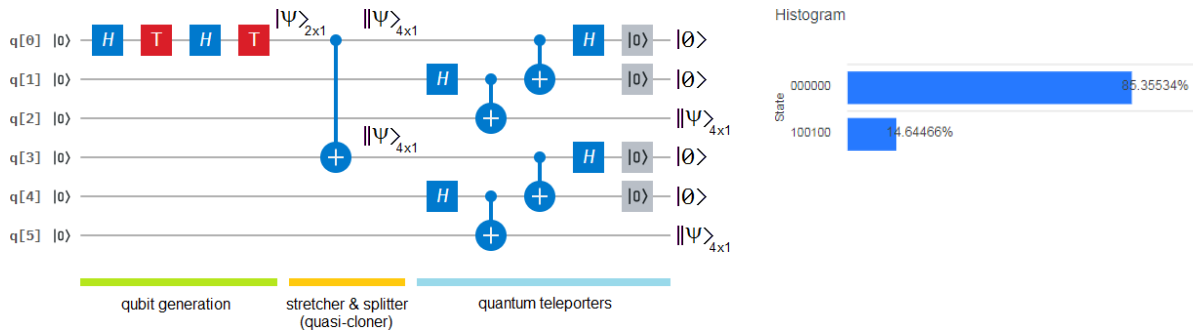

Figure 89 On the left, the quantum circuit for this experiment begins with the qubit generation, and continues with a quantum stretching, where each branch goes to its respective teleporter. On the right, the histogram with the real part of the state.

Figure 90 shows a similar case to the previous one but using a robust version of the controlled quantum teleporters, with a statevector [0.354-0.146j "19 zeros" 0.854+0.354j "11 zeros"]^T.

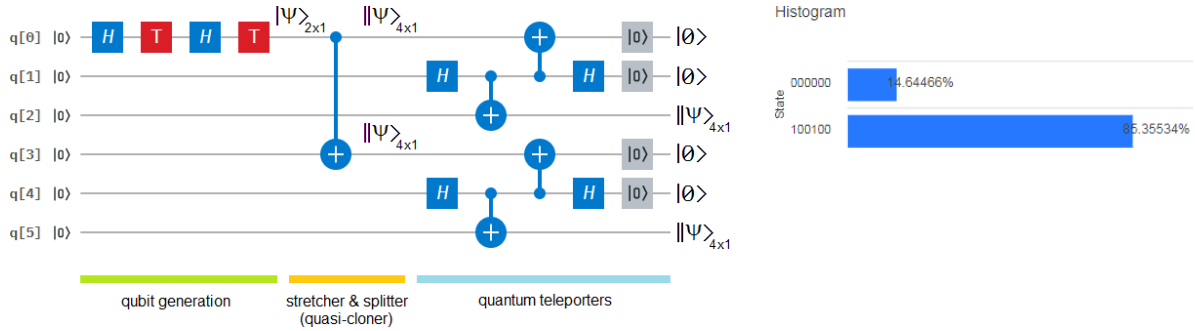

Figure 90 Idem to the previous case, however, using a robust version for each teleporter.

Next experiment is similar to that of **Figure 89**, but with a robust version in its teleporters, where the statevector will be [0.854+0.354j "44 zeros" 0.354-0.146j "18 zeros"]^T. This configuration will provoke a multiple stretching allowing us to distribute the same message to two different destinations at the same time, conserving quasi-copies of them.

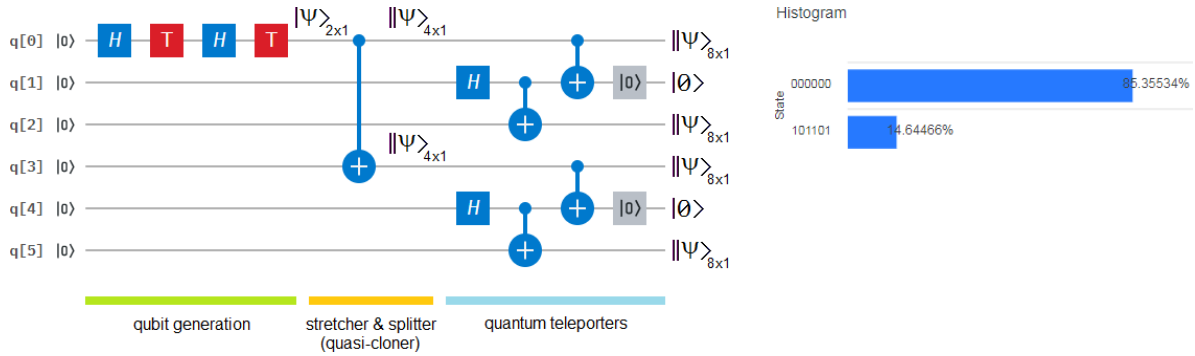

Figure 91 Identical considerations about the previous cases, however, the use of a simplified version of the teleporters generates more stretching at the output of the configuration.

Undoubtedly, all the states involved in relation to this configuration must inexorably comply with the rule of inverse-of-the-sizes conservation, whose graphic representation can be seen in **Figure 92**, being its values: 1/2 = 1/4 + 1/4 = 1/8 + 1/8 +1/8 + 1/8.

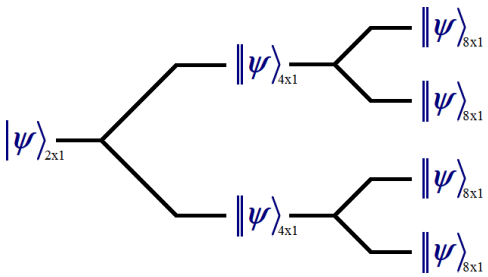

Figure 92 Graphic representation of the rule of inverse-of-the-sizes conservation for this experiment.

Figure 93 shows a similar case to the previous one but replacing the teleporters by their robust version with a statevector like ["6 zeros" 0.854+0.354j "41 zeros" 0.354-0.146j "15 zeros"]^T and four identical outputs q[1] = q[2] = q[4] = q[5] = [0.854+0.354j 0 0 0 0 0 0 0.354-0.146j]^T.

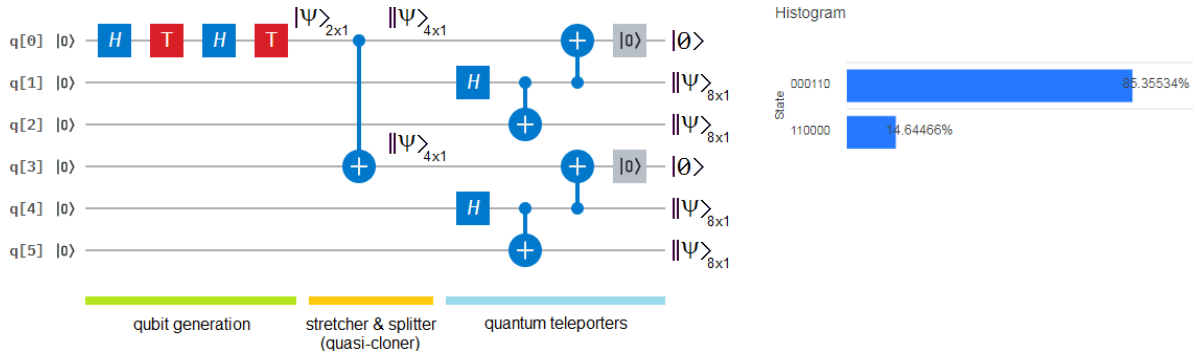

Figure 93 Idem to the previous case, but using a robust version of the simplified teleporters.

4.7. Quantum splitters and repeaters

Finally, we access to the possibility of copying, distributing, and multiplying the range (as in the case of the classical Internet) of a message from *1* to *N* points, thanks to quantum stretching. **Figure 94** shows this first version, with two lines of teleporters: a first line, and a second line or repeaters line. IBM Q [42] delivers only the statevector [-0.854-0.354j "271 zeros" 0.354-0.146j "239 zeros"]^T due to the big number of qubits involved.

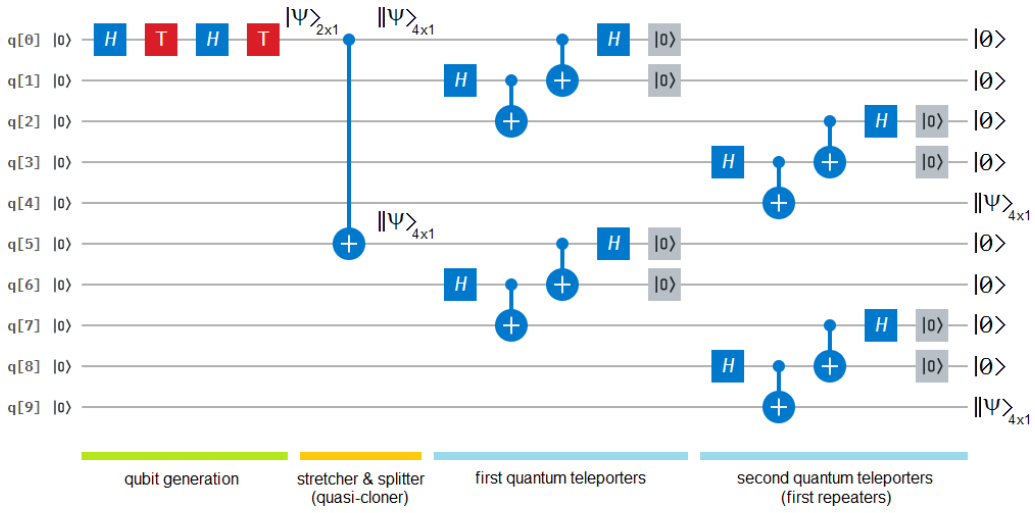

Figure 94 Complete configuration with qubit generation, quantum stretching, two lines of teleporters: the first line and their respective repeaters, i.e., the second line.

Figure 95 represents a similar case to the previous one but with a robust version of the teleporters. The statevector delivered by IBM Q is [0.354-0.146j “527 zeros” -0.854-0.354j “495 zeros”]^T.

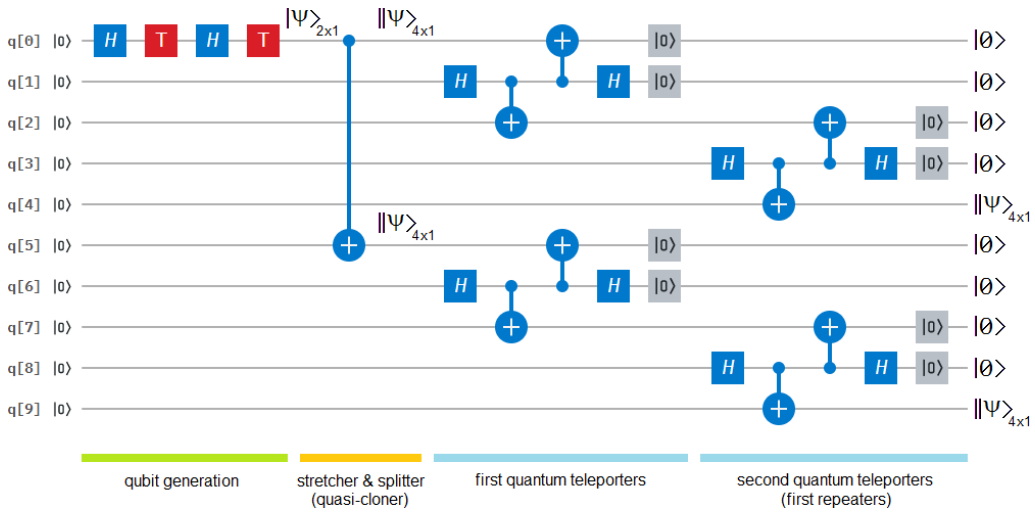

Figure 95 Idem to the previous case but replacing each teleporter by the robust version.

Figure 96 is an identical case to that of **Figure 94** but with a simplified version of the teleporters, with a statevector: [“128 zeros” 0.854+0.354j “180 zeros” 0.354-0.146j “202 zeros”]^T. The rule of inverse-of-the-sizes is conserved: 1/2 = 1/4+1/4 = 1/8+1/16+1/16+1/8+1/16+1/16, as we can see in **Figure 97**.

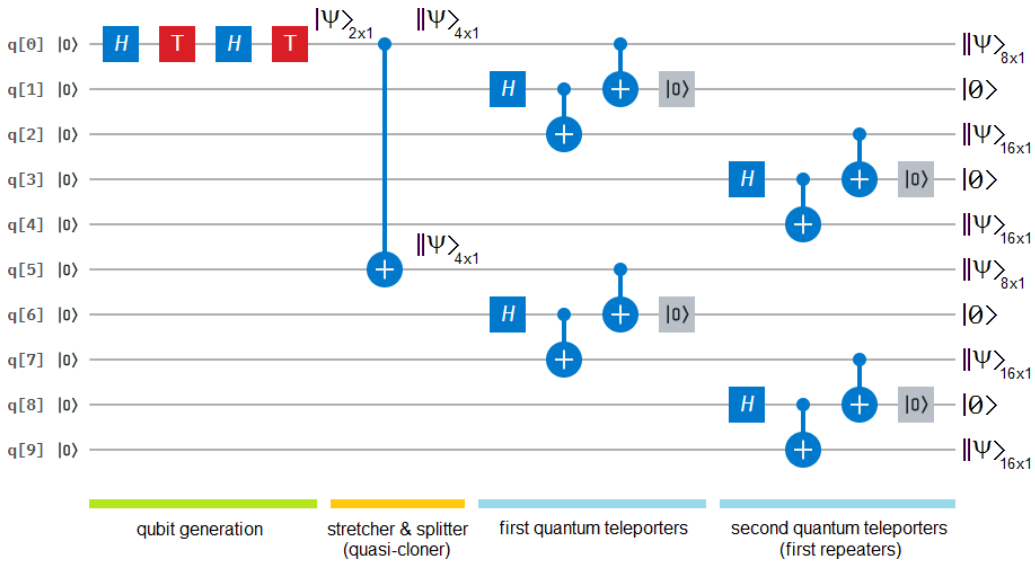

Figure 96 Identical version to **Figure 94** but using a simplified version of its teleporters.

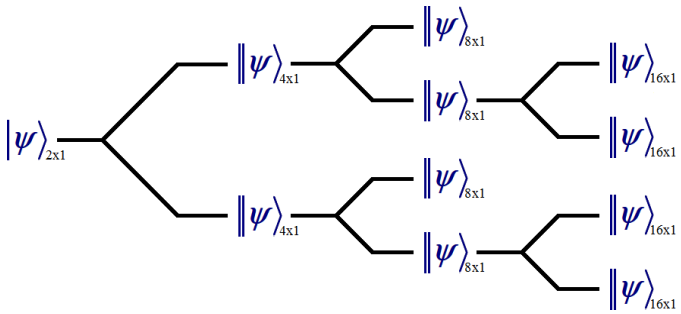

Figure 97 Graphic representation of the rule of inverse-of-the-sizes conservation for this experiment.

Figure 98 represents an identical case to the previous one, except for a simple difference, the replacement of the teleporters for a robust version with respect to those used in the configuration of **Figure 97**, with a statevector equal to ["26 zeros" 0.354-0.146j "805 zeros" 0.854+0.354j "191 zeros"]^T, however, we get six outputs:

q[1] = q[6] = [0.854+0.354j "6 zeros" 0.354-0.146j]^T,
q[3] = q[4] = q[8] = q[9] = [0.854+0.354j "14 zeros" 0.354-0.146j]^T.

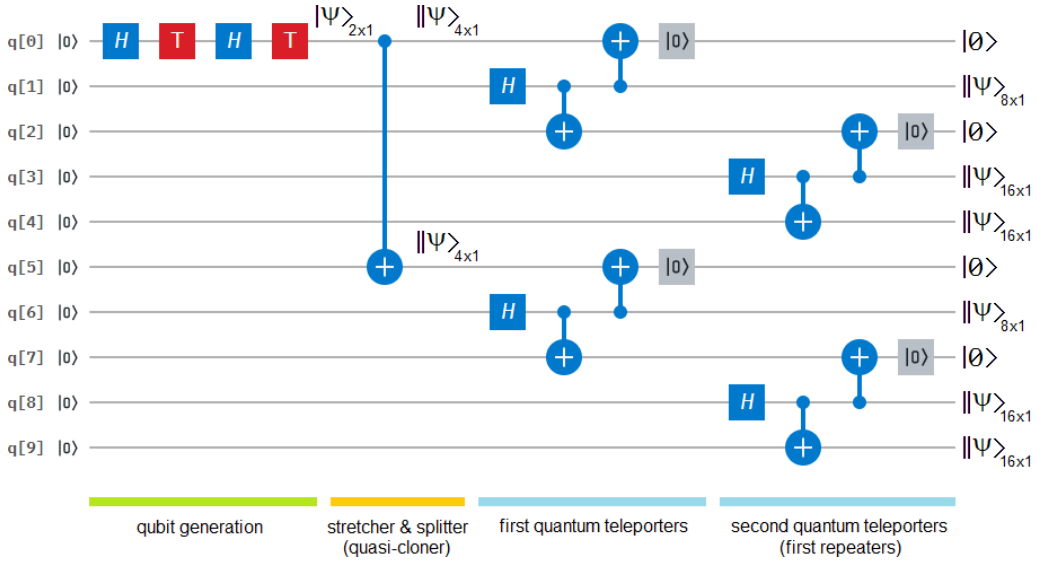

Figure 98 Idem to the previous case but employing a robust version of its protocols.

Finally, by combining all the techniques seen throughout this work, the power of dissemination of the same message on the quantum internet is immense, however, always taking into account the dimensional dilatation caused precisely by the use of these techniques.

5. Conclusions and future works

5.1. Conclusions

The technique used to solve Problem #1 of the quantum internet established in Section 1 of this work was presented in a previous work [30], another technique that mitigates Problem #2 was presented here, where the latter allows that modulus (see Quasi-Cloning Theorem) and orientation of the original qubit to be quasi-cloned to be present in its both quasi-copies. For this reason, we say that quantum stretching procedure is a lossless technique with a great future over the quantum internet.

Finally, as it has been mentioned in Subsection 3.3 and experimentally verified in Subsection 4.2, entanglement is part of a broader process, i.e., it is a particular case of stretching. Precisely, **Figure 99** shows that all forms of entanglement are particular cases of quantum stretching.

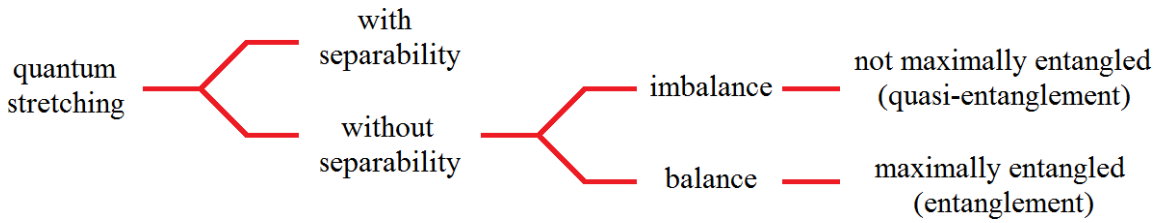

Figure 99 Graph showing that all forms of entanglement are particular cases of quantum stretching.

5.2. Future works

Some future works will be in charge of companies such as IBM Q [42] and Rigetti [46], e.g.:

- the implementation of the qubit reset gate [|0>] on their quantum physical machines (QPU) necessary for all the controlled protocols of teleportation, in fact, whoever achieves it first, will dominate the world of quantum communications, in general, and the quantum internet, in particular, and

- the extention of the coherence time of the entangled pairs, which is Problem #4 of Section 1 of this work,

while other future works will be under our charge, specifically, the resolution of Problems #3 and #5 of Section 1 of this work.

Competing interests. The author declares that there are no competing interests.

Funding. The author acknowledges funding by LosWW under contract QComm-02#10/28/2018.

Acknowledgements. The author thanks to the board of directors of LosWW for all their support.

References

1. Bennett, C.H., *et al.*: Teleporting an Unknown Quantum State via Dual Classical and Einstein-Podolsky-Rosen Channels. *Phys. Rev. Lett*. 70, 1895. (1993)
2. Bouwmeester, B.D., *et al.*: Experimental quantum teleportation, *Phil. Trans. R. Soc. Lond. A*, 356, 1733-1737. (1998)
3. Bouwmeester, D., *et al.*: Experimental Quantum Teleportation. *Nature*, 390, 575–579. (1997)
4. Boschi, D., *et al.*: Experimental Realization of Teleporting an Unknown Pure Quantum State via Dual Classical and Einstein-Podolsky-Rosen Channels. *Phys. Rev. Lett.*, 80, 1121. (1998)
5. Kurucz, Z., Koniorczyk, Z., Janszky, J.: Teleportation with partially entangled states. *Fortschr. Phys.* 49:10–11, 1019–1025. (2001)
6. Walleczek, J., Grössing, G.: The Non-Signalling theorem in generalizations of Bell's theorem. (2014).
7. Bacciagaluppi, G.: Insolubility from No-Signalling. *Int. J. Theo. Phys*. 53, 3465-3474. (2013)
8. De Martini, F., Santamato, E.: Nonlocality, No-Signalling and Bell's Theorem investigated by Weyl's Conformal Differential Geometry, *Physica Scripta*, T163, 014015. (2014)
9. Abramsky, S., Brandenburger, A., Savochkin, A.: No-Signalling is Equivalent to Free Choice of Measurements. (2014)
10. Walleczek, J., Grössing, G.: Nonlocal Quantum Information Transfer Without Superluminal Signalling and Communication, *Found Phys*, 46, 1208–1228. (2016)
11. Ghirardi, G.C., *et al.*: A General Argument against Superluminal Transmission through the Quantum Mechanical Measurement. Process. *Lettere al Nuovo Cimento*, 27:10, 293-298. (1980)
12. Einstein, A., Podolsky, B., Rosen, N.: Can Quantum-Mechanical Description of Physical Reality Be Considered Complete? *Phys. Rev.* 47:10, 777–780. (1935)
13. Bell, J.: On the Einstein Podolsky Rosen paradox. *Physics Physique Fizika*. 1:3, 195-200. (1969)
14. Clauser, J.F., *et al.*: Proposed experiment to test local hidden-variable theories. *Phys. Rev. Lett.*, 23, 15, 880-884. (1969)
15. Aspect, A., Grangier, P., Roger, G.: Experimental Realization of Einstein-Podolsky-Rosen-Bohm Gedankenexperiment: A New Violation of Bell's Inequalities. *Phys. Rev. Lett*. 49:2, 91-94. (1982)
16. Hensen, B., *et al.*: Experimental loophole-free violation of a Bell inequality using entangled electron spins separated by 1.3 km. (2015) arXiv:quant-ph/1508.05949v1
17. Einstein, A., *et al.*: The Principle of Relativity: a collection of original memoirs on the special and general theory of relativity. Courier Dover Publications, N.Y. (1952)
18. Phillips, A.C.: Introduction to Quantum Mechanics. Wiley, N.Y. (2003)

19. Penrose, R.: The road to reality: A complete guide to the laws of the universe. Johathan Cape. London, UK. (2004)
20. Weinstein, S.: Superluminal Signaling and Relativity. *Synthese*, 148:2, 381-399. (2006)
21. Weinstein, G.: Einstein on the Impossibility of Superluminal Velocities. (2012) arXiv: physics.hist-ph/1203.4954
22. Kimble, H.J.: The quantum internet. Nature 453, 1023–1030. (2008)
23. Lloyd, S., *et al.*: Infrastructure for the Quantum Internet. ACM SIGCOMM Computer Communications Review, 34:5, 9-20. (2004) doi: 10.1145/1039111.1039118
24. Azuma, K., Kato, G.: Aggregating quantum repeaters for the quantum internet. *Phys. Rev. A.* 96, 032332. (2017)
25. Bradler, K., Siopsis, G., Wozniakowski, A.: Covert Quantum Internet. (2017) arXiv:quant-ph/1704.07281
26. Yu, N., Lai, C.-Y., Zhou, L.: Protocols for Packet Quantum Network Intercommunication. (2019) arXiv:quant-ph/1903.10685
27. Pant, M., *et al.*: Routing entanglement in the quantum internet, *npj Quantum Information*, 5:25. (2019) doi:10.1038/s41534-019-0139-x
28. Hellemans, A.: Two steps closer to a quantum Internet. *IEEE Spectrum*, 53:1, 11–13. (2016)
29. ETSI: Quantum Key Distribution (QKD); Component characterization: characterizing optical components for QKD systems. ETSI GS QKD 011 V1.1.1. (2016)
30. Mastriani, M.: Is instantaneous quantum internet possible? ResearchGate (2019) doi:10.13140/RG.2.2.35132.08329/3
31. https://www.qubitreset.com
32. Nielsen, M.A., Chuang, I.L.: Quantum Computation and Quantum Information. Cambridge University Press, Cambridge. (2004)
33. Wootters, W.K., Zurek, W.H.: A single quantum cannot be cloned. *Nature*, 299, 802-803. (1982)
34. Audretsch, J.: Entangled Systems: New Directions in Quantum Physics. Wiley-VCH Verlag GmbH & Co., Weinheim, Germany. (2007)
35. Jaeger, G.: Entanglement, Information, and the Interpretation of Quantum Mechanics. The Frontiers Collection. Springer-Verlag. Berlin, Germany. (2009)
36. Horodecki R, *et al.*: Quantum entanglement. (2007) arXiv:quant-ph/0702225
37. Herbst, T., *et al.*: Quantum teleportation over a 143 km free-space link, International Conference on Space Optics (ICSO'2014) Tenerife, Canary Islands, Spain. (2014)
38. Valivarthi, R., *et al.*: Quantum teleportation across a metropolitan fibre network. (2016) arXiv: quant-ph/1605.08814
39. Kaye, P., Laflamme, R., Mosca, M.: An Introduction to Quantum Computing. Oxford University Press, Oxford. (2004)
40. Stolze, J., Suter, D.: Quantum Computing: A Short Course from Theory to Experiment. WILEY-VCH Verlag GmbH & Co. KGaA. Weinheim, Germany. (2007)
41. MacKay, D.J.C.: Information Theory, Inference, and Learning Algorithms. Cambridge University Press, Cambridge. (2003)
42. https://quantum-computing.ibm.com/
43. Arul, A.J.: Impossibility of comparing and sorting quantum states. (2001) arXiv:quant-ph/0107085
44. Mastriani, M.: Every entangled stuff has its own avatar. ResearchGate (2018) doi:10.20944/preprints201809.0221
45. Bang, J., Ryu, J., Kaszlikowski, D.: Fidelity deviation in quantum teleportation. (2018) arXiv:quant-ph/1801.06115
46. https://www.rigetti.com/